5459324

KAPL, Inc.
Knolls Atomic Power Laboratory
Post Office Box 1072 Schenectady, N.Y 12301-1072
Telephone (518) 395-4000 Facsimile (518) 395-4422

LOCKHEED MARTIN

MDO-723-0042
November 2, 2005

To: C. D. Eshelman, Manager
Space Reactor Engineering, Bettis

D. F. McCoy, Manager
Space Reactor Engineering, KAPL

Subject: Reflector and Shield Material Properties for Project Prometheus (U)

References:
a) SPP-67410-0004, dated December 22, 2004
b) B-SE-0106, dated April 28, 2005
c) SM-7231-0009/B-MT (SPME)-3, dated April 28, 2005
d) MDO-723-0021/B-MT (SRME)-21, dated April 18, 2005
e) S#05-01741, dated May 3, 2005
f) MDO-723-0012/B-MT(SPME)-002, dated February 21, 2005
g) S#05-02377, dated July 15, 2005
h) MDO-723-0048, to be issued

Attachments:
1) Reflector Material Properties for Project Prometheus
2) Shield Material Properties for Project Prometheus

Abstract
This letter provides updated reflector and shield preliminary material property information to support reactor design efforts. The information provided herein supersedes the applicable portions of Revision 1 to the Space Power Program Preliminary Reactor Design Basis (Reference (a)). This letter partially answers the request in Reference (b) to provide unirradiated and irradiated material properties for beryllium, beryllium oxide, isotopically enriched boron carbide ($^{11}B_4C$) and lithium hydride. With the exception of $^{11}B_4C$, the information is provided in Attachments 1 and 2. At the time of issuance of this document, $^{11}B_4C$ had not been studied.

Background
Reference (a) provided a set of assumptions and information used for early reactor sizing studies enabling various reactor concepts to be evaluated and compared on a common basis. These sizing studies and comparisons were used to support the recommendation for a gas cooled reactor. With the selection of a gas cooled reactor, the project transitioned to pre-conceptual design studies to further define the geometry and identify preferred reflector and shield materials. Reference (b) requested updated material properties and guidance for use in the pre-conceptual design process. In particular, Reference (b) requested the following properties for beryllium (Be), beryllium oxide (BeO), and lithium hydride (LiH) reflector and shield materials:

- Composition, density, maximum use temperature, melting temperature
- Thermal conductivity
- Thermal expansion (mean and instantaneous)
- Specific heat
- Modulus of elasticity
- Emissivity
- Yield strength
- Ultimate tensile strength
- Poisson's ratio
- *Irradiation swelling*

Discussion

Attachments 1 and 2 to this letter provide material properties for reflector and shield materials, respectively. These documents provide the available information requested in Reference (b) together with a discussion of data sources, with the exception of $^{11}B_4C$, which is not addressed herein.

The attachments include data for reflector materials Be and BeO as well as shielding materials LiH and Be. A significant amount of literature review and analysis was performed as part of this effort. To the extent possible, the available data, NRPCT-recommended equations, and competing equations were provided. However, more work remains to be done, both in terms of literature review and analysis to identify further data, and further testing to generate new data. For instance, the following properties are not included due to lack of information:

- Ultimate tensile strength of BeO. There is limited data on the tensile properties of BeO. (Attachment 1, Section 1.2.8)
- Yield strength of LiH. No data is available at the current time. (Attachment 2, Section 1.1.8)
- Poisson's ratio of LiH. No data is available at the current time. (Attachment 2, Section 1.1.10)

Since the majority of the data presented in Attachments 1 and 2 was obtained from open source literature, the measurement uncertainties in the data are not quantified. For example, it is commonly understood that the measurement uncertainty associated with thermocouples alone can be ± 0.5 to 1.0%. These and other uncertainties are not accounted for specifically in data presented herein. Statistical analysis and review included linear regression and curve-fitting techniques for the raw data, which provides some confidence, but is not a replacement for full understanding of the experiments. Therefore, the robustness of the data is questionable. Since the recommended equations were generated using all available data from the literature, additional data may be required to validate these equations and relationships.

BeO has been studied on and off for several decades, however most of the testing was on different grades of BeO that are no longer commercially available. This is significant since the irradiated material performance of BeO (specifically swelling) has been shown to be sensitive to grain size and processing techniques (Reference (c) and Section 1.2.13 of Attachment 1). Prior to close-out of the project, technical approval was sought to test a current form of BeO in the JOYO test reactor in Reference (d) and approved by Reference (e). For the reflector application, the most uncertain BeO irradiated properties include thermal conductivity, swelling and compressive strength.

Irradiated material properties for commercially available grades of Be are available in the literature. Prior to close-out, there was no testing planned for Be. Further efforts are necessary to identify gaps in the irradiated material property data where limited testing may be required. However, irradiated material property testing of Be should not be considered a high priority.

Prior to close-out of the project, technical approval was sought to fabricate lithium hydride specimens for shield materials testing in Reference (f) and approved by Reference (g). The primary goal of this testing was to determine the swelling properties of LiH, however other properties would be tested as well. Additionally, the NRPCT is investigating the applicability of quantum mechanical modeling and its ability to help in the understanding of swelling mechanisms. These results will be included in Reference (h), the shield materials portion of the close out report. Both testing and analysis were intended to reduce the uncertainty associated with the use of lithium hydride.

Conclusion

Reflector and shield material properties for Prometheus project pre-conceptual design efforts are provided in Attachments 1 and 2, respectively. The information has not been validated and is not sufficient to support final reactor design. Equations and correlations presented herein are not considered to be a final design basis. Both the reflector and shield attachments were independently reviewed, which included review of the calculations, methods used, and technical content.

Future Work

Revisions to the attachments will be necessary as further data is obtained. This data will allow for the quantification of measurement uncertainty and result in better characterized confidence intervals, as well as validation of the recommended equations. Lessons learned from future testing can be applied to determine what if any measurement uncertainty is applicable to previously gathered data.

Concurrence

This letter has the concurrence of the Bettis Manager of Space Plant Materials (Ohlinger), and the KAPL Manager of Space Materials (Simonson).

Very Truly Yours,

James Nash, Engineer
Fuel and Shield Technology
Space Materials, KAPL

Barri Gurau, Engineer
Fuel and Shield Technology
Space Materials, KAPL

Approved,

Brian Campbell, Manager
Fuel and Shield Technology
Space Materials, KAPL

This Page Intentionally Left Blank

Attachment 1:
Reflector Material Properties for Project Prometheus (U)

Author:
James Nash

Reviewed by:
Brian Campbell
MC Chen
Amitava Guha
Barri Gurau
Wayne Ohlinger
Jane Oppenlander
Dean Poeth

1.0 Reflector Materials

All data was plotted with Microsoft Excel and JMP, statistical analysis software (SAS Institute). JMP was used to fit data using the least squares method. Residual plots were examined to determine the quality of the regression data fit. In some analyses Cook's D statistics were used to examine the influence of individual data points on the least squares model (Reference 1.1.a). Where applicable, 95% prediction intervals were determined which specify the confidence on a single future value. However, these confidence intervals do not account for uncertainty associated with the individual measurements. Results from future test programs are required to quantify the measurement uncertainty.

1.1 Beryllium (Be)

Many different industrial grades of Be are available (Brush Wellman, Elmore, OH). Data for the structural grades of Be (S-65, S-65H, S-200F and S-200FH) are most commonly reported in the literature. The main differences between the various grades are impurity levels (particularly the BeO content) and processing/fabrication method. S-65 and S-200F grade Be are vacuum hot pressed (VHP) materials while S-65H and S-200FH grade Be are hot isostatically pressed (HIP) materials. The S-65 and S-65H material has a maximum BeO content of 1% while the S-200 and S-200FH material has a maximum BeO content of 1.5%. Further information on the effect of processing and impurities in Be can be found in Reference 1.1.b and 1.1.c. Generally, Be is not recommended as a structural material for radiation environments due to loss of ductility at relatively low fluences (References 1.1.d and 1.1.e). Ductility and elongation are not presented here in, but could be studied if later needed.

1.1.1 Composition

Table 1.1.1 gives the composition of S-65 structural grade beryllium from Reference 1.1.f (Brush Wellman).

Table 1.1.1: S-65 Beryllium Composition (Brush Wellman)

Element (max unless otherwise stated)	wt%
Be (min %)	99
BeO	1.0
Al	0.06
C	0.10
Fe	0.08
Mg	0.06
Si	0.06
Other metallic impurities	0.04

1.1.2 Melting Temperature and Maximum Use Temperature

The melting temperature of beryllium is (Reference 1.1.g):

$T_{melt} = 1558 \pm 10\ K$

For structural application in a radiation environment, the maximum use temperature is 823K. Above 873K embrittlement and reduction in strength are limiting factors (section 1.1.8 and 1.1.10).

1.1.3 Density

From Scaffidi-Argentina (Reference 1.1.b) for all grades of Be, the room temperature (293K) theoretical density is 1.85 g/cm^3. The following curve is recommended for the temperature range 293K $\leq$T $\leq$1500K.

$$\rho = 1.823 - 6.933x10^{-5} \cdot (T - 273) - 1.514x10^{-8} \cdot (T - 273)^2$$

where
ρ = density, g/cm^3
T = temperature, K

Dombroski (Reference 1.1.c) includes a data table of the variation in density of S-65 grade beryllium (Brush Wellman) with temperature (Table 1.1.2). Figure 1.1.1 shows some slight variation (+/-0.02) is observed at higher temperatures because the equation was fit to data from industrially available Be grades and the tabular data is only for S-65 grade Be, shown in Figure 1.1.1.

For the density of Be, the equation given by Scaffidi-Argentina (Reference 1.1.b) is recommended.

Table 1.1.2: Density data for Be

	Scaffidi-Argentina (2000)	S-65 Dombrowski (1995)
T (K)	Density (g/cc)	Density (g/cc)
324	1.819	1.82
412	1.813	1.814
456	1.810	1.811
515	1.805	1.806
564	1.802	1.801
609	1.798	1.797
673	1.793	1.791
737	1.788	1.785
816	1.781	1.777
892	1.774	1.769
973	1.767	1.76
1127	1.753	1.742
1269	1.739	1.725

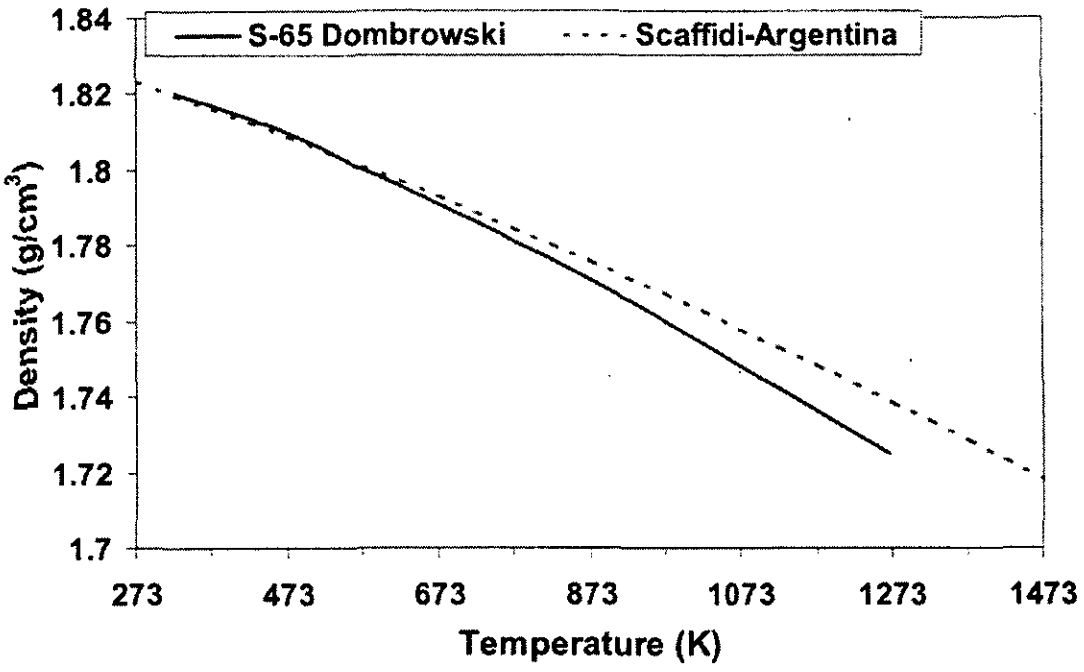

Figure 1.1.1: Density of Be

1.1.4 Thermal Conductivity

1.1.4.1 Unirradiated

From Scaffidi-Argentina (Reference 1.1.b) the unirradiated, thermal conductivity of Be is given by the following curve for the temperature range 293K ≤T ≤1500K.

$$k = 189.8 - 0.2694 \cdot (T - 273) + 2.543x10^{-4} \cdot (T - 273)^2 - 1.010x10^{-7} \cdot (T - 273)^3$$

where
k = thermal conductivity, W/m-K
T = temperature, K

Billone (Reference1.1.h) also proposed an equation for the thermal conductivity of Be based on data from various grades of Be up to 973K. This equation accounts for the fact that thermal conductivity is dependent upon the porosity of the material. This equation for the effective thermal conductivity is for hot pressed Be in the 0-50% porosity range.

$$k = \left(\frac{1 - p}{1 + 3.7p^2} \right) \cdot \left(291 - 0.48015 \cdot T + 4.2602x10^{-4} \cdot T^2 - 1.4914x10^{-7} \cdot T^3 \right)$$

where
k = thermal conductivity, W/m-K
p = fraction porosity
T = temperature, K

Dombroski (Reference 1.1.c) includes a data table of the variation in thermal conductivity of S-65 grade Be with temperature. Again, some variation is observed at higher temperatures (T>1073K) because the equation was fit to data from industrially available Be grades and the tabular data is only for S-65 grade Be.

The tabulated data (Table 1.1.3) for S-65 grade Be from Reference 1.1.c and the predicted values from the equations given in Reference 1.1.b and Reference 1.1.g assuming zero porosity are plotted in Figure 1.1.2. At temperatures between 400 – 973K, little variation is observed between the three sources.

For the thermal conductivity of Be, the equation given by Billone (Reference 1.1.h) is recommended. This curve is recommended because it accounts for the porosity of the material (0-50% range). This curve is given for T ≤973K.

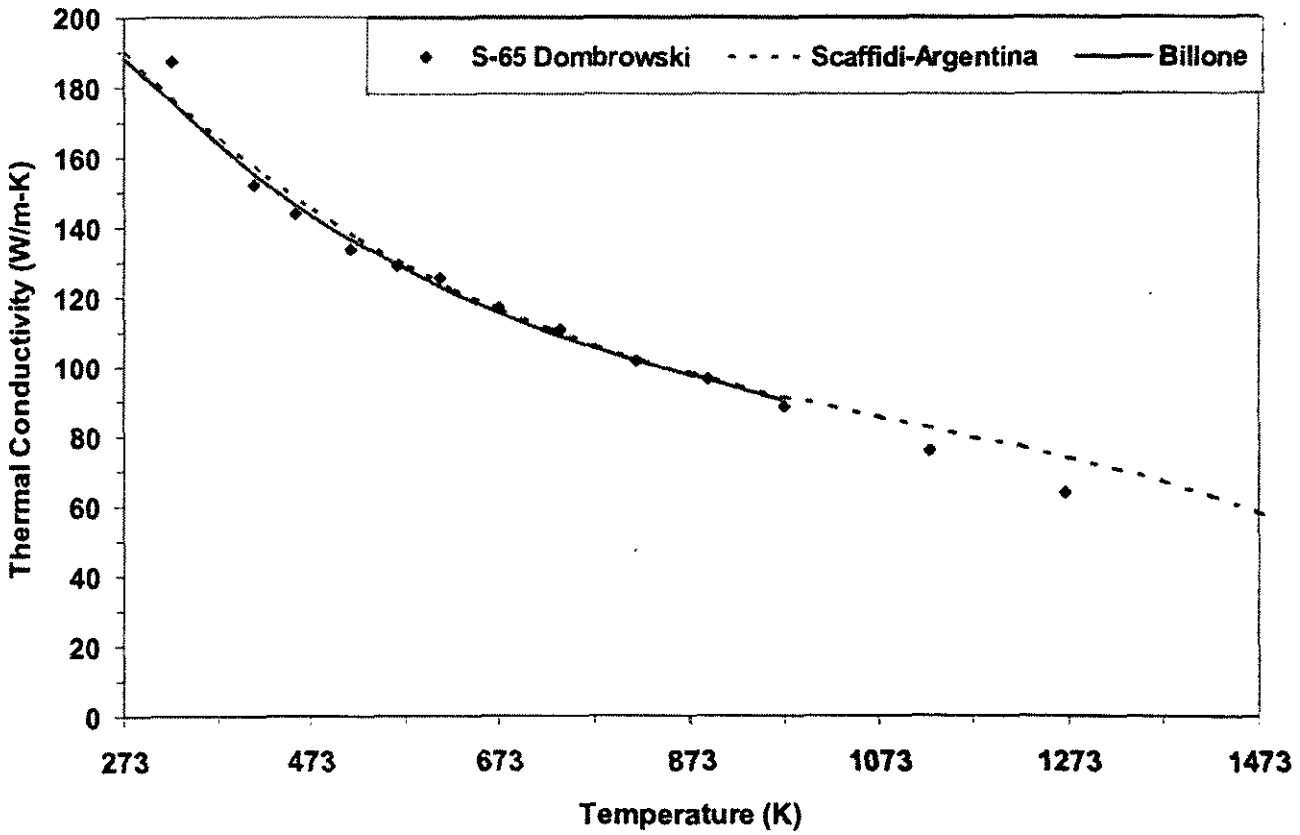

Figure 1.1.2: Thermal Conductivity of Be

Table 1.1.3: Thermal Conductivity Data for Be

S-65	Dombrowski (1995)
T (K)	Thermal Conductivity (W/m-K)
324	187.3
412	152.3
456	143.8
515	133.8
564	128.8
609	125.2
673	116.6
737	110.4
816	101.8
892	96.1
973	88.4
1127	75.8
1269	63.8

	Scaffidi-Argentina (2000)	Billone (1995)
T(K)	W/m-K	W/m-K
273	189.8	188.6
373	165.3	163.4
473	145.3	143.4
573	129.1	127.7
673	116.3	115.4
773	106.0	105.5
873	97.88	97.28
973	91.17	89.76
1073	85.29	
1173	79.66	
1273	73.65	
1373	66.67	
1473	58.10	
1573	47.35	

1.1.4.2 Irradiated

The irradiated thermal properties, including thermal conductivity, have been studied for beryllium. Snead and Barabash (References 1.1.i and 1.1.j) summarize the neutron irradiation data for S-65 and S-200F Brush Wellman beryllium grades. Snead (Reference 1.1.i) reported that significant reductions in thermal conductivity of Be are not expected until He bubbles and swelling become more prominent (He bubbles form at grain boundaries from 598 – 873K and form at dislocations within the grain at temperatures around 723 – 823K). This is because for irradiations above 573 K the He is no longer in solid solution and therefore He diffusion and bubble formation begin to occur. Snead (Reference 1.1.i) showed that the effect of radiation on the thermal conductivity of S-65 Be at ~$1x10^{21}$ n/cm^2 (E>0.1 MeV) and approximately 573K was within the ~4% experimental error of the unirradiated value. For S-200F Be irradiated to fluences of $4.5x10^{20}$ n/cm^2 (E>1MeV) at 473K, the thermal conductivity decreased approximately 5% (Reference 1.1.j). At this time there is no recommended equation for irradiated thermal conductivity of Be.

1.1.5 Thermal Expansion

It should be noted that due to the anisotropic nature of the hexagonal lattice, some amount of anisotropy is expected in thermal expansion. However, as described by Scaffidi-Argentina (Reference 1.1.b), there is little difference (less than a few percent) observed for polycrystalline, isotropic sintered Be parts (S-65 Brush Wellman grade Be). Extruded grades of Be may exhibit 15-20% differences in the longitudinal and transverse thermal expansion, while HIP Be (S-65H and S-200FH) are more isotropic.

1.1.5.1 Unirradiated Linear Expansion

Billone (Reference 1.1.h) reports the following equation, plotted in Figure 1.1.3, developed for the percent change in length ($\Delta L/L_0$) of Be based on data up to 1558K. The unirradiated percent change in length ($\Delta L/L_0$) is given by:

$$\frac{\Delta L}{L_0} = 8.43x10^{-4} \cdot (1 + 1.36x10^{-3} \cdot T - 3.53x10^{-7} \cdot T^2) \cdot (T - 298)$$

where
$\Delta L/L_0$ = change in length from 298K, percent
T = temperature, K

T (K)	% Linear Expansion
298	0
373	0.092
473	0.231
573	0.386
673	0.555
773	0.737
873	0.930
973	1.13

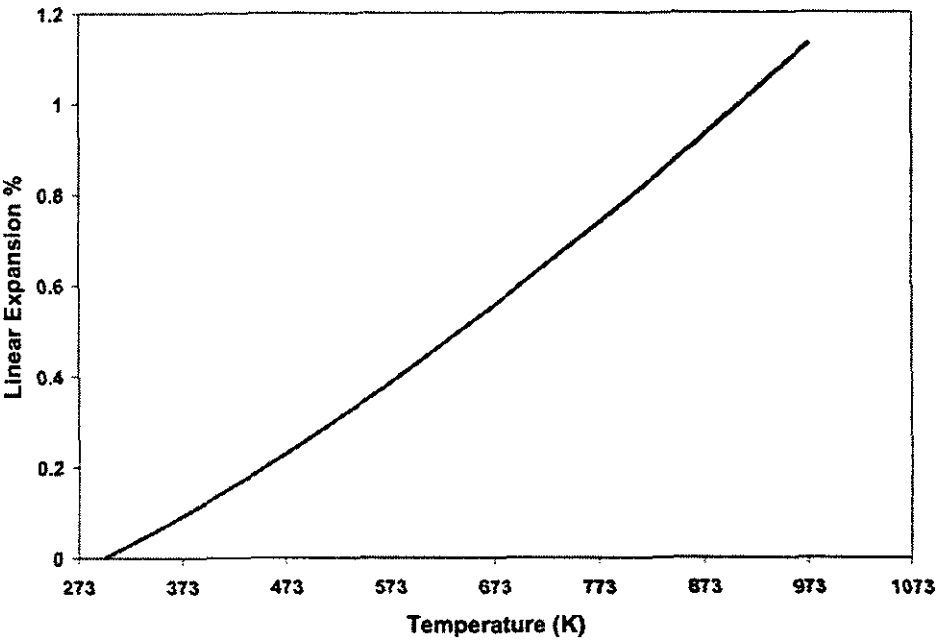

Figure 1.1.3: Linear Expansion of Be with Data Table Included

1.1.5.2 Unirradiated Instantaneous Coefficient of Thermal Expansion

From Scaffidi-Argentina (Reference 1.1.b), for the temperature range 293K ≤T ≤1473K the unirradiated instantaneous coefficient of thermal expansion (α_i) is given by the following equation.

$$\alpha_i = 10.8 + 0.022 \cdot (T - 273) - 1.35x10^{-5} \cdot (T - 273)^2 + 3.45x10^{-9} \cdot (T - 273)^3$$

where
α_i = instantaneous coefficient of thermal expansion, 10^{-6} K^{-1}
T = temperature, K and the reference temperature is 293K

1.1.5.3 Unirradiated Mean Coefficient of Thermal Expansion

From Scaffidi-Argentina (Reference 1.1.b), for the temperature range 293K < T < 1473K the unirradiated mean coefficient of thermal expansion (α_m) is given by:

$$\alpha_m = 11.04 + 0.0109 \cdot (T - 273) - 4.474x10^{-6} \cdot (T - 273)^2 + 8.631x10^{-10} \cdot (T - 273)^3$$

where
α_m = mean coefficient of thermal expansion, 10^{-6} K^{-1}
T = temperature, K and the reference temperature is 293K

Figure 1.1.4 includes the instantaneous coefficient of thermal expansion (α_i) and the mean coefficient of thermal expansion (α_m) as determined by Scaffidi-Argentina (Reference 1.1.b) for all grades of Be, and the mean thermal expansion coefficient as determined by Dombrowski (Reference 1.1.c) for S-65 Be containing 0.9% BeO. The values are tabulated in Table 1.1.4.

For the mean coefficient of thermal expansion of Be, the equation given by Scaffidi-Argentina (Reference 1.1.b) is recommended.

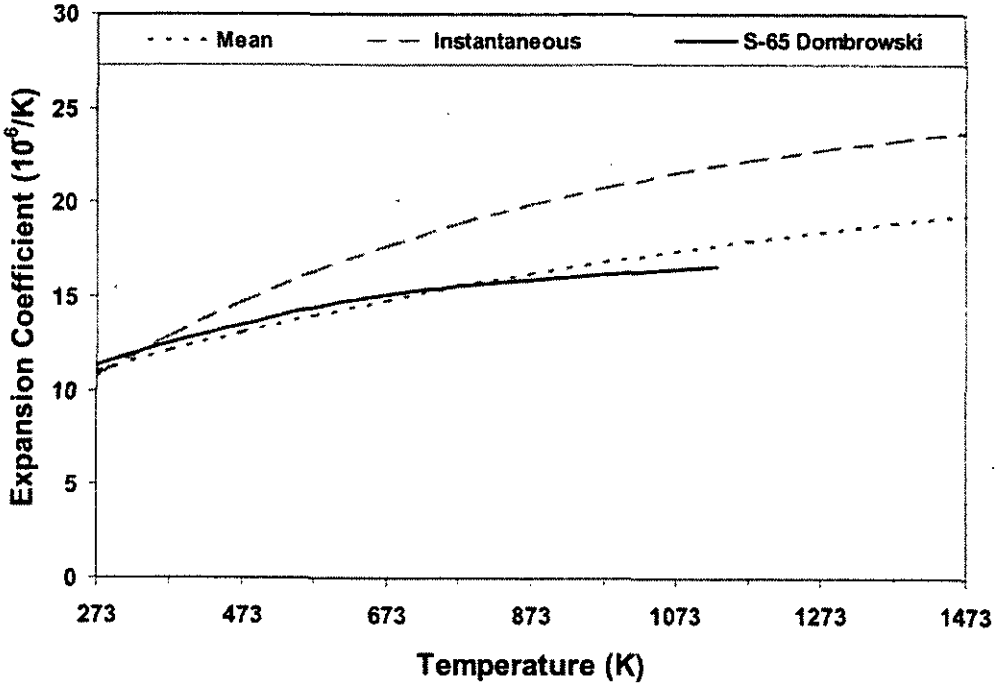

Figure 1.1.4: Mean and Instantaneous Thermal Expansion Coefficient of Be

Table 1.1.4: Mean and Instantaneous Thermal Expansion Data for Be

S-65	Dombrowski (1995)
T (K)	CTE (10^{-6})/K
270	11.32
381	12.58
524	14.00
607	14.66
688	15.14
758	15.44
952	16.10
1130	16.61

	Scaffidi-Argentina (2000)	
	instantaneous	mean
T(K)	CTE (10^{-6})/K	CTE (10^{-6})/K
273	10.80	11.04
373	12.87	12.10
473	14.69	13.07
573	16.28	13.96
673	17.66	14.78
773	18.86	15.53
873	19.89	16.22
973	20.77	16.85
1073	21.53	17.42
1173	22.18	17.95
1273	22.75	18.43
1373	23.26	18.88
1473	23.72	19.29
1573	24.16	19.68

1.1.5.4 Irradiated

From Reference 1.1.b it is expected that the coefficient of thermal expansion in isotropic Be grades is not affected by neutron irradiation.

1.1.6 Specific Heat

1.1.6.1 Unirradiated

From Scaffidi-Argentina (Reference 1.1.b), the unirradiated specific heat of Be is given by the following equation. This equation is based on experimental data from Be grades with ≤1% BeO content (S-65 Brush Wellman Be). The equation is valid for 293 ≤T ≤1558K.

$$C_p = 1741.8 + 3.3358 \cdot (T - 273) - 3.1125x10^{-3} \cdot (T - 273)^2 + 1.2748x10^{-6} \cdot (T - 273)^3$$

where
C_p = specific heat, J/kg-K
T = temperature, K

Billone (Reference 1.1.h) proposed an equation for the specific heat based on data from various grades of Be up to 973K.

$$C_p = 2432 + 0.6428 \cdot (T - 273) - 0.7111 \cdot (T - 273)^{-2}$$

where
C_p = specific heat, J/kg-K
T = temperature, K

Dombrowski (Reference 1.1.c) includes a data table of the variation in specific heat of S-65 grade Be with temperature. Figure 1.1.5 is of the tabular data, given in Table 1.1.5, for S-65 Be from Reference 1.1.c and the predicted values from the equations given in Reference 1.1.a and Reference 1.1.h for the unirradiated specific heat of Be. Some variation is observed between Reference 1.1.a and 1.1.h at lower temperatures (T<573K).

For the specific heat of Be, the equation given by Scaffidi-Argentina (Reference 1.1.b) is recommended.

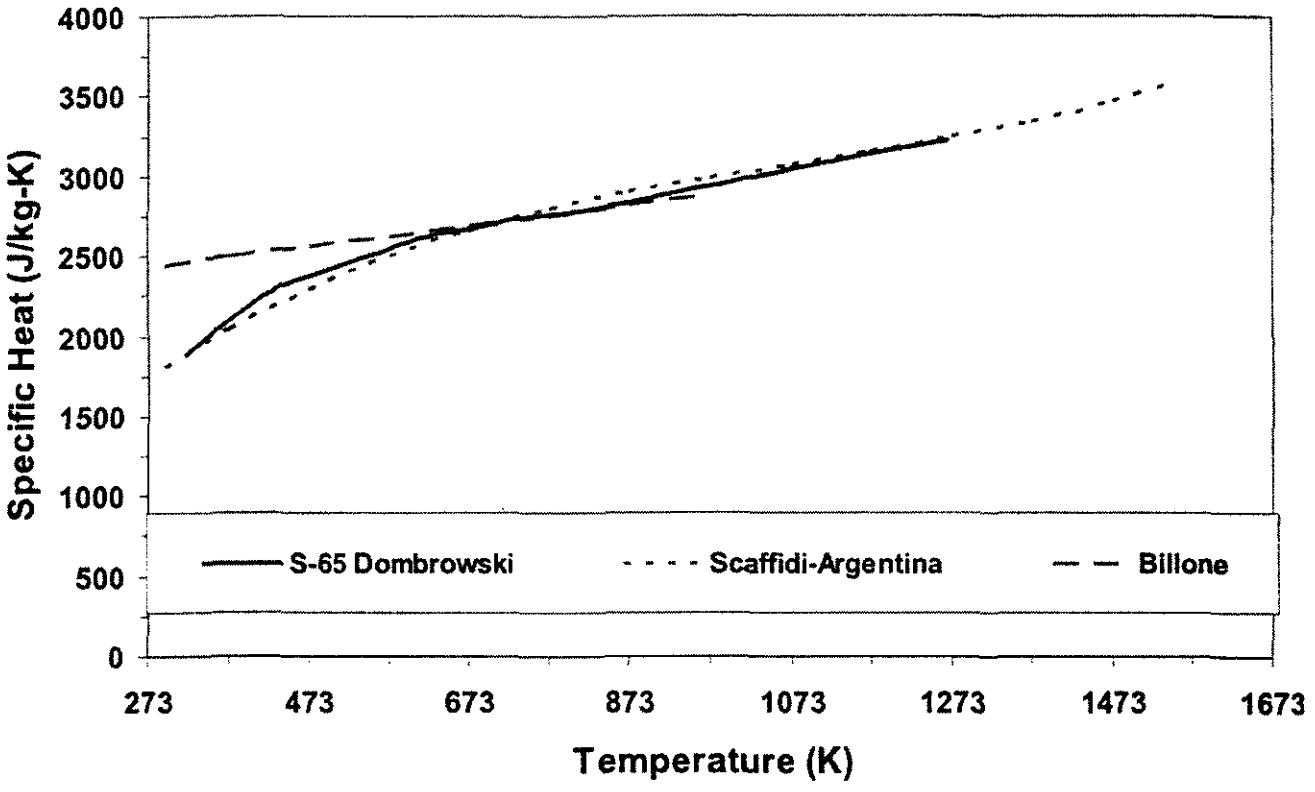

Figure 1.1.5: Specific Heat of Be

Table 1.1.5: Specific Heat Data for Be

S-65	Dombrowski (1995)
T (K)	Cp (J/kg-K)
324	1905
412	2240
456	2344
515	2441
564	2529
609	2613
673	2667
737	2734
816	2780
892	2860
973	2939
1127	3086
1269	3220

	Scaffidi-Argentina (2000)	Billone (1995)
T(K)	Cp (J/kg-K)	Cp (J/kg-K)
293	1807	2445
373	2046	2496
473	2295	2561
573	2497	2625
673	2660	2689
773	2791	2753
873	2898	2818
973	2989	2882
1073	3071	
1173	3152	
1273	3240	
1373	3342	
1473	3466	
1550	3581	

1.1.6.2 Irradiated

Scaffidi-Argentina (Reference 1.1.b) reports minimal effects on the specific heat of irradiated Be. It was also reported that the specific heat remains fairly independent of the Be grade. At this time it is assumed that the specific heat of Be will remain independent of irradiation.

1.1.7 Modulus of Elasticity

1.1.7.1 Unirradiated

Variation in the elastic modulus of S-65 Be with temperature is given by Dombrowski (Reference 1.1.c) over the temperature range 273K ≤T ≤1273K, shown in Figure 1.1.6. Based on the limited data points reported, no equation is given at this time.

T (K)	Young's Modulus (GPa)
273	310
473	300
673	290
873	230
1073	97
1273	48

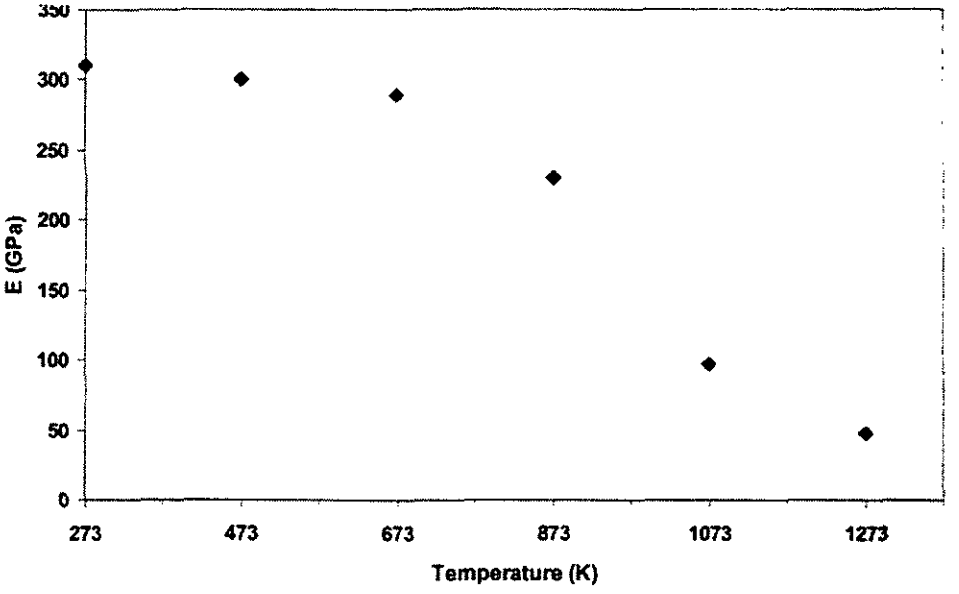

Figure 1.1.6: Elastic Modulus of Be with Data Table Included.

1.1.7.2 Irradiated

Hickman (Reference 1.1.e) reports that radiation effects in Be are expected to be negligible because of the lack of significant displacement type damage above 373K (no fluence limit was reported by Hickman). Some variation in the elastic modulus of Be may occur due to helium bubble formation and swelling. Generally, variations in the elastic modulus are related to temperature as shown above.

1.1.8 Tensile Yield Strength

1.1.8.1 Unirradiated

Multiple references have reported on the unirradiated tensile yield strength of Be (References 1.1.d, 1.1.k, 1.1.l and 1.1.m). The below equations are based on data from unirradiated VHP (S-65 and S-200F Brush Wellman) and HIP (S-65H and S-200FH Brush Wellman) Be grades. In general, HIP grade Be exhibits a higher tensile yield strength than VHP grade Be. These equations are linear regressions of the data in the temperature range 293K ≤T ≤1228K (See Figures 1.1.7 and 1.1.8 below in section 1.1.8.2).

$$VHP\ \ YS = -0.2574 \cdot T + 350.1$$

$$HIP\ \ YS = -0.3289 \cdot T + 449.3$$

where

VHP YS = tensile yield strength of VHP Be, MPa
HIP YS = tensile yield strength of HIP Be, MPa
T = temperature, K

1.1.8.2 Irradiated

Irradiation effects on the tensile yield strength of multiple grades of Be (S-65, S-65H, S-200F and S-200FH) have been studied by many references (References 1.1.d, 1.1.k, 1.1.l and 1.1.m) Irradiated Be exhibits a higher yield strength than in the unirradiated state. Below is a linear regression fit to the irradiated VHP Be and HIP Be data over a temperature range of 293K ≤T ≤823K and fluence range of 0.75 – 2.45x10^{21} n/cm^2 (E>1 MeV). The plot of irradiated and unirradiated tensile yield strength data for multiple grades of Be is also shown below (Figure 1.1.7 and 1.1.8). Neutron irradiation studies have observed that above 823K the strength of irradiated Be dramatically decreases due to He bubble formation. In beryllium He bubbles begin to form at grain boundaries at T>673K and at dislocations within the grains at T>823K. Additionally, Be has a high fast neutron cross-section for (n,α) reactions and therefore at higher temperatures He embrittlement becomes a concern (corresponding to 0.5 T_{melt}). All high temperature irradiated data (T ≥823K) was excluded from the regression analysis. Additionally, Moons (Reference 1.1.d) performed thermal ageing studies to isolate thermal effects from radiation effects. The thermal results are not included in this linear regression analysis. Data reported from Reference 1.1.d, 1.1.k, 1.1.l and 1.1.m were from samples tested at the irradiation temperature. The equations exhibit a good fit for 293 – 823K.

$$VHP\ YS_{irr} = -0.6270 \cdot T + 692.5$$

$$HIP\ YS_{irr} = -0.6985 \cdot T + 791.7$$

where
VHP YS_{irr} = irradiated tensile yield strength of VHP Be, MPa
HIP YS_{irr} = irradiated tensile yield strength of HIP Be, MPa
T = temperature, K

The unirradiated and irradiated tensile yield strength of Be is plotted in Figure 1.1.7 for VHP and HIP grades are plotted in Figure 1.1.8. The 95% confidence intervals for the least square fits to the data are shown on the graphs. Further study is required to define the effects on yield strength for fluences below 0.75x10^{21} n/cm^2 (E>1MeV).

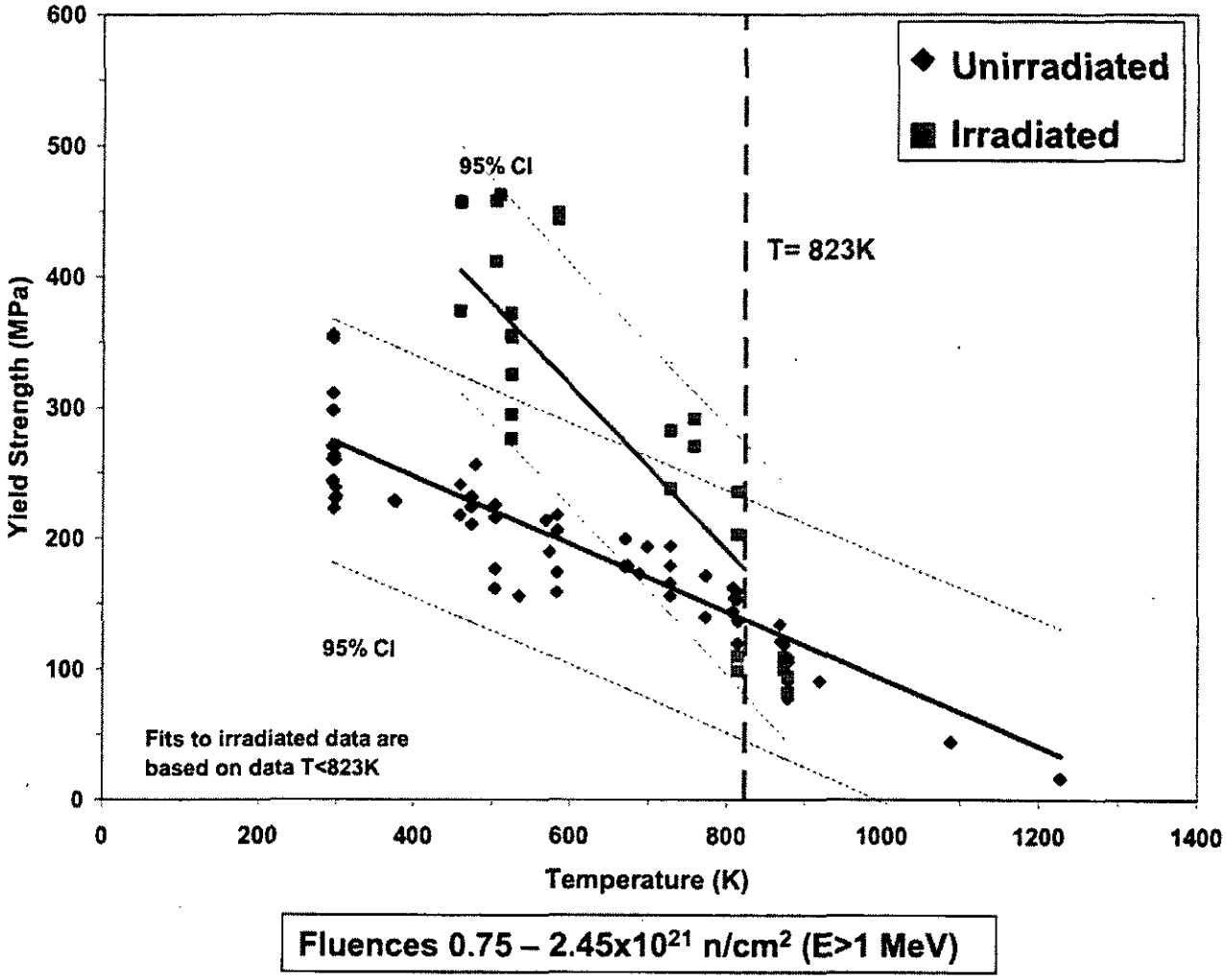

Figure 1.1.7: Irradiated and Unirradiated Tensile Yield Strength of VHP Be

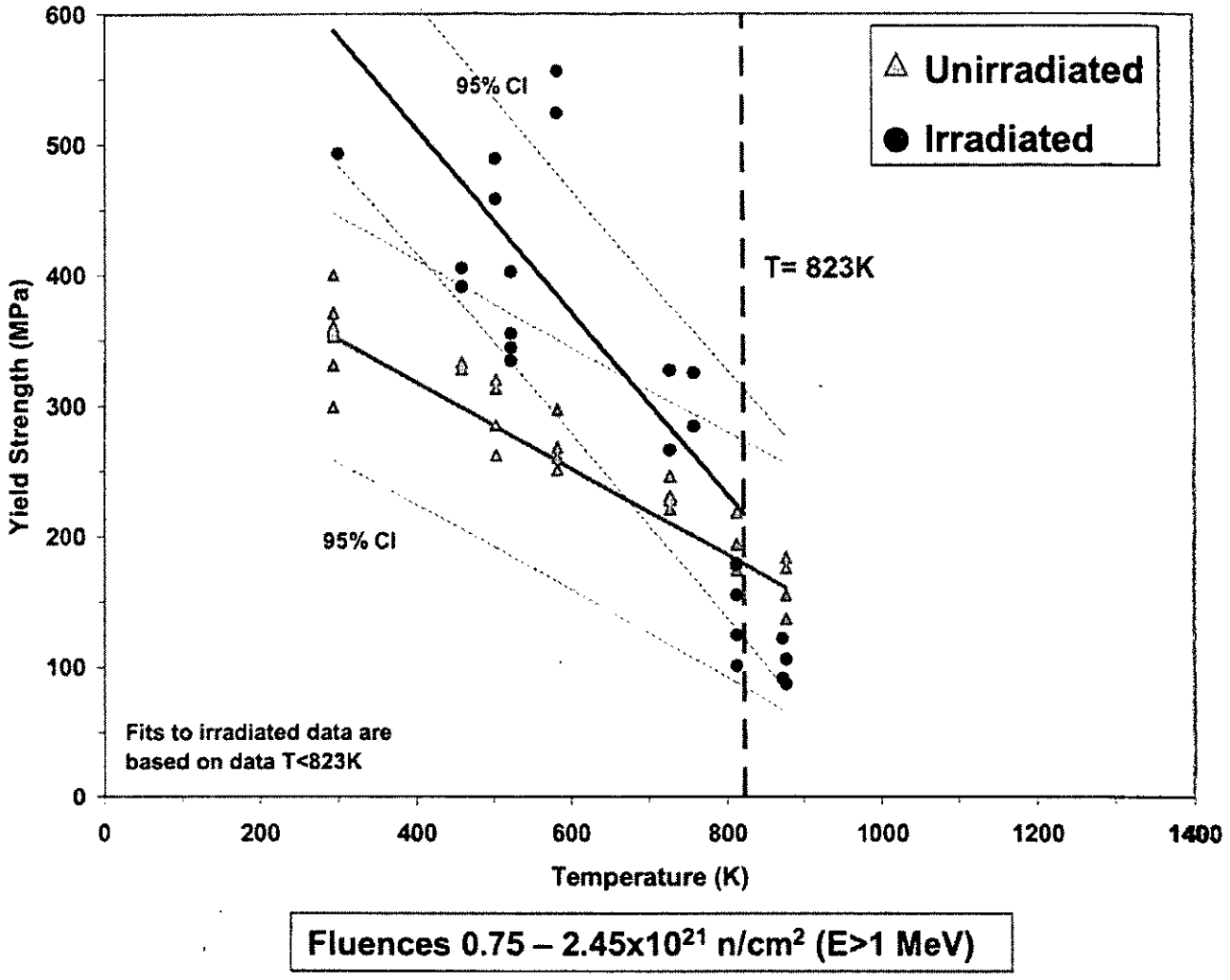

Figure 1.1.8: Irradiated and Unirradiated Tensile Yield Strength of HIP Be

1.1.9 Emissivity

Reference 1.1.g reports the emissivity of Be for $T < T_m$:

$$\varepsilon = 0.61$$

The emissivity of Be is not expected to vary with irradiation, however the emissivity may vary with material processing (i.e. surface finish).

1.1.10 Ultimate Tensile Strength

1.1.10.1 Unirradiated

Multiple references have reported on the unirradiated ultimate tensile strength of Be (References 1.1.d, 1.1.k, 1.1.l and 1.1.m). The below equations are based on data from unirradiated VHP (S-65 and S-200F Brush Wellman) and HIP (S-65H and S-200FH Brush Wellman) Be grades. In general,

HIP grade Be exhibits a higher ultimate tensile strength than VHP grade Be. These equations are based on data in the temperature range 293K ≤T ≤923K (See Figures 1.1.9 and 1.1.10 below in section 1.1.10.2).

$$VHP\ UTS = -0.4139 \cdot T + 515.3$$

$$HIP\ UTS = -0.4897 \cdot T + 609.9$$

where
VHP UTS = ultimate tensile strength of VHP Be, MPa
HIP UTS = ultimate tensile strength of HIP Be, MPa
T = temperature, K

1.1.10.2 Irradiated

Irradiation effects on the ultimate tensile strength of multiple grades of Be (S-65, S-65H, S-200F and S-200FH) have been studied by many references (References 1.1.d, 1.1.k, 1.1.l and 1.1.m). Irradiated Be exhibits a slightly higher ultimate tensile strength than in the unirradiated state. Below is a fit to the VHP Be and HIP Be data over a temperature range of 293K ≤T ≤823K and fluence range of 0.75 – 2.45x10^{21} n/cm^2 (E>1 MeV). The plot of irradiated and unirradiated ultimate tensile strength data for multiple grades of Be are shown in Figure 1.1.9 and Figure 1.1.10. Neutron irradiation studies have observed that above 823K the strength of irradiated Be dramatically decreases due to He bubble formation. In beryllium He bubbles begin to form at grain boundaries at T>673K and at dislocations within the grains at T>823K. Additionally, Be has a high fast neutron cross-section for (n,α) reactions and therefore at higher temperatures He embrittlement becomes a concern (corresponding to 0.5 T_{melt}). All high temperature irradiated data (T ≥823K) was excluded from the regression analysis. Additionally, Moons (Reference 1.1.d) performed thermal ageing studies to isolate thermal effects from radiation effects. The thermal results are not included in this linear regression analysis. Data reported from Reference 1.1.d, 1.1.k, 1.1.l and 1.1.m were from samples tested at the irradiation temperature. The equations exhibit a good fit for 293 – 823K.

$$VHP\ UTS_{irr} = -0.7980 \cdot T + 849.0$$

$$HIP\ UTS_{irr} = -0.8738 \cdot T + 943.6$$

where
VHP UTS_{irr} = irradiated ultimate tensile strength of VHP Be, MPa
HIP UTS_{irr} = irradiated ultimate tensile strength of HIP Be, MPa
T = temperature, K

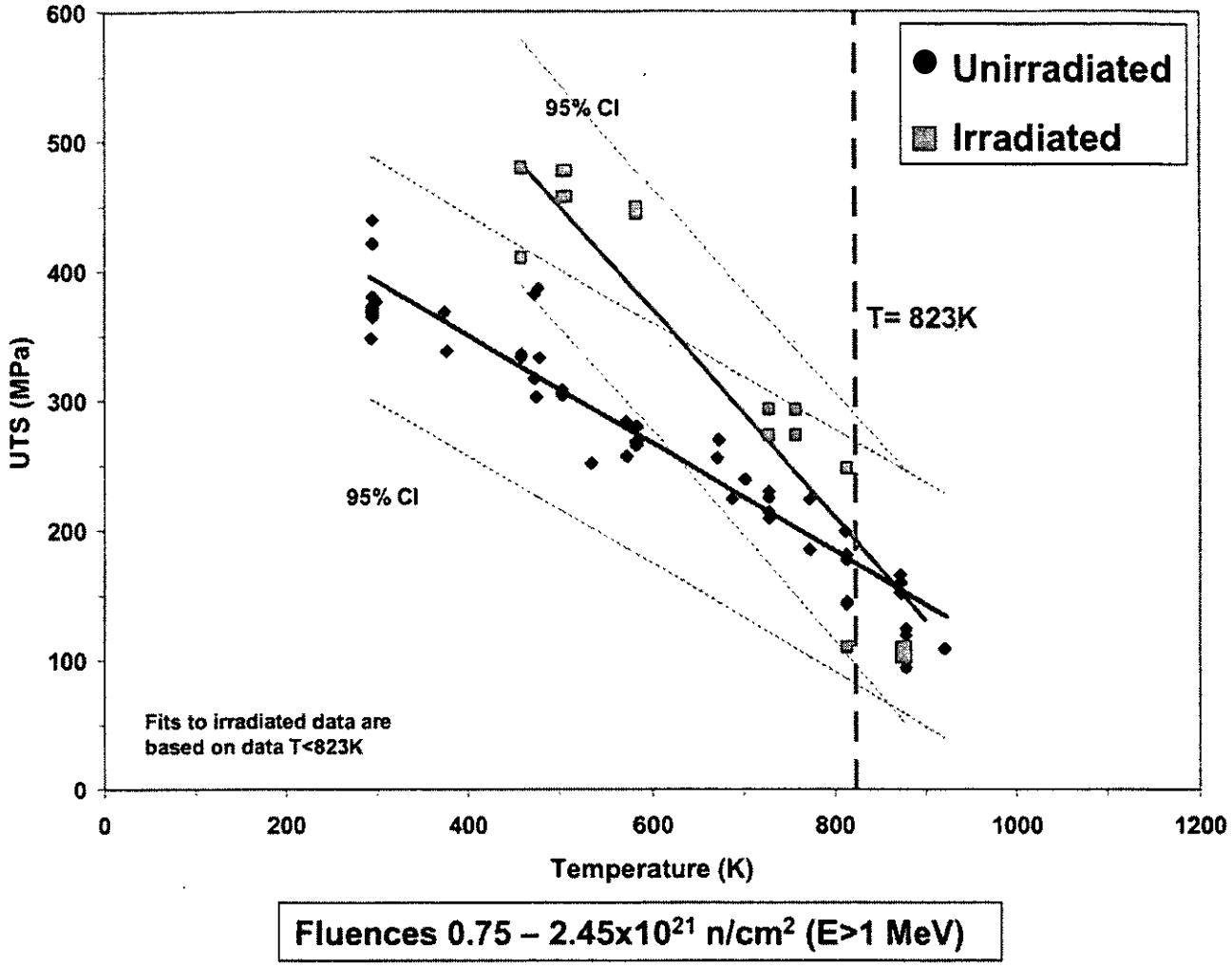

Figure 1.1.9: Irradiated and Unirradiated Ultimate Tensile Strength of VHP Be

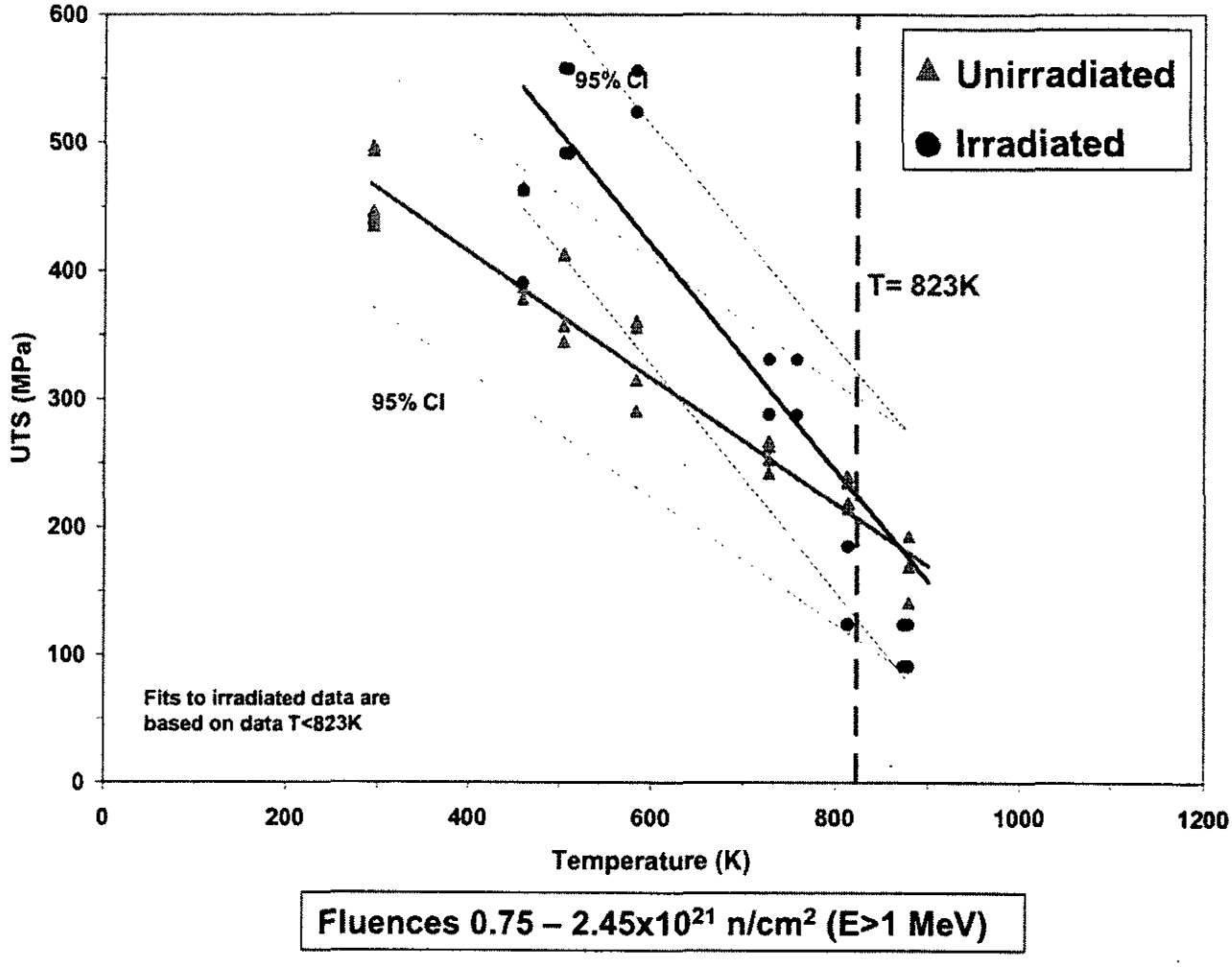

Figure 1.1.10: Irradiated and Unirradiated Ultimate Tensile Strength of HIP Be

1.1.11 Poisson's Ratio

Dombrowski (Reference 1.1.c) gives a table (Table 1.1.6) of room temperature data for Poisson's ratio of Brush Wellman Be grade S-200F. Note, scatter in the data is possibly attributed to the low value of the measurements. Because Be grades S-200F and S-65 are similarly processed, these results should be similar for S-65 grade Be.

Table 1.1.6: Poisson Ratio Data for S-200F Be

Orientation	Stress Axis	Direction of Orthogonal Strain	Poisson's Ratio
LC	Longitudinal	Circumferential	0.102 0.064 0.072
LR	Longitudinal	Radial	0.102 0.080 0.105

Orientation	Stress Axis	Direction of Orthogonal Strain	Poisson's Ratio
TL	Transverse	Longitudinal	0.069 0.071 0.108
TR	Transverse	Radial	0.102 0.058 0.066

Scaffidi-Argentina (Reference 1.1.b) reported that Poisson's ratio ranges between 0.01 – 0.13 (0.07 +/- 0.06) while Billone (Reference 1.1.h) reported Poisson's ratio at room temperature to be 0.08 +/- 0.02. Reference 1.1.a also reported that Poisson's ratio is generally independent of temperature, grain size, porosity and radiation damage. Additional data on S-65 grade Be may be required to validate these assumptions.

1.1.12 Irradiation Swelling

As described by Scaffidi-Argentina and Gelles (References 1.1.b and 1.1.n), damage due to irradiation in Be occurs primarily from fast neutron transmutation reactions resulting in the formation of helium (He) and tritium (^{3}H) via the following reactions:

$$^9Be + n \rightarrow {}^8Be + 2n \text{ (threshold energy 2.7 MeV)}$$

$$^8Be \rightarrow 2\ {}^4He$$

$$^9Be + n \rightarrow {}^6He + {}^4He \text{ (threshold energy 1.4MeV)}$$

$$^6He \rightarrow {}^6Li$$

$$^6Li + n \rightarrow {}^4He + {}^3H \text{ (primarily thermal neutrons)}$$

Swelling is considered an important irradiation effect. The He formed by the transmutation reactions is responsible for swelling at high fluences and high temperatures. Gelles (Reference 1.1.n) determined that minimum swelling at high temperatures occurred in Be grades with the smallest grain size and highest BeO content. Helium migration and the formation of large helium bubbles are limited by the large quantity of small BeO particles. The swelling of Be was also examined by Dalle Donne (Reference 1.1.o) in an attempt to characterize the behavior of the material in solid breeder blanket applications. It was established by Scaffidi-Argentina (Reference 1.1.b) that swelling generated from a given gas concentration was dependent on the He bubble size and therefore dependent upon the bubble density. Dalle Donne (Reference 1.1.o), using this and other constitutive relationships for Be (surface tension, grain boundary energy, self-diffusion, He diffusion, vapor pressure etc.) created the computer code ANFIBE (Analysis of Fusion Irradiated Beryllium). The ANFIBE code accounts for the important mechanistic processes that affect the gas generation and swelling behavior in Be.

Reference 1.1.o illustrates how the ANFIBE code has shown agreement with a variety of experimental data. Experimental data ranges from 2.1-50 x 10^{21} n/cm^2 (E>1MeV) from 300-973K. Experimental data was obtained from S-65 and S-200F beryllium irradiated in the EBR-II (fast reactor), BR2 (fast reactor) and the ATR (PWR reactor). Swelling predictions from the ANFIBE model were reported by Dalle Donne to fluences of 25x10^{21} n/cm^2 (E>1MeV) and temperatures of 973K. Dalle Donne (Reference 1.1.o) presented a comparison of the ANFIBE calculated swelling versus experimental

swelling shown for a range of data (Figure 1.1.11). Additionally, the ANFIBE predictions for swelling at 0.5-10 x 10^{21} n/cm^2 (E>1MeV) over the temperature range of 273-973K are shown in Figure 1.1.12.

Efforts continue to develop the ANFIBE code, providing greater capability and confidence in the model (References 1.1.b and 1.1.p). While much of the data used in validating the code is for higher fluences at lower temperatures or lower fluences at higher temperatures, the model is expected to yield reasonable predictions at higher temperatures and higher fluences.

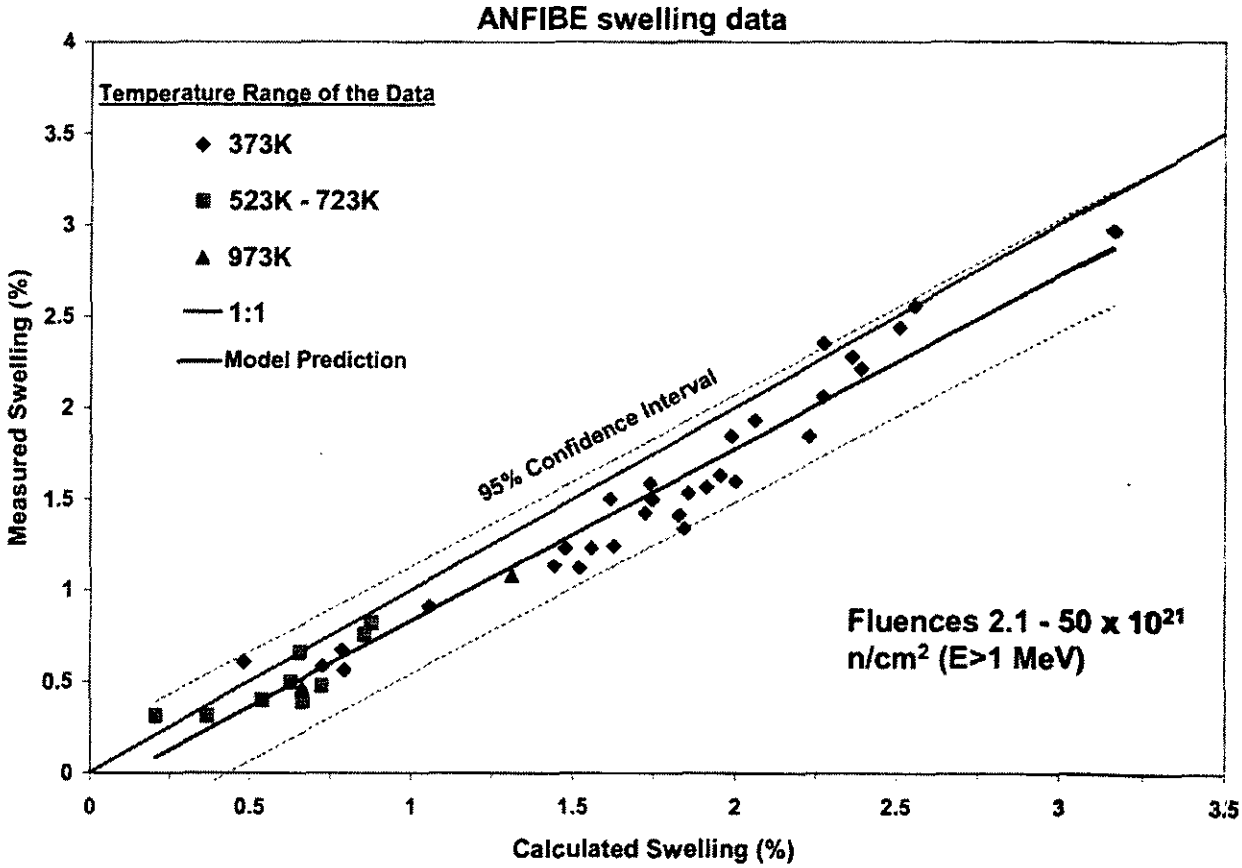

Figure 1.1.11: Measured Be Swelling Data Versus the ANFIBE Calculated Swelling

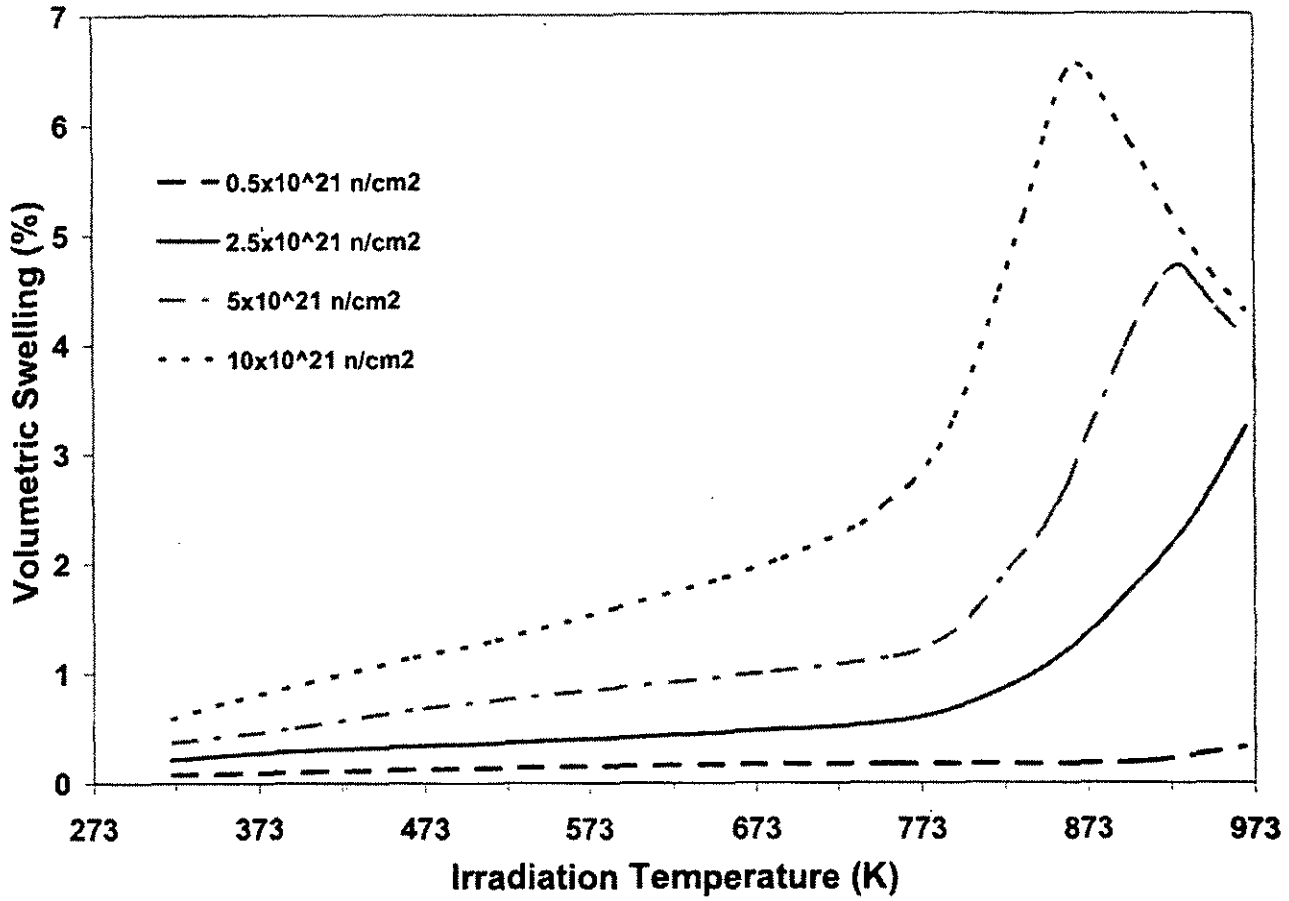

Figure 1.1.12: Predicted Be Swelling Based on ANFIBE Code

1.1.13 References

1.1.a J. Neter, M. H. Kutner, C. J. Nachtsheim and W. Wasserman, *Applied Linear Statistical Models* 4th ed., McGraw-Hill (1996).

1.1.b F. Scaffidi-Argentina, G. R. Longhurst, V. Shestakov and H. Kawamura, "Beryllium R&D for fusion applications", *Fusion Eng. and Design*, **51-52** (2000) 23-41.

1.1.c D. E. Dombrowski, E. Deksnis and M. A. Pick, "Thermomechanical Properties of Beryllium", Brush Wellman Report TR-1182, February 20, 1995.

1.1.d SCK CEN Progress report FT/Mol/96-03 ITER Task 23 "Beryllium Characterization: Tensile tests on neutron irradiated and reference beryllium", F. Moons, February 1996.

1.1.e B. S. Hickman, "Radiation Effects in Beryllium and Beryllium Oxide", *Studies in Radiation Effects, Series A Physical and Chemical Vol. 1*, 1966.

1.1.f Brush Wellman specification, S-65 Structural Grade Beryllium Block, Rev C, July 1, 1987.

1.1.g J. M. Beeston, "Beryllium metal as a neutron moderator and reflector material", *Nuclear Eng. and Design*, **14** (1970) 445-474.

1.1.h M. C. Billone, "Recommended design correlations for S-65 beryllium", Proceedings 2nd IEA International Workshop on Beryllium Technology for Fusion, September 6-8, 1995 pp. 348 – 363.

1.1.i L. L. Snead, "Low-temperature low-dose irradiation effects on beryllium", *J. Nucl. Mat.*, **326** (2004) 114-124.

1.1.j V. Barabash, G. Federici, M. Rödig, L. L. Snead and C. H. Wu, "Neutron irradiation effects on plasma facing materials", *J. Nucl. Mat.*, **283-287** (2000) 138-146.

1.1.k M. F. Smith, R. D. Watson, J. B. Whitley and J. M. McDonald, "Thermomechanical testing of beryllium for limiters in ISX-B and JET", *Fusion Technology*, **8** (1985) 1174-1183.

1.1.l S. H. Goods and D. E. Dombrowski. 1997. "Mechanical properties of S-65C grade beryllium at elevated temperatures", Proceedings of the 3rd IEA International Workshop on Beryllium Technology for Fusion, Mito City, Japan, 22-24 October.

1.1.m R. Chaouadi, F. Moons and J. L. Puzzolante. 1997. "Tensile and fracture toughness test results of neutron irradiated beryllium", Proceedings of the 3rd IEA International Workshop on Beryllium Technology for Fusion, Mito City, Japan, 22-24 October.

1.1.n D. S. Gelles, G. A. Sernyaev, M. Dalle Donne and H. Kawamura, "Radiation effects in beryllium used for plasma protection", *J. Nucl. Mat.*, **212-215** (1994) 29-38.

1.1.o M. Dalle Donne, F. Scaffidi-Argentina, C. Ferrero and C. Ronchi, "Modeling of swelling and tritium release in irradiated beryllium", *J. Nucl. Mat.*, **212-215** (1994) 954-960.

1.1.p E. Rabaglino, C. Ferrero, J. Reimann, C. Ronchi and T. Schulenberg, "Study of the microstructure of neutron irradiated beryllium for the validation of the ANFIBE code", *Fusion Eng. and Design*, **61-62** (2002) 769-773.

1.2 Beryllium Oxide (BeO)

1.2.1 Composition

Table 1.2.1 gives a typical composition of Thermalox 995 BeO (Brush Ceramic Products Reference 1.2.a).

Table 1.2.1: Composition of Thermalox 995 BeO

Thermalox 995 BeO	
Element (max unless otherwise stated)	**wt%**
BeO (min %)	99.5
Al	0.035
Cr	0.0015
Ca	0.015
Fe	0.015
Mg	0.13
Ni	0.0015
Si	0.25
Na	0.015
Zn	0.002

Si and Mg are added to the Thermalox 995 as sintering aids.

1.2.2 Melting Temperature and Maximum Use Temperature

The melting temperature of beryllium oxide is (Reference 1.2.b):

$$T_{melt} = 2843 \pm 30K$$

A practical maximum use temperature (unirradiated) is approximately 2300K (Reference 1.2.b). Irradiation may affect other properties (thermal conductivity and compressive strength) and lower this maximum use temperature.

1.2.3 Density

Busboom (Reference 1.2.b) reported the room temperature (298K), theoretical density of BeO is 3.010 g/cm^3. The actual BeO density is calculated by:

$$\rho_{actual} = TD \cdot (1 - P)$$

where
TD = theoretical density
P = volume fraction porosity

1.2.4 Thermal Conductivity

1.2.4.1 Unirradiated

Data given from Reference 1.2.c for the temperature range 273K ≤T ≤2300K is shown in Figure 1.2.1. The following equation is for the unirradiated thermal conductivity of BeO. This equation is based on data from various grades of BeO with densities varying from 2.60 – 2.97 g/cm^3 (86 – 99% TD). From Figure 1.2.1 it is observed that there is some slight dependence of thermal conductivity on porosity. Generally in ceramics, increasing the porosity decreases the thermal conductivity (Reference 1.2.d). The effect of porosity is not accounted for in the following equation.

$$k = 8.31 x 10^5 \cdot T^{-1.42}$$

where
k = thermal conductivity, W/m-K
T = temperature, K

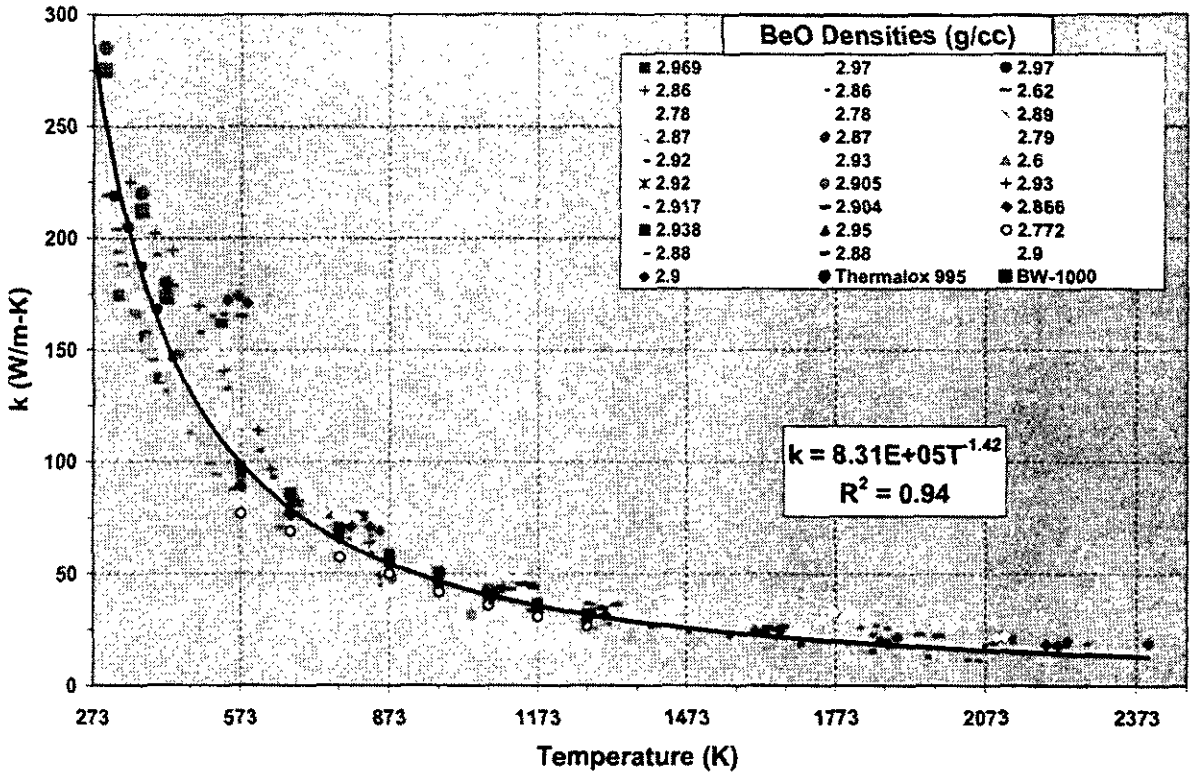

Figure 1.2.1: Thermal Conductivity of BeO

1.2.4.2 Irradiated

Low temperature (350 – 373K) thermal conductivity studies by Pryor (Reference 1.2.e) reported a reduction in BeO thermal conductivity at doses as low as $2x10^{18}$ n/cm^2 (E>1MeV). Pryor (Reference 1.2.e) found large reductions in thermal conductivity as dose increased. The thermal conductivity decreased as the dose increased up to the highest dose evaluated, $0.2x10^{21}$ n/cm^2 (E>1MeV). Measurements at higher doses were not performed due to microcracking in the material, which is expected to affect thermal conductivity (see swelling discussion). Hickman (Reference 1.2.f) estimated values of thermal conductivity at elevated temperatures based on the low temperature data. Predictions indicated that as irradiation temperature increased the degradation in thermal conductivity may be minimal in the vicinity of 1073K. More data is required to validate the predictions from Reference 1.2.f on currently available grades of BeO at higher temperatures and fluences.

Snead (Reference 1.2.g) reported effects of neutron irradiation at 333K on the thermal conductivity of currently available Brush Wellman Thermalox 995 grade BeO. Minimal changes in thermal conductivity were observed at fluences of $1x10^{18}$ n/cm^2 (E>0.1MeV).

Touloukian (Reference 1.2.c) provided limited irradiation data for BeO irradiated at $8.6x10^{18}$, $2x10^{20}$ and $3.7x10^{20}$ n/cm^2 (E>1MeV) over the narrow temperature range of 330 – 560K. Figure 1.2.2 illustrates the degradation in the thermal conductivity of BeO, similar to the trends in Reference 1.2.f.

Due to limited thermal conductivity data for currently available grades of BeO irradiated at high temperatures and high fluence, irradiation testing of BeO was planned in the JOYO fast reactor to characterize the material.

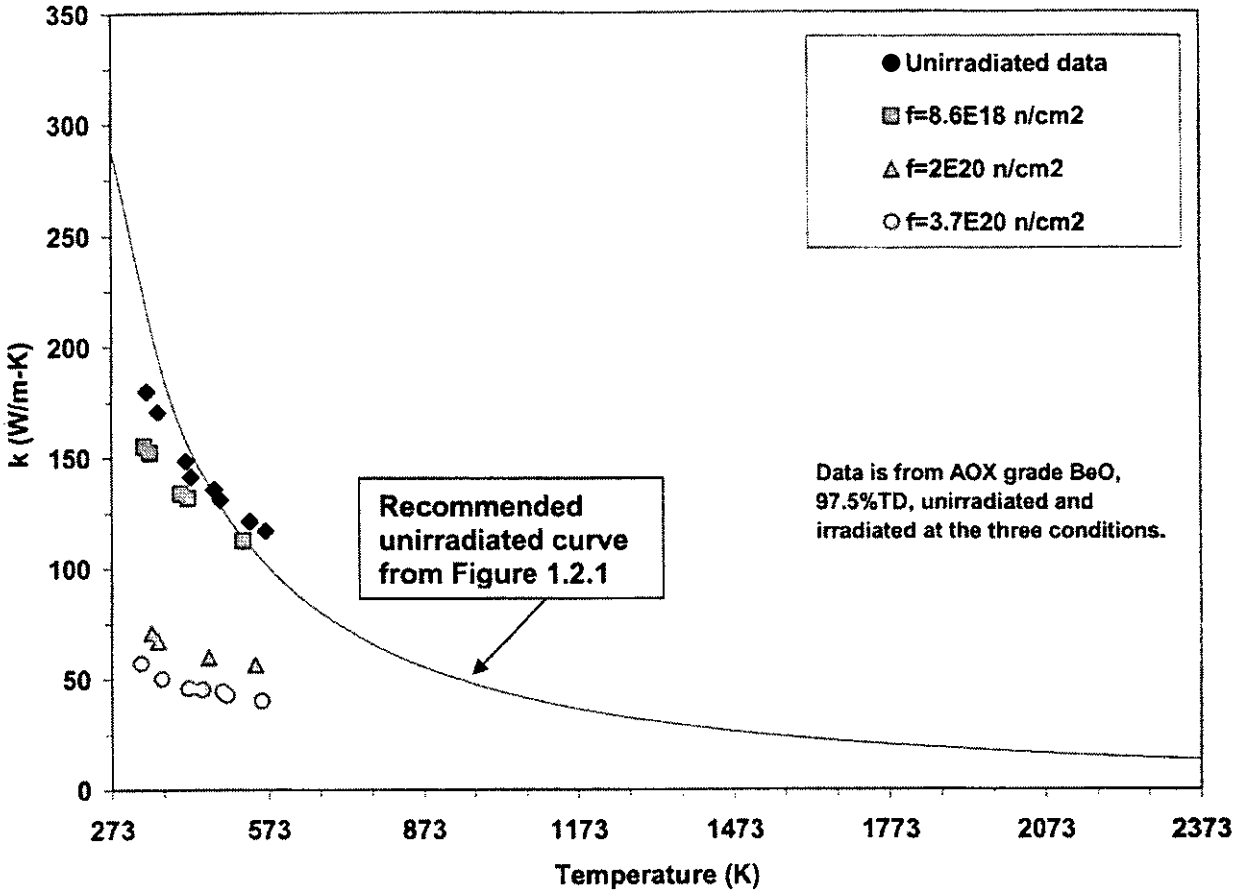

Figure 1.2.2: Irradiated Thermal Conductivity of BeO Compared to Curve Fit in Figure 1.2.1

1.2.5 Thermal Expansion

1.2.5.1 Unirradiated Linear Expansion

Data compiled by Touloukian (Reference 1.2.h) over the temperature range 293K ≤T ≤2300K is shown in Figure 1.2.3. From the data it is observed that there is no correlation between changes in the density of BeO and linear expansion (Figure 1.2.3). The unirradiated percent change in length ($\Delta L/L_0$) is given by the following equation. This equation is based on data from various grades of BeO with densities varying from 2.68 – 2.99 g/cm^3.

$$\frac{\Delta L}{L_0} = 1.69x10^{-7} \cdot T^2 + 6.65x10^{-4} \cdot T - 0.229$$

where
$\Delta L/L_0$ = change in length from 293K, percent
T = temperature, K

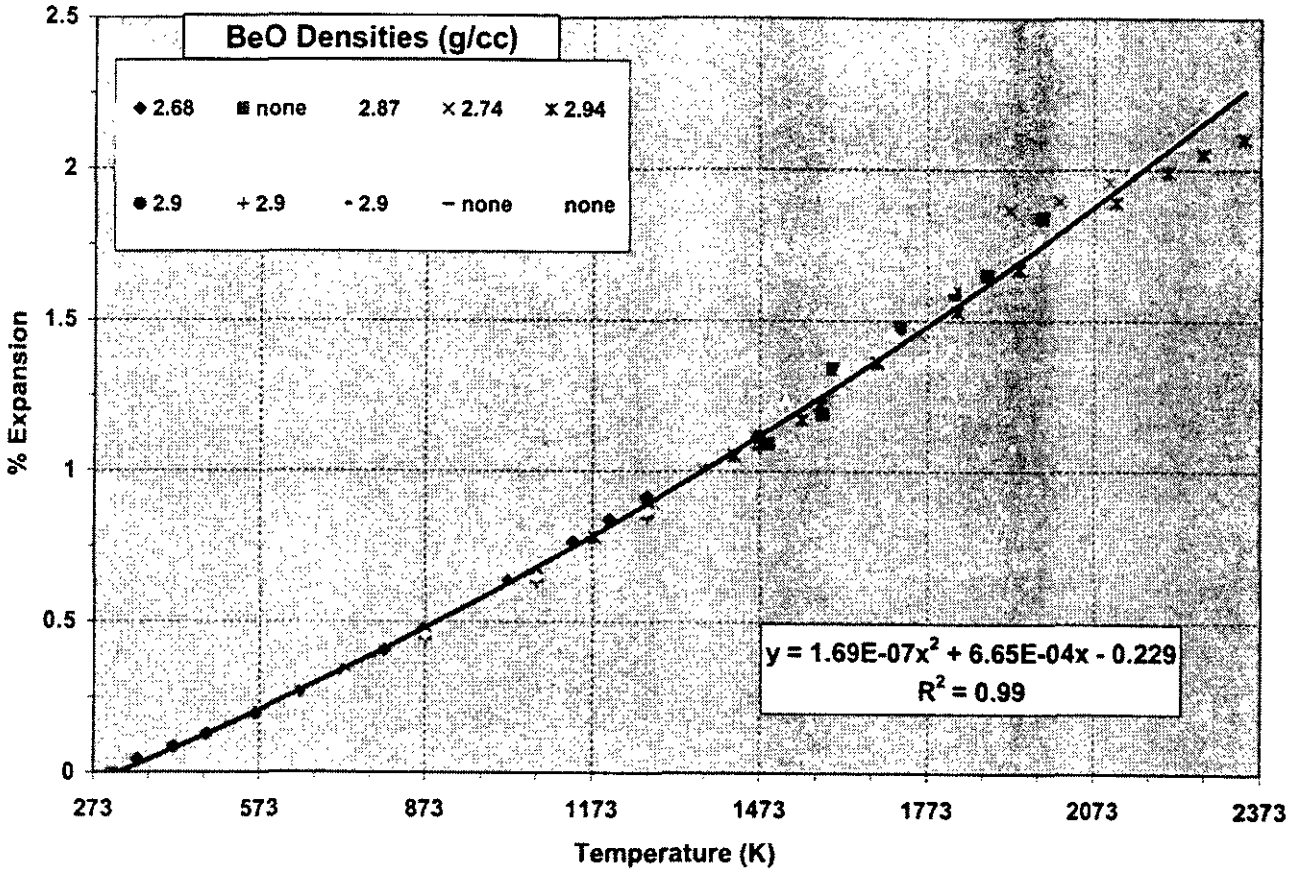

Figure 1.2.3: Linear Expansion of BeO

1.2.5.2 Unirradiated Instantaneous Coefficient of Thermal Expansion (CTE)

From Reference 1.2.b for the temperature range 293K ≤T ≤2300K the unirradiated instantaneous coefficient of thermal expansion (α_i) is given by:

$$\alpha_i = 4.433x10^{-6} + 6.552x10^{-9} \cdot T - 8.262x10^{-13} \cdot T^2$$

where
α_i = instantaneous linear coefficient of thermal expansion, K^{-1}
T = temperature, K

1.2.5.3 Unirradiated Mean Coefficient of Thermal Expansion (CTE)

The definition of mean coefficient of thermal expansion (α_m) is given by:

$$\alpha_m = \frac{\left(\frac{\Delta L}{L_0}\right)}{100 \cdot (T - T_{ref})}$$

where
α_m = mean linear coefficient of thermal expansion, K^{-1}

$\Delta L/L_0$ = change in length, percent (section 1.2.5.1)
T = temperature, K
T_{ref} = average reference temperature

Data from Touloukian (Reference 1.2.h) for the linear expansion ($\Delta L/L_0$) of BeO was used to determine the mean coefficient of thermal expansion over the temperature range 353K ≤T ≤2300K. Because the reference temperature (T_{ref}) varied for different data sets, an average value was used for the reference temperature (299 K). The change in slope of the mean CTE curve, shown in Figure 1.2.4, around 473K appears reasonable based on the single data point at 299 K [curve 53, Reference 1.2.h]. The reference temperature used to calculate the mean CTE of the curve 53 point is 79 K.

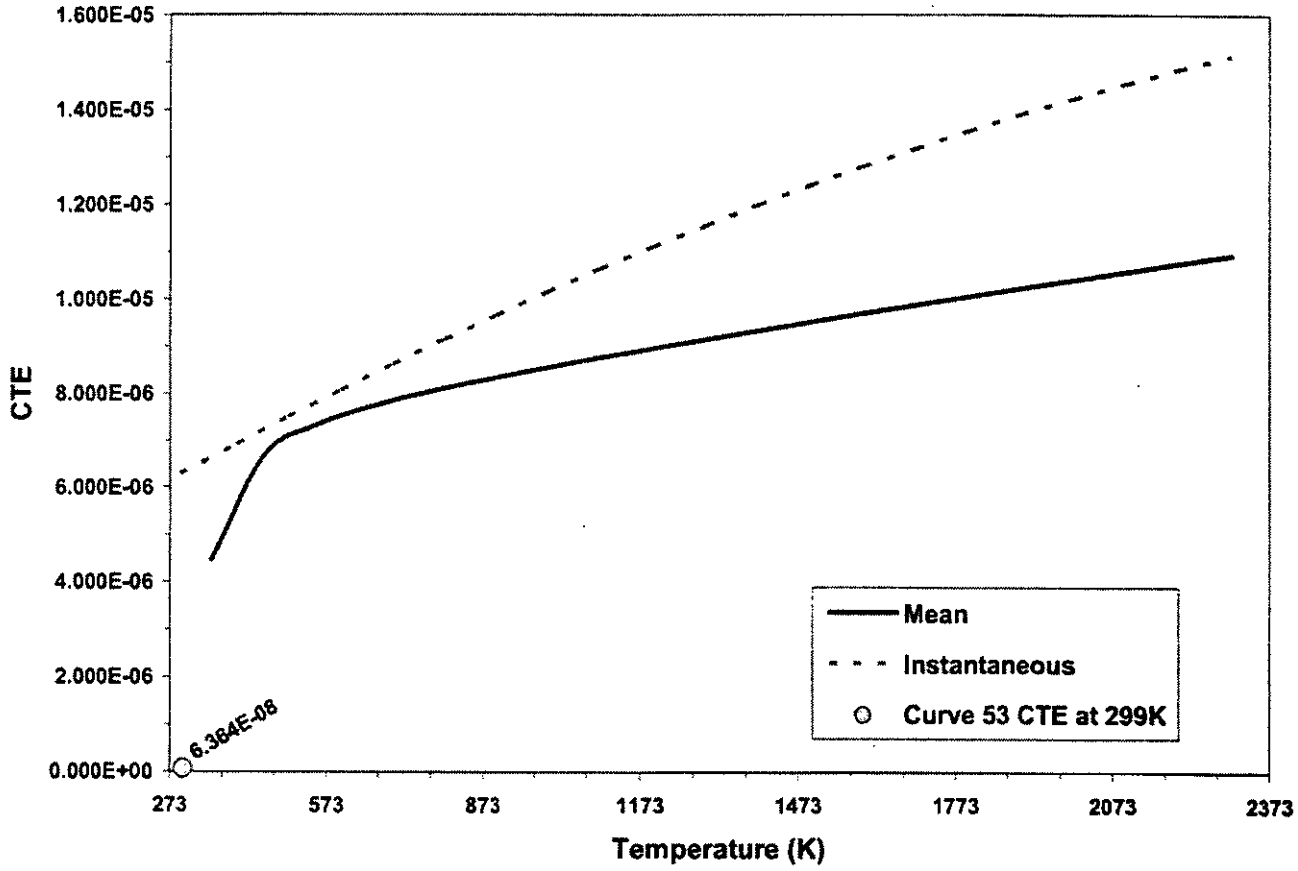

Figure 1.2.4: Mean and Instantaneous Coefficient of Thermal Expansion of BeO

The recommended equation over the range 353K ≤T ≤2300K for the mean CTE of BeO is given by:

$$\alpha_{mean} = \frac{\left(1.69x10^{-7} \cdot T^2 + 6.65x10^{-4} \cdot T - 0.229\right)}{100 \cdot \left(T - 299\right)}$$

where
α_{mean} = mean coefficient of thermal expansion
T = temperature, K

1.2.5.4 Irradiated

It is expected that the coefficient of thermal expansion is not affected by irradiation. Collins (Reference 1.2.i) reported no change (+/-5%) in the coefficient of thermal expansion for BeO irradiated at 373K. Additionally, Walker (Reference 1.2.j) reported no change (+/- 0.02%) in the coefficient of thermal expansion of BeO irradiated to 0.65×10^{21} n/cm^2 (E>1MeV) at 923 – 963K.

1.2.6 Specific Heat

1.2.6.1 Unirradiated

From Reference 1.2.k (Table 1.2.2 and Figure 1.2.5) for the temperature range 298K ≤T ≤2820K the unirradiated specific heat of BeO is given by the following equation:

$$C_p = 3.61x10^{-7} \cdot T^3 - 1.69x10^{-3} \cdot T^2 + 2.87 \cdot T + 418$$

where
C_p = specific heat, J/kg-K
T = temperature, K

Table 1.2.2: Data Reported in Figure 1.2.5 for Specific Heat of BeO

Curve Number	Specifications and Remarks
2	99.9 BeO, with impurities of Al, Ni, Cu, Zn, Ag, Fe and Ti; pressed and sintered at 1673 – 2073K.
3	No description of sample given.
4	99.96 BeO, 0.01 Si, 0.007 Al, 0.002 Na, 0.001 Cs, 0.001 Fe, <0.001 Ca, <0.001 Cu, <0.00005 Li, <0.00005 Mg; supplied by Norton Co.; pressed, fired at 2073K and sintered.
5	99.5 BeO, 0.0090 si, 0.0050 Al, 0.0020 Mo, 0.0010 Ca, 0.0010 Cr, 0.0010 Fe, 0.0010 Na, 0.0010 Ni, 0.0003 Mn, <0.0001 B, Cd, Li, <0.0001 Co, Cu; supplied by Brush Beryllium Co.; cold pressed; density 2.87 g/cm^3.
6	Sample supplied by Zirconium Corp. of America; crushed in hardened steel mortar to pass 100-mesh screen; pressed and sintered; density at 298K before exposure: apparent density (ASTM method B311-58) 2.93 g/cm^3, true density (by immersion in xylene) 3.00 g/cm^3.

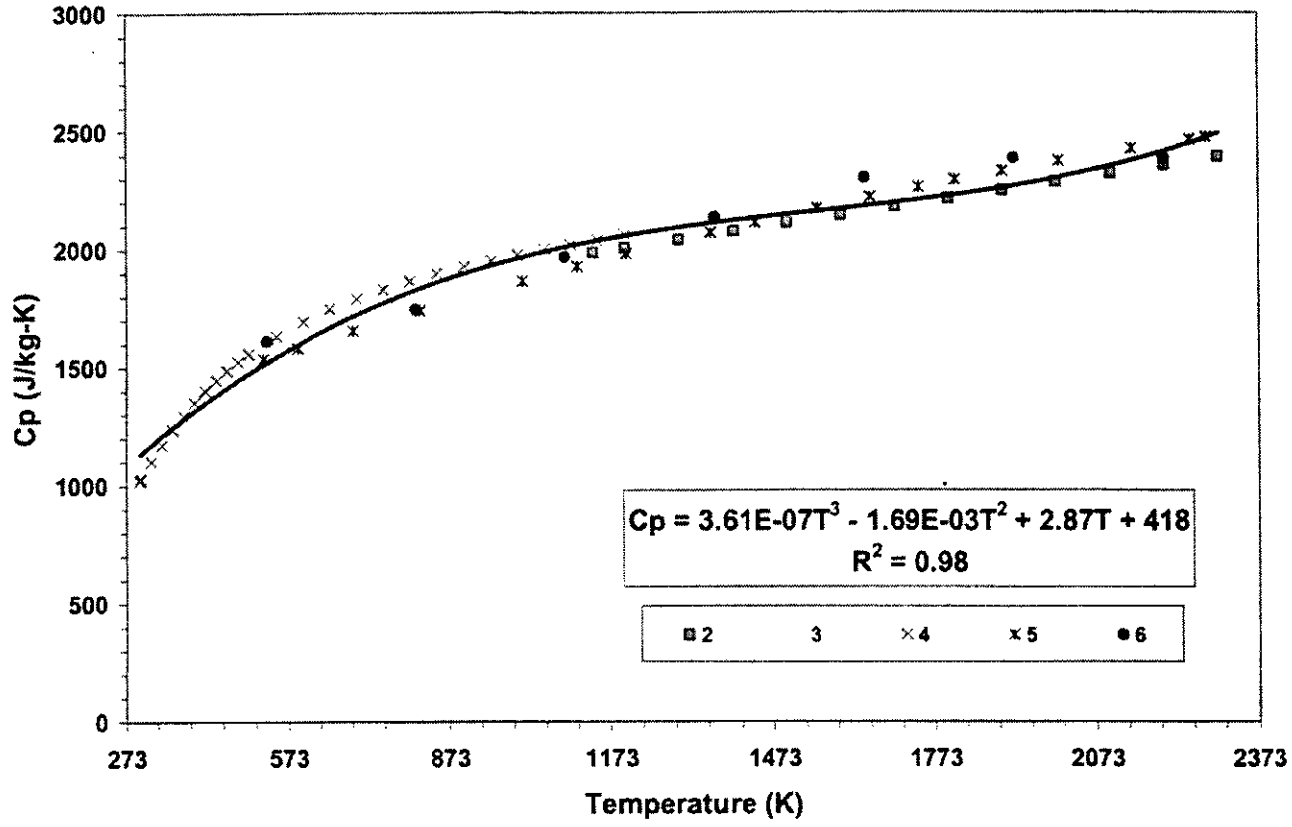

Figure 1.2.5: Specific Heat of BeO

1.2.6.2 Irradiated

Hickman (Reference 1.2.l) reported no measurable change in enthalpy of irradiated BeO at 573K, 873K and 1173K after removing the effects due to stored energy. Measurements of stored energy in irradiated BeO samples indicate a significant amount of energy is stored at high fluences. However, the stored energy has minimal effects on the specific heat of irradiated BeO at or below the irradiation temperature.

1.2.7 Modulus of Elasticity

1.2.7.1 Unirradiated

From Reference 1.2.b the elastic modulus (Figure 1.2.6) is given over two temperature ranges with porosity ranging from 0 – 30% for BeO by the following:

For 298K < T < 800K

$$E = 344.7 - 805.7 \cdot P$$

For 800K < T < 1500K

$$E = \left(344.7 - 805.7 \cdot P\right) \cdot \left(1.31 - 1.75x10^{-3} \cdot T + 2.82x10^{-6} \cdot T^2 - 1.39x10^{-9} \cdot T^3\right)$$

where
E = modulus of elasticity, GPa

P = volume fraction porosity, 0 < P < 0.3
T = temperature, K

T (K)	E (GPa)
300	304.4
400	304.4
500	304.4
600	304.4
700	304.4
800	304.4
801	304.4
805	304.5
850	305.2
900	305.0
1000	299.8
1100	286.4
1200	262.2
1300	224.7
1400	171.3
1500	99.43

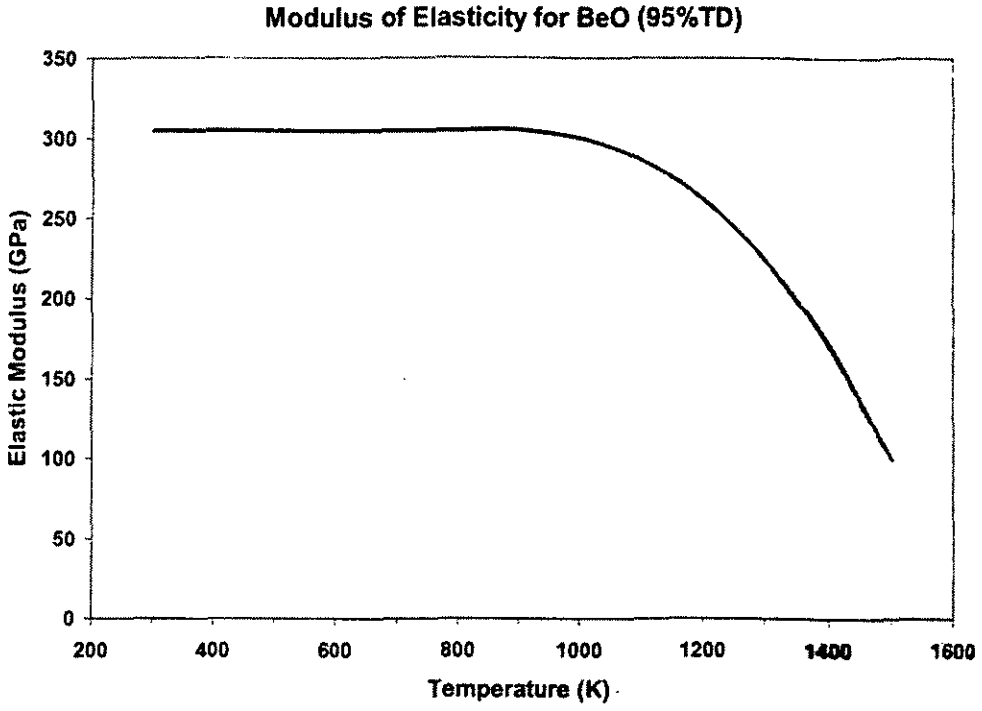

Figure 1.2.6: Elastic Modulus of 95% Theoretical Density BeO with Data Table Included

1.2.7.2 Irradiated

The modulus of elasticity remains independent of irradiation effects. Using resonance frequency methods, Collins (Reference 1.2.i) reported a small decrease in the elastic modulus of BeO as a function of irradiation dose, which is consistent with the decrease in density to the point at which microcracking occurred. The elastic modulus of samples that experienced microcracking could not be determined. Generally, variations in the elastic modulus are related to temperature as shown in section 1.2.7.1.

1.2.8 Compressive Strength

1.2.8.1 Unirradiated

From Reference 1.2.b (Figure 1.2.7) the compressive strength for BeO over the temperature range 293K ≤T ≤1500K and porosity range of 0 – 30% is given by the following:

$$C = (1585 - 3273 \cdot P) \cdot (1.232 - 8.284x10^{-4} \cdot T + 1.142x10^{-7} \cdot T^2)$$

where
C = compressive strength, MPa
P = volume fraction porosity, 0 < P < 0.3

T = temperature, K

T (K)	CS (MPa)
293	1420
400	1306
500	1203
600	1103
700	1006
800	913
900	823
1000	736
1100	652
1200	572
1300	495
1400	421
1500	350

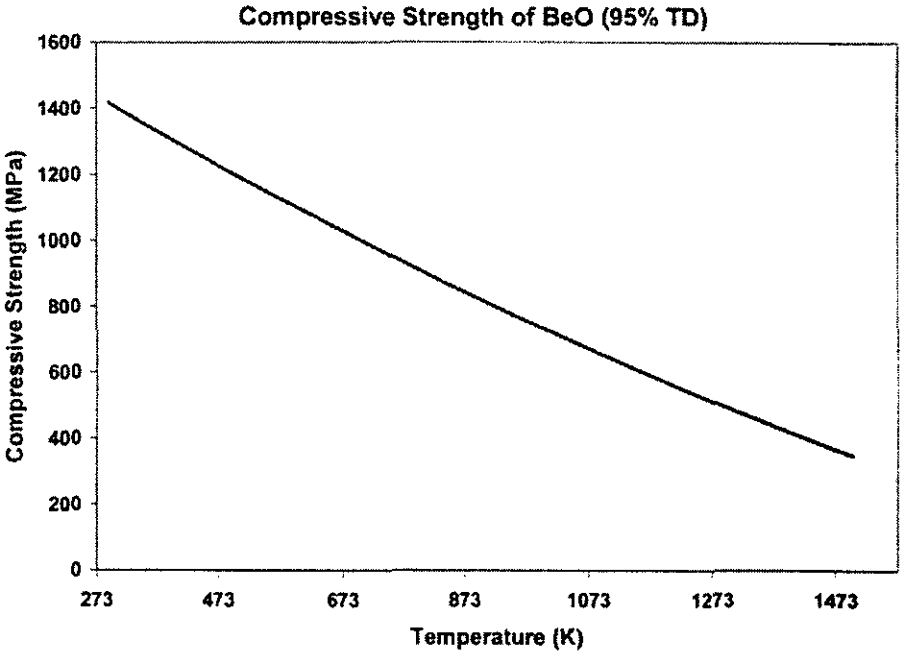

Figure 1.2.7: Compressive Strength of 95% Theoretical Density BeO with Data Table Included

1.2.8.2 Irradiated

There is limited data on irradiated compressive strength of BeO. Elston and Labbe (Reference 1.2.m) reported the compressive strength of BeO irradiated at 373K. Measurements were performed at T< 373K and T< 673K. This reference shows that the strength dramatically decreases at doses above $6x10^{19}$ n/cm^2 (E>1 MeV). Note that the material tested had an average grain size of 50 – 100 microns; therefore significant microcracking from irradiation likely occurred (see swelling).

Due to limited compressive strength data for currently available grades of BeO irradiated at high temperatures and high fluence, irradiation testing of BeO was planned in the JOYO fast reactor to characterize the material.

1.2.9 Tensile Yield Strength

The compressive strength of BeO is given above in section 1.2.8. There is limited data on the tensile properties of BeO due to the brittle nature of ceramics.

1.2.10 Emissivity

From Reference 1.2.b the emissivity is given over three temperature ranges for BeO by the following equations. These equations fit the data presented by Touloukian (Reference 1.2.n) as shown in Figure 1.2.8.

For 300K < T < 800K
$\varepsilon = 0.2$

For 800K < T < 2200K

$$\varepsilon = -0.235 + 6.65x10^{-4} \cdot T - 1.51x10^{-7} \cdot T^2$$

For 2200 < T
$\varepsilon = 0.5$

where
ϵ = emissivity
T = temperature, K

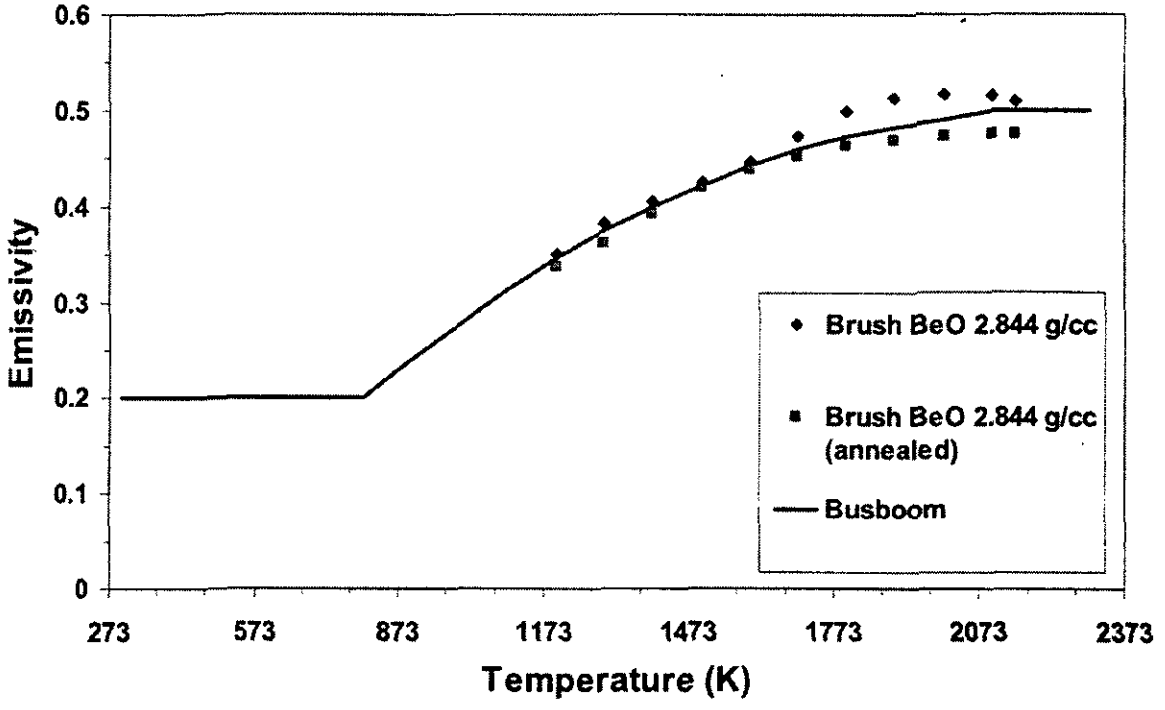

Figure 1.2.8: Emissivity of BeO

1.2.11 Ultimate Tensile Strength

The compressive strength of BeO is given above in section 1.2.8. There is limited data on the tensile properties of BeO due to the brittle nature of ceramics.

1.2.12 Poisson's Ratio

From Reference 1.2.b the best estimate for Poisson's ratio is 0.3 for 298K to 1400K. It is expected that Poisson's ratio for BeO will remain independent of irradiation effects, similar to the elastic modulus.

1.2.13 Irradiation Swelling

Several factors are believed to influence the swelling behavior of BeO exposed to neutron irradiation, primarily grain size, temperature, fluence, flux and density. Plumlee (Reference 1.2.o) reported expressions based on lattice defects ($\Delta V/V_D$), microcracking ($\Delta V/V_{MC}$) and helium bubble formation ($\Delta V/V_{He}$) to predict the swelling of BeO. The grain size, temperature, fluence, flux and density affect these swelling mechanisms and are summarized in the table below. It should be noted that these

equations have been developed with relatively limited data, flux range (0.65 – 3.2x10^{14} n/cm^2-s) (E>1MeV) and fine grain size (5 – 20 microns) BeO.

$$\frac{\Delta V}{V_{total}} = \frac{\Delta V}{V_D} + \frac{\Delta V}{V_{MC}} + \frac{\Delta V}{V_{He}}$$

where
$\Delta V/V$ = total volume expansion fraction
$\Delta V/V_D$ = volume expansion fraction due to lattice defect mechanisms
$\Delta V/V_{MC}$ = volume expansion fraction due to microcracking
$\Delta V/V_{He}$ = volume expansion fraction due to helium bubble formation

Collins (Reference 1.2.i) formulated an expression for the volume expansion due to lattice defects ($\Delta V/V_D$). Collins assumed high temperature damage is due to competing processes of annealing and production. Collins accounts for the rate of atomic displacements, K, and annealing effects, A_m and A_i. These annealing constants are proportional to the diffusion rate of defects (interstitials and vacancies). Assuming first order kinetics the following expression describes the volume expansion due to lattice defect mechanisms ($\Delta V/V_D$). At temperature above 1073K, this equation underestimates the volume change $\Delta V/V_D$.

$$\frac{\Delta V}{V_D} = \frac{K}{A_m}(1 - e^{-A_m t}) + \frac{K}{A_i}(1 - e^{-A_i t})$$

where
$K = 3.3x10^{-23} \cdot F$
F = neutron flux, n/cm^2-s (E>1MeV)
$A_m = 6.1x10^{-5}\ e^{-10300/RT}$
$A_i = 0.113e^{-22100/RT}$
R = gas constant = 1.987 cal/mol-K
T = temperature, K
t = time, sec

Based on Reference 1.2.b and 1.2.o, the predicted volume expansion due to microcracking, $\Delta V/V_{MC}$ (grain boundary separation), is described by the following equation when $\Delta V/V_D \geq \Delta V/V_{threshold}$. This equation accounts for the fact that microcracking does not initiate until $\Delta V/V_D \geq \Delta V/V_{threshold}$.

$$if\ \frac{\Delta V}{V_D} < \frac{\Delta V}{V_{threshold}} \qquad then\ \frac{\Delta V}{V_{MC}} = 0$$

$$if\ \frac{\Delta V}{V_D} \geq \frac{\Delta V}{V_{threshold}} \qquad then\ \frac{\Delta V}{V_{MC}} = 5.7x10^{-24}(Ft - f)$$

where
$\Delta V/V_{MC}$ = volume expansion due to microcracking
$\Delta V/V_D$ = volume expansion due to lattice defects
$\Delta V/V_{threshold}$ = microcracking threshold
F = neutron flux, n/cm^2-s (E>1MeV)
t = time, sec

f = microcracking fluence threshold where $\Delta V/V_D = \Delta V/V_{threshold}$

For BeO there is a microcracking threshold ($\Delta V/V_{threshold}$) at which microcracking initiates for a given temperature. When the swelling due to lattice defects ($\Delta V/V_D$) is greater than the microcracking threshold ($\Delta V/V_{threshold}$), microcracking initiates and contributes to the total swelling. The following equation for the microcracking threshold illustrates that microcracking is a function of irradiation temperature.

$$\frac{\Delta V}{V_{threshold}} = 2.16x10^{-3} + 6.27x10^{-6} \cdot T$$

where
$\Delta V/V_{threshold}$ = microcracking threshold
T = temperature, K

Plumlee (Reference 1.2.o) states that for the temperature range 373K < T <873K, the volume expansion of BeO should be attributed only to defect growth and microcracking. At T>873K helium bubbles begin to form and become a significant mechanism contributing to swelling in BeO above 1173K. Helium bubbles first form at grain boundaries and later with increasing fluence, bubbles begin to form within the grains. Reference 1.2.o states that He bubble size and density increase with increasing grain size. Helium release from BeO and volume expansion due to He bubbles are difficult to correlate. It was reported in Reference 1.2.o that substantial experimental data will be required for adequate correlation of the volume expansion due to He bubble formation. For the volume expansion due to helium bubble formation ($\Delta V/V_{He}$) the following equation was proposed, accounting for the theoretical density of the BeO. This equation is based on limited data and more effort is required to verify the theory. This equation assumes that the volume expansion due to He bubble formation varies linearly between 86% and 96% theoretical density (Reference 1.2.o).

$$\frac{\Delta V}{V_{He}} = 4.40x10^{-24}(0.036D - 2.456)Ft$$

where
F = neutron flux, n/cm^2-s (E>1MeV)
t = time, sec
D = percent of theoretical density

1.2.13.1 Grain Size Effect on Swelling

Previous irradiation testing results (Reference 1.2.o) have shown that grain size is a key factor influencing swelling; however the functionality is not known. Testing in Reference 1.2.f has focused on BeO with fine grain sizes (~5 microns) and limited testing of materials with grain size up to 100 microns. Plumlee (Reference 1.2.o) demonstrated that larger grain sizes decreased the threshold fluence at which microcracking of BeO occurred near room temperature irradiation. Figure 1.2.9 shows the neutron dose required to produce microcracking during irradiation at 323 – 373K as a function of grain size. Increased microcracking results in increased swelling. It should be noted that this figure is valid only at lower temperatures (~373K).

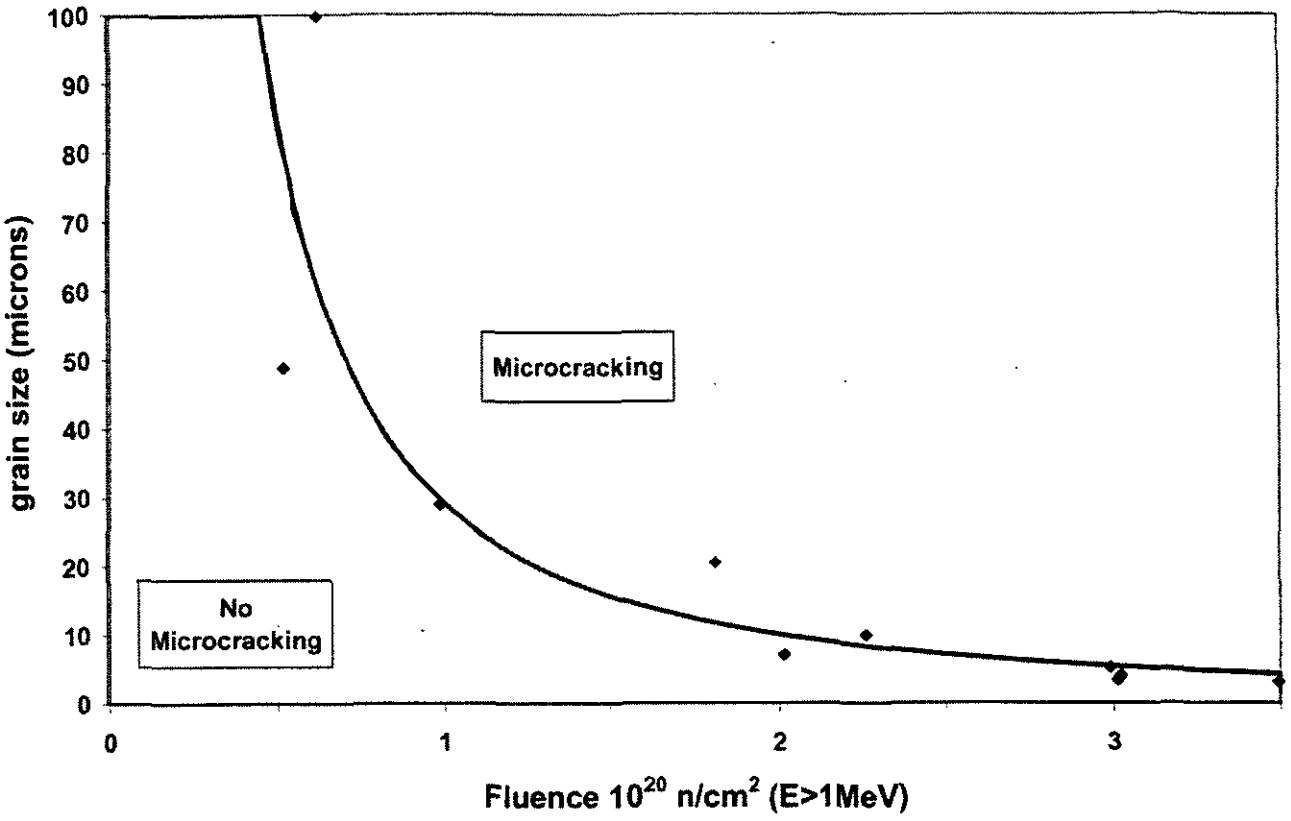

Figure 1.2.9: Neutron Dose Required to Produce Microcracking in BeO

1.2.13.2 Temperature Effect on Swelling

Figure 1.2.10 from Plumlee (Reference 1.2.o) presents data from fine grain size (nominally 5μm, 96%TD) BeO at 373K, 873K and 1273K and the model described in section 1.2.13. It is observed that as the irradiation temperature increases the swelling begins to anneal out of the BeO and the swelling rate decreases. Recall that over the temperature range $373 < T < 873$ the volume expansion of BeO should be attributed to defect growth and microcracking only. At T>873K helium bubbles begin to form and become a significant mechanism contributing to swelling in BeO above 1173K.

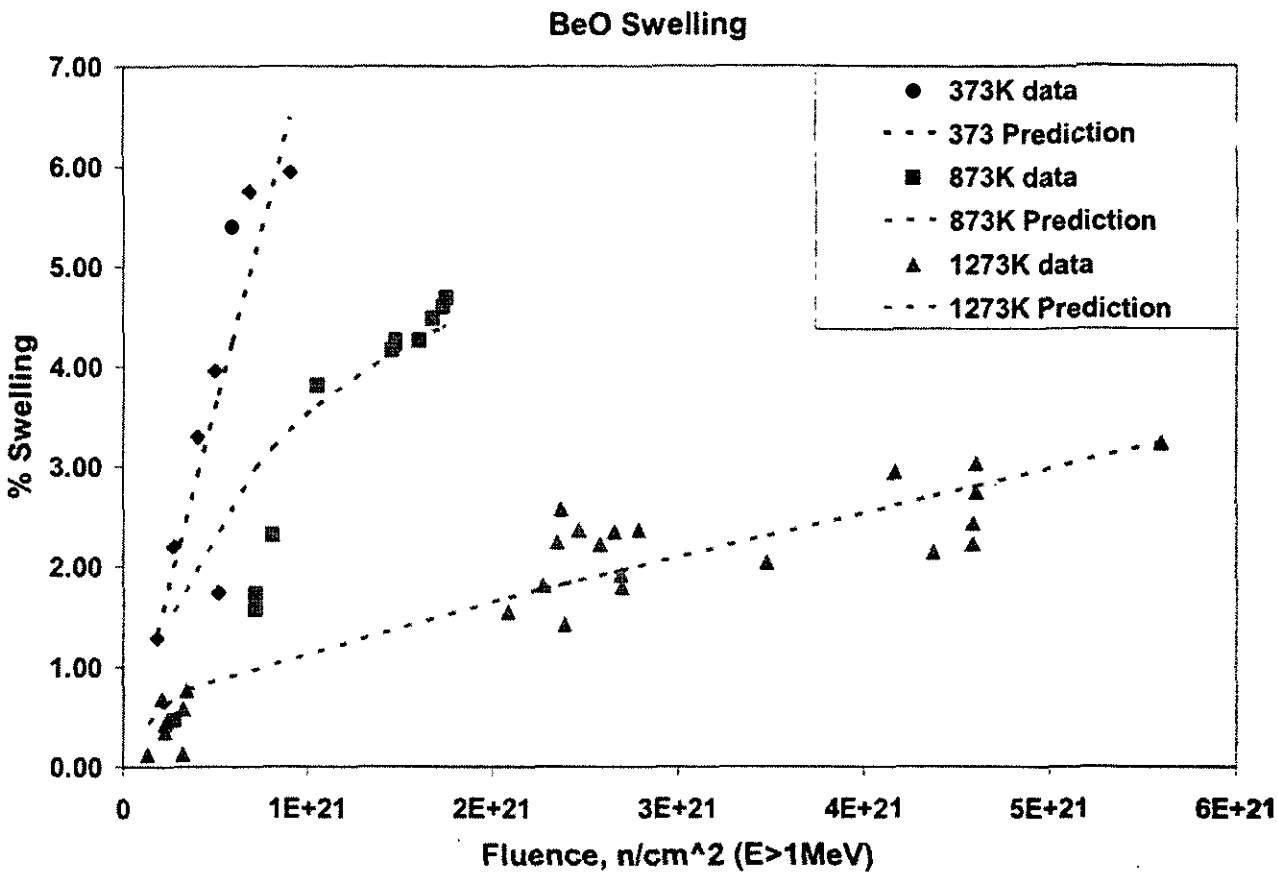

Figure 1.2.10: Irradiation Swelling of BeO with Predicted Curves from Plumlee (Reference 1.2.o)

1.2.13.3 Fluence Effect on Swelling

From Figure 1.2.10 above (section 1.2.13.2), Plumlee (Reference 1.2.o) reports that as the fluence increases, the swelling in BeO also increases. At lower temperatures (T<873K) increased fluence leads to increased anisotropic swelling and microcracking. At higher temperatures (T>873K) the increasing fluence levels, increase the formation of helium. Irradiation testing was proposed to help identify irradiation behavior and performance such as maximum swelling boundaries at each temperature.

1.2.13.4 Flux Effect on Swelling

In the definition of volume expansion due to lattice defects ($\Delta V/V_D$), Collins (Reference 1.2.i) defines the rate of atomic displacements, K, based on lattice expansion data, which increases with flux over a range of ~0.55 – 3.2 x10^{14} n/cm^2-sec (E>1MeV). Therefore, the correlation given for volume expansion due to lattice defects ($\Delta V/V_D$) (section 1.2.13), predicts an increase in swelling with increasing flux at constant fluence. It should be noted that for these correlations the rate of atomic displacements, K, only covers a small experimental range of fluxes. It is not clear if the correlation is valid over a broader range than initially defined. Additionally, the extent to which flux affects swelling at constant fluence, needs to be confirmed with experimental data. Data from future BeO irradiation testing is required to refine the correlation and better predict swelling over a larger flux range.

1.2.13.5 Theoretical Density Effect on Swelling

There is some evidence to suggest that density plays a role in determining swelling behavior – perhaps due to increased ability to accommodate helium bubble formation, or an increased ability to release helium outside the BeO volume. Plumlee (Reference 1.2.o) shows that in particular, sub-dense (86% TD) BeO appears to swell less than full dense (95% TD) BeO at higher temperatures (T>1173) and the model by Plumlee overpredicts the swelling. Recall that at T>873K helium bubbles begin to form and become a significant mechanism contributing to swelling in BeO above 1173K. It is expected that for lower temperature applications (T<873K), there may be little advantage to using sub-dense BeO.

1.2.13.6 Swelling Predictions for BeO

Based on the above correlations for the swelling of BeO, swelling values were extrapolated above the known range of temperatures (373K, 873K and 1273K) and fluences (0.37 – $12x10^{21}$ n/cm^2). Predictions assumed the same flux level used in Reference 1.2.o, $2.3x10^{14}$ n/cm^2-s (E>1MeV). Results of these extrapolations yielded results which do not appear to be reasonable based on the limited amount of data. It should be noted that in the literature reviewed, no swelling above ~6% has been observed, however some irradiated samples have disintegrated to powder (Reference 1.2.p). Future testing is required to validate these predictions over a range of fluxes, fluences, temperatures and BeO grain sizes.

Table 1.2.3 summarizes how the various parameters (grain size, temperature, fluence, flux and density) influence the swelling of BeO. References for each parameter are also given.

Table 1.2.3: Key Parameters that Effect Irradiation Swelling of BeO

Parameter	Result	Reference
Increasing Grain Size	Increased Swelling	1.2.f 1.2.i 1.2.o
Increasing Temperature (at fixed fluence)	Decreased Swelling	1.2.f 1.2.i 1.2.o
Increasing Fluence (at fixed temperature)	Increased Swelling	1.2.f 1.2.i 1.2.o
Increasing Flux	Increased Swelling (based on correlation)	1.2.f 1.2.i 1.2.p
Increasing % Theoretical density	Increased Swelling (due to He bubble retention) T>1173K	1.2.o

1.2.14 References

1.2.a K. Harrison. 2005. Brush Ceramic Products, personal communication, 15 April.
1.2.b H. Busboom, "Material Properties for Beryllium Oxide (BeO)", GE specification 23A3186, (1989).

1.2.c Y. S. Touloukian, R. W. Powell, C. Y. Ho and P. G. Klemens, Thermophysical Properties of Matter Vol. 2 (1970) 123.

1.2.d J. Francl and W. D. Kingery, "Thermal Conductivity: IX, Experimental investigation of effect of porosity on thermal conductivity", *J. Am. Ceram. Soc.*, **37** [2] (1954) 99-107.

1.2.e A. W. Pryor, R. J. Tainsh and G. K. White, "Thermal conductivity at low temperature of neutron irradiated BeO", *J. Nucl. Mat.*, **14** (1964) 208-219.

1.2.f B. S. Hickman and A. W. Pryor, "The effect of neutron irradiation on beryllium oxide", *J. Nucl. Mat.*, **14** (1964) 96-110.

1.2.g L. L. Snead and S. J. Zinkle, "Use of beryllium and beryllium oxide in space reactors", ORNL report

1.2.h Y. S. Touloukian, R. W. Powell, C. Y. Ho and P. G. Klemens, Thermophysical Properties of Matter Vol. 13 (1970) 195.

1.2.i C. G. Collins, "Radiation effects in BeO", *J. Nucl. Mat.*, **14** (1964) 69-86.

1.2.j D. G. Walker, R. M Mayer and B. S. Hickman, "X-ray diffraction studies of irradiated beryllium oxide", *J. Nucl. Mat.*, **14** (1964) 147-158.

1.2.k Y. S. Touloukian, R. W. Powell, C. Y. Ho and P. G. Klemens, Thermophysical Properties of Matter Vol. 5 (1970) 45.

1.2.l B. S. Hickman, "Radiation Effects in Beryllium and Beryllium Oxide", *Studies in Radiation Effects, Series A Physical and Chemical Vol. 1*, 1966.

1.2.m J. Elston and C. Labbe, *J. Nucl. Mat.*, **4** (1961) 143-164.

1.2.n Y. S. Touloukian, R. W. Powell, C. Y. Ho and P. G. Klemens, Thermophysical Properties of Matter Vol. 8 (1970) 201.

1.2.o D. E. Plumlee, "BeO Performance Lessons Learned", SP-100 Program, Martin Marietta, March 2, 1994.

1.2.p G. W. Keilholtz, J. E. Lee, Jr. and R. E. Moore, "Irradiation Damage to Sintered Beryllium Oxide as a Function of Fast-Neutron Dose and Flux at 110, 650 and 1100°C", *Nuclear Science and Engineering*, **26** (1966) 329-338.

This Page Intentionally Left Blank

Attachment 2:
Shield Material Properties for Project Prometheus (U)

Authors:
Barri Gurau
James Nash

Reviewed by:
Brian Campbell
MC Chen
Amitava Guha
Wayne Ohlinger
Jane Oppenlander
Dean Poeth

1.0 Shield Materials

All data was plotted with Microsoft Excel and JMP, statistical analysis software (SAS Institute). JMP was used to fit data using the least squares method. Residual plots were examined to determine the quality of the regression data fit. In some analyses Cook's D statistics were used to examine the influence of individual data points on the least squares model (Reference 1.1.a). Where applicable, 95% prediction intervals were determined which specify the confidence on a single future value. However, these confidence intervals do not account for uncertainty associated with the individual measurements. Results from future test programs will be necessary to quantify the measurement uncertainty.

1.1 Lithium Hydride (LiH)

The following properties are for natural lithium hydride (~7.6% Li^6, 92.4% Li^7) (Reference 1.1.b).

1.1.1 Composition

Table 1.1.1 gives the typical composition of LiH as described in Reference 1.1.h. It is recognized that the typical composition adds up to greater than 100%. However, these are the values reported for as procured material from the Union Carbide Nuclear Company, Y-12 Plant, Oak Ridge, Tennessee.

Table 1.1.1: Composition of LiH as Given by Welch

Element	Typical	Minimum	Maximum
	wt%		
Li	86.6	85.5	-
H	12.4	12.0	-
OH	1.0	-	2.5
CO_3	0.75	-	1.5
Cl	0.05	-	0.1
Na (ppm)	100	-	300
Ba (ppm)	30	-	80
Ca (ppm)	40	-	200
Cr (ppm)	6	-	25
Co (ppm)	40	-	60
Fe (ppm)	500	-	1500
K (ppm)	100	-	400

1.1.2 Melting Temperature and Maximum Use Temperature

The melting temperature of lithium hydride is 961K, given by the phase diagram from References 1.1.e and 1.1.h.

$$T_{melt} = 961 \text{ K}$$

For a high dose region, the SP-100 project limited the use of LiH to a temperature range of 600-800K to prevent unacceptable swelling (Reference 1.1.c). The unacceptable swelling was observed in several gamma irradiation tests, all of which were not in the dose range of Prometheus.

The operating temperature range for LiH is bounded at the upper end by T_{melt} – offset, shown on the phase diagram (Figure 1.1.1). SP-100 set the upper temperature limit at 800K (Reference 1.1.c), but the basis for this limit has not been verified by the NRPCT. The lower temperature limit is a function of the environment and design. At this time the lower temperature limit has not been set, and in fact, having no minimum temperature is the most desirable case. In SP-100, 600K was set as the lower temperature limit because recombination of radiolytically decomposed LiH is very fast, resulting in near zero swelling at far higher dose rates than those under consideration for Prometheus shields. However, the SP-100 lower temperature limit of 600K would possibly require incorporation of heaters in the Prometheus shield, which introduces cost, complexity and reliability concerns. A lower temperature limit for the Prometheus shield LiH will be a trade off between the amount of swelling that is allowable in the design, and the swelling characteristics of the LiH due to environmental conditions (temperature, dose and dose rates). The composition of the LiH is also believed to be a factor. The design space for LiH use has yet to be defined.

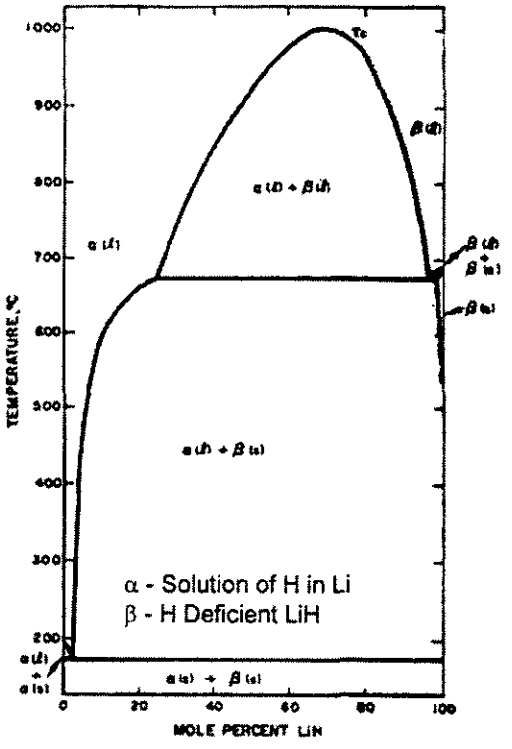

Figure 1.1.1 Phase Diagram for LiH

1.1.3 Density

The density correlation for LiH given by below is generated using linear regression of data from References 1.1.d and 1.1.e. A sharp decrease in density, related to the change in slope is observed at the melting temperature of LiH (961K). Individual confidence bands (95%) are also shown in Figure 1.1.2. The raw data points are given in Table 1.1.2. The equations are valid for 298 -1233K.

For T ≤961K

$$\rho = -1.3x10^{-4} \cdot T + 0.82$$

T > 961K

$$\rho = -2.6x10^{-4} \cdot T + 0.815$$

where
ρ = density, g/cm^3
T = temperature, K
R^2 = 0.995

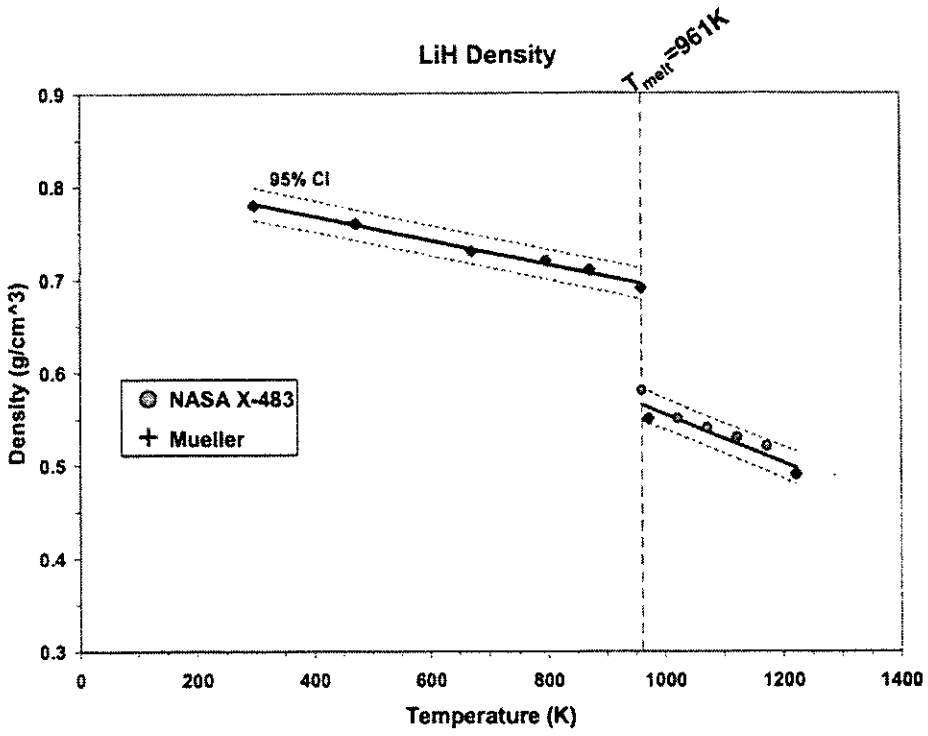

Figure 1.1.2: Density of LiH

Table 1.1.2: Data for Density of LiH

T (K)	Density	Source
298	0.78	NASA
473	0.76	NASA
673	0.73	NASA
798	0.72	NASA
873	0.71	NASA
961	0.69	NASA
961	0.58	NASA
973	0.55	NASA
1023	0.55	NASA
1073	0.54	NASA
1123	0.53	NASA
1173	0.52	NASA
1223	0.49	NASA
298	0.78	Mueller
473	0.76	Mueller
673	0.73	Mueller
798	0.72	Mueller
873	0.71	Mueller
961	0.69	Mueller
973	0.55	Mueller
1223	0.49	Mueller

1.1.4 Thermal Conductivity

LiH has a high specific heat but low thermal conductivity. Therefore, the regions at elevated temperatures tend to sustain the temperature. The following correlation is given by a power fit of thermal conductivity data (Figure 1.1.3) and correlations given by References 1.1.d and 1.1.f for LiH. The equation is valid for 200-961K.

$$k = 456.31 \cdot T^{-0.71}$$

where
k = thermal conductivity, W/m-K
T = temperature, K
$R^2 = 0.993$

T (K)	Thermal Conductivity (W/m-K)	Source
335	7.31	NASA
374	6.50	NASA
445	5.92	NASA
509	5.56	NASA
539	5.37	NASA
577	5.07	NASA
625	4.73	NASA
681	4.50	NASA
722	4.36	NASA
786	4.09	NASA
200	11.06	NRL
300	7.88	NRL
400	6.29	NRL
500	5.33	NRL
600	4.69	NRL
700	4.24	NRL
800	3.90	NRL
900	3.63	NRL
961	3.50	NRL
350	10.87	ORNL
375	9.94	ORNL
400	8.99	ORNL
438	7.79	ORNL
450	7.28	ORNL
475	7.01	ORNL
500	6.60	ORNL
550	5.93	ORNL
600	5.57	ORNL

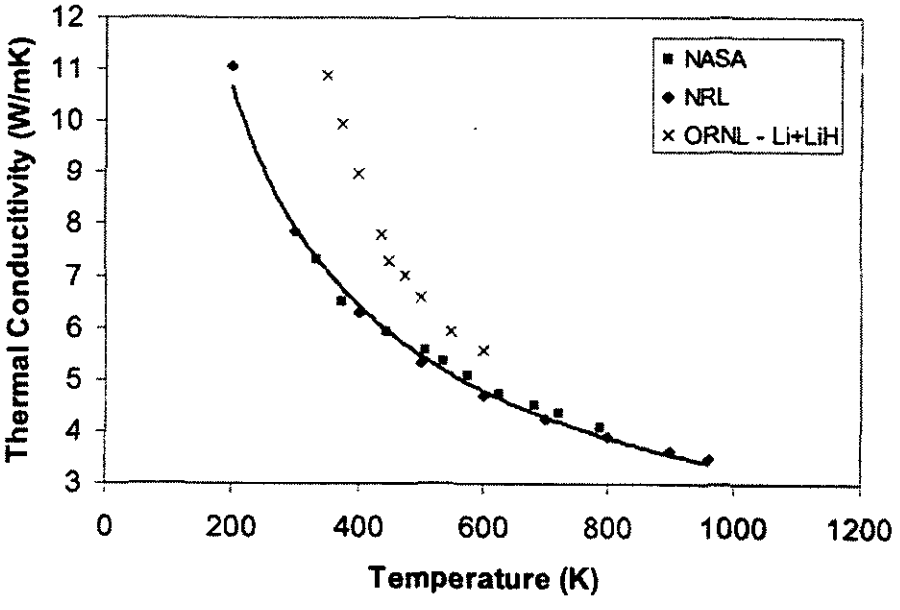

Figure 1.1.3: Thermal Conductivity of LiH with Tabular Data Included

Figure 1.1.3 displays thermal conductivity data for LiH + 2% Li (Reference 1.1.g). The additional Li increases the thermal conductivity by adding additional free electrons. Since at elevated temperatures conducting electrons are the dominant method of energy transport, the difference between LiH and LiH + 2% Li decreases as temperature increases.

1.1.5 Specific Heat

NASA (Reference 1.1.d) uses Lang's data obtained using a drop calorimeter to measure enthalpy to fit a specific heat curve. The specific heat curve, adjusted to metric units, valid for 298-838 K is given in Figure 1.1.4.

$$C_p = 6.01 \cdot T + 2013.7$$

where
C_p = specific heat, J/kg-K
T = temperature, K

Terry (Reference 1.1.f) of the Naval Research Laboratory used the superposition of the acoustic and optical lattice vibrations to determine the heat capacity of LiH, which is valid above 298 K.

$$C_p = b_0 + \sum_{m=1}^{5} b_m (T - 280)^m$$

m	b_m
0	27.08
1	0.109
2	-2.80×10^{-4}
3	4.75×10^{-7}
4	-2.94×10^{-10}
5	5.60×10^{-14}

where
C_p = molar specific heat, J/mol-K
m = index
b_m = coefficients for molar specific heat
T = temperature, K

T (K)	Cp (J/kg-K)	Source
311	3882	NASA
422	4550	NASA
533	5218	NASA
644	5886	NASA
755	6554	NASA
839	7055	NASA
298	3643	Terry
300	3668	Terry
400	4643	Terry
500	5276	Terry
600	5789	Terry
700	6333	Terry
800	6996	Terry
900	7815	Terry

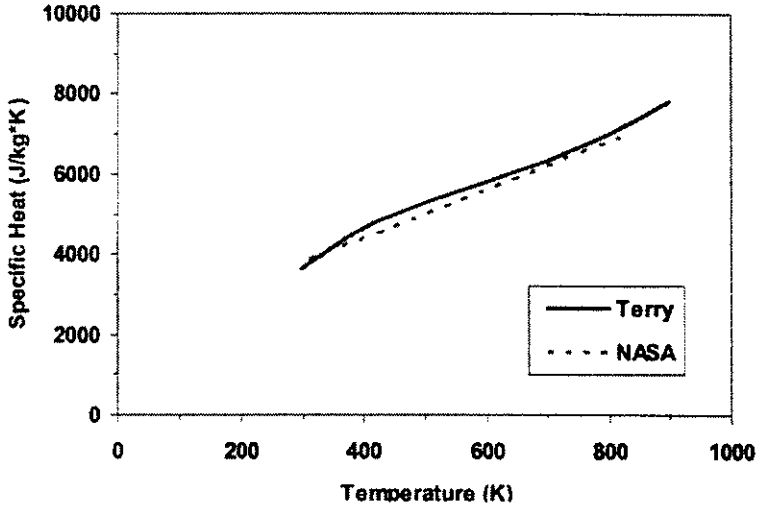

Figure 1.1.4: Specific Heat of LiH with Tabular Data Included

Since the primary mode of energy transport in LiH is through lattice vibration and Terry's fundamental specific heat curve exhibits similar trend and values as the 1958 drop calorimeter measurements made by Lang, the equation presented by Terry, which has a greater range of applicability is the preferred specific heat curve.

For the specific heat of LiH, the curve given by Terry (Reference 1.1.f) is recommended.

1.1.6 Thermal Expansion

Mel'nikova (Reference 1.1.j) calculated the coefficient of thermal expansion and lattice constant of natural lithium hydride (as well as isotopic compositions) using a quasi-harmonic approximation. This equation assumes that the Grüneisen constant is independent of temperature, volume, and isotopic composition, which lithium hydride satisfies fairly well (Reference 1.1.j).

$$\alpha(T) = 1.1837 \cdot 10^{-6} \cdot c_p(T)$$

where
$\alpha(T)$=coefficient of linear expansion of crystalline lithium hydride
c_p = molar specific heat (J/mol-K)

The calculation is accurate to within 2% of the experimental data used to verify the equation (Zalkin Reference 1.1.k), which is single crystal x-ray diffraction data.

Mel'nikova presents the results of his equation using the Zalkin data, which is presented in Figure 1.1.5. The fundamentally derived thermal expansion is valid from 0K to the melting point; however, it was validated for temperatures 298-798K. For comparison, the Mel'nikova equation is evaluated using both the Terry (Reference 1.1.f) and NASA (Reference 1.1.d) specific heat equations presented in section 1.1.5. The uncertainty associated with the Mel'nikova equation increases based on the uncertainty associated with the specific heat used to evaluate the equation.

Using the Terry equation for specific heat (Section 1.1.5) with the Mel'nikova equation above, is the preferred equation for the thermal expansion coefficient of LiH. The Mel'nikova derivation can be used for all temperatures with increasing uncertainty at temperatures greater than 798K.

	Mel'nikova	Equation (Terry)	Equation (Nasa)
Temp	α	α	α
K	*10^{-6} 1/K	*10^{-6} 1/K	*10^{-6} 1/K
100	7.5	-5.56	
150	16	8.34	
200	22.5	19.3	
250	28.4	27.9	
298.15	34.3	34.3	
300	34.6	34.5	35.9
350	39.7	39.7	38.7
400	43.7	43.7	41.6
450	46.9	46.9	44.4
500	49.6	49.6	47.2
550	52.1	52.1	50.0
600	54.5	54.5	52.9
650	56.9	56.9	55.7
700	59.5	59.6	58.5
750	62.5	62.5	61.4
800	65.8	65.8	64.2
850	69.4	69.5	
900	73.5	73.5	
950	77.8	77.9	
965	79.2	79.3	

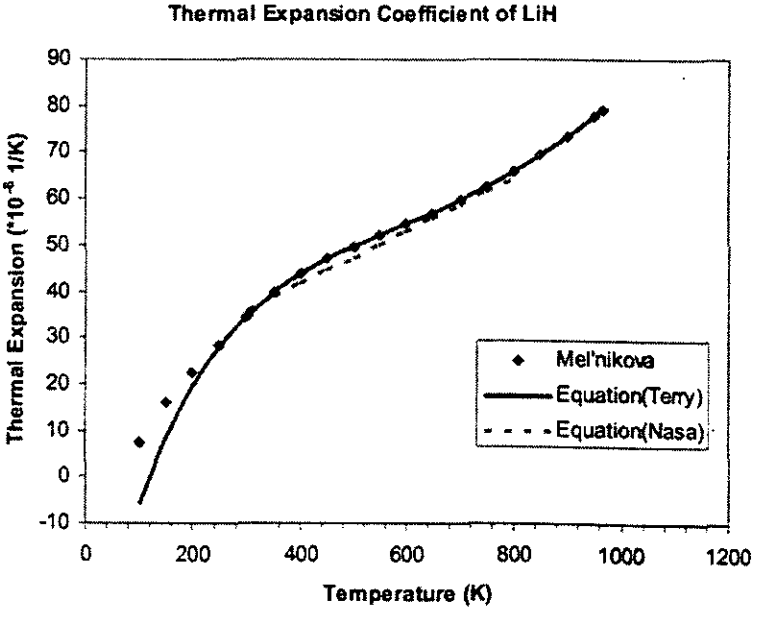

Figure 1.1.5: Thermal Expansion Coefficient of LiH with Tabular Data Included

1.1.7 Modulus of Elasticity

Lundberg (Reference 1.1.l) published data for the Young's Modulus of LiH in flowing helium. The moduli were calculated from a rough stress-strain plot obtained by plotting the crosshead motion versus the load on the sample. Due to the systematic error associated with the strain measurement techniques, according to Lundberg, "the absolute values are probably not too accurate (Reference 1.1.l)." A power law equation can be fit using least squares fitting techniques, given in Figure 1.1.6. The equation is valid for 339 – 689K.

$$E = 6.516x10^{16} \cdot T^{-5.191}$$

where
E = Young's Modulus, MPa
T = temperature, K

Temperature	Young's Modulus
K	MPa
339	3654
339	6826
339	6205
339	5792
539	285.4
539	---
539	298.5
539	---
555	167.5
689	87.56
689	208.2
689	206.2
689	165.5

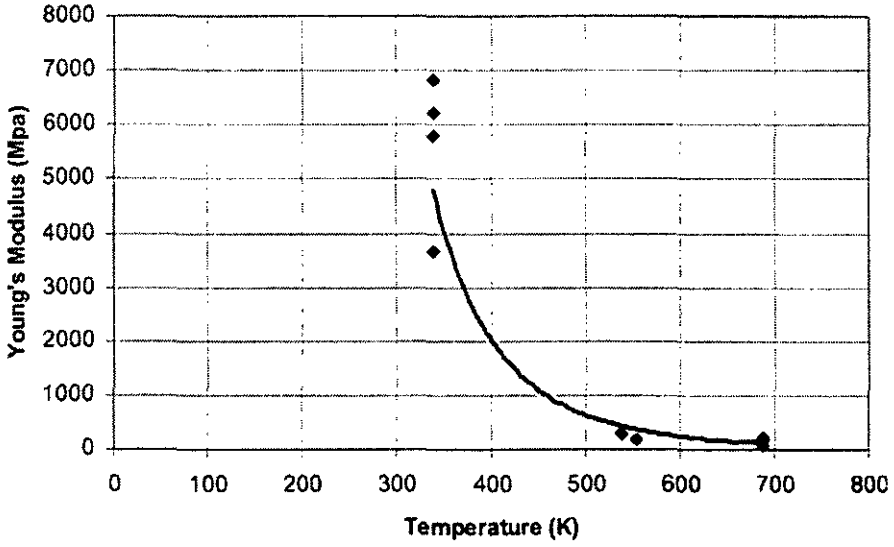

Figure 1.1.6: Elastic Modulus of LiH with Tabular Data Included

Welch states that the average Young's modulus for cold-pressed and sintered LiH at room temperature is $7.24x10^4$ MPa ($10.5x10^6$ psi) (Reference 1.1.h). Young's modulus decreases by an order of magnitude over the temperature range of the data. The large decrease in elasticity occurs at approximately 435 K. At approximately 435 K a liquid alpha phase appears in the solid lithium hydride. The presence of the liquid phase causes the material to become weaker and less resistant to deformation when under stress. The NRPCT has not verified this.

Since the modulus is strongly dependent on the strain rate at elevated temperatures, LiH does not behave elastically (Reference 1.1.h). Stress-strain rate curves are given in Section 1.1.9 that demonstrate the non-linearity of the stress-strain rate relationship.

Therefore, the recommended equation for the Young's Modulus of LiH is the power law equation given above.

1.1.8 Yield Strength

Data for the yield strength of LiH has not been located.

1.1.9 Ultimate Tensile Strength

Welch (Reference 1.1.h) demonstrated the ultimate tensile strength of cold-pressed and sintered LiH is a function of strain rate (Figure 1.1.7). The tests were ultimately tested in static helium atmosphere. Originally, the tests at elevated temperature were attempted in a vacuum, but the extensometer consistently slipped off the samples. The stress-strain rate plot (below) shows that the LiH does not obey Hooke's law to the fracture point. Therefore, LiH is not truly a brittle material.

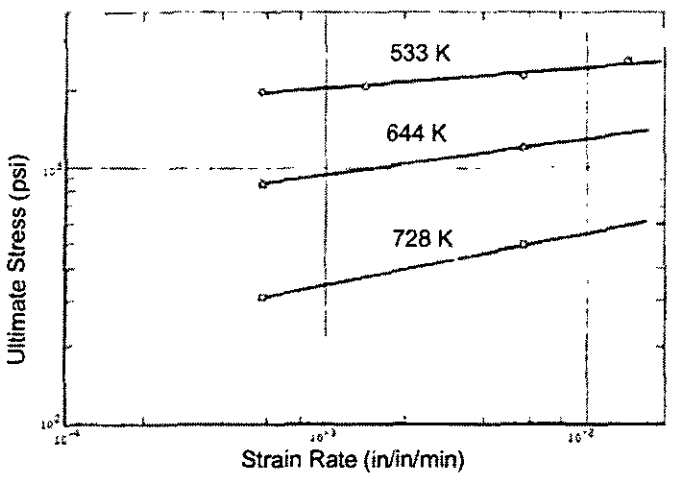

Figure 1.1.7: Ultimate Tensile Strength Curves of LiH from Welch

The ultimate tensile strength as a function of temperature and strain rate for LiH is given in Table 1.1.3 below. From the data it is observed that LiH is not that strain rate sensitive.

Table 1.1.3: Ultimate Tensile Strength Data for LiH

T (K)	UTS (MPa)	strain rate in/in/min
533	13.72	0.00057
533	13.21	0.00057
644	5.72	0.00057
644	6	0.00057
728	2.43	0.00057
728	1.71	0.00057
728	1.63	0.00057
728	2.73	0.00057
533	15.31	0.0057
533	15.38	0.0057
644	8	0.0057
644	8.2	0.0057
728	3.35	0.0057
533	14.07	0.00143
533	14	0.00143
533	17.79	0.0143
533	17.37	0.0143
298	17.17	0.001
298	19.55	0.001

The NRPCT cannot recommend an equation for ultimate tensile strength of LiH, more data is necessary to reach a conclusion.

1.1.10 Poisson's Ratio

Data for the Poisson's ratio of LiH has not been located.

1.1.11 Irradiation Swelling

1.1.1.1. Gamma Irradiation

Disney (Reference 1.1.i) reported gamma irradiation swelling of 25% at 500K for a dose of 14.7 Grad: Dose was ~ 15X of what was expected on Prometheus (nominally 1 Grad), and dose rate was ~1500X of expected (15E6 Rad/hr versus 1E4 Rad/hr). In the 400 to 500K temperature range, lower doses produced lower swelling, e.g., ~2% at 0.5 Grad at ~500K, or ~8% at 1 Grad at ~500K. Although 1 Grad is the currently predicted max gamma dose for the Prometheus shield, the dose rate was still far in excess of prototypical, as shown in Figure 1.1.8. Given that the gamma-induced swelling is expected to be a rate balance between ionization and thermal recombination, dose rate is a key variable to understand. Reference 1.1.i showed that decreasing dose rate resulted in reduced swelling, however, the lowest dose rate tested (~1E6 Rad/hr) was still far above expected. At SP-100 proposed temperature range of >600K, prior gamma testing reported <0.2% swelling regardless of dose and dose rate (up to 717K) (Reference 1.1.i).

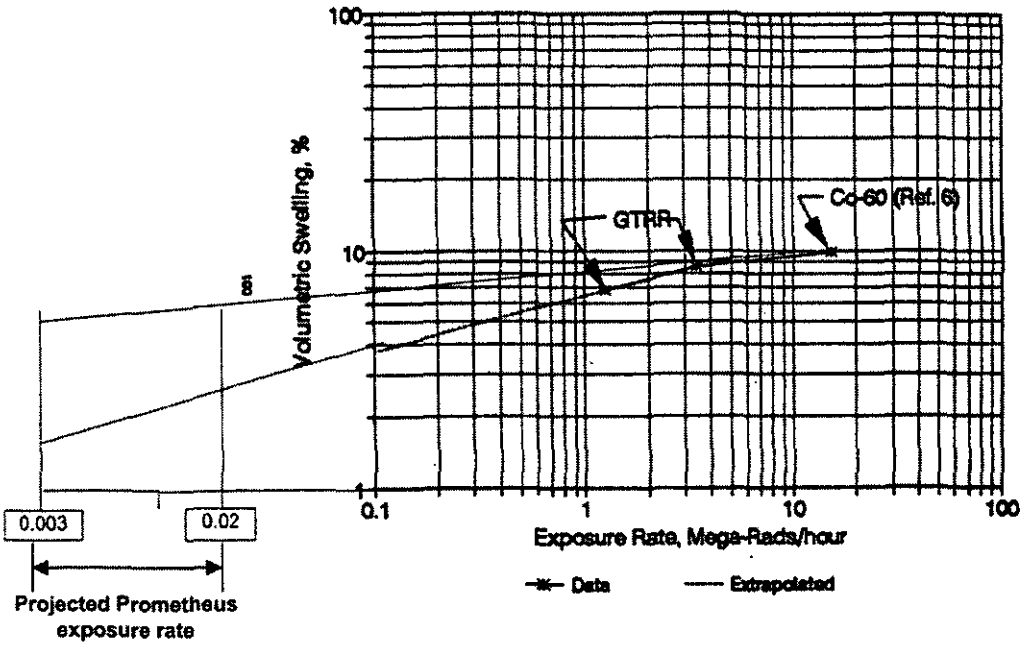

Figure 1.1.8: LiH Swelling Due to Gamma Irradiation

Early gamma irradiation testing of LiH produced results not prototypic of the doses or temperatures seen by a shield for a 200 MW_{th} Prometheus reactor. Table 1.1.4 summarizes the previous LiH irradiation experiment conditions and the expected Prometheus conditions.

Table 1.1.4: Summary of Gamma Irradiation Swelling of LiH

	Prometheus Shield Target Range	Intended NRPCT Testing	Prior Irradiation Programs Ranges & Example Results							
			Co-60 gamma					GTRR gamma		
Temperatures (K)	600 - 800	300 - 850	450		500		600	450	500	600
Dose Rates (Mega Rad/hr)	.003 to .02	.001 to .1	15					1.25	3.4	3.4
Doses (G rad)	0.3 to 2 Grad	.1 to 5	0.2	0.5	0.5	3.5	28	2.5		
Fast Flux (n/cm2/s)	1e6 to 1 e10	1e5 to 1e11								
Fast Fluence (n/cm2)	5e14 to 5e18	1e14 to 1e19								
Swelling %	< 2	Key Metric	0.4	~2	~2	12	~.15	7	10	<0.2

1.1.1.2. Neutron

The NRPCT is currently evaluating data from the earlier space nuclear power programs. Refer to Reference 1.1.o for information regarding LiH performance in a neutron environment.

1.1.12 References

1.1.a. J. Neter, M. H. Kutner, C. J. Nachtsheim and W. Wasserman, *Applied Linear Statistical Models* 4th ed., McGraw-Hill (1996).

1.1.b. Baum, Edward M. et al. 2002. *Nuclides and Isotopes, Sixteenth Edition.* Lockheed Martin.

1.1.c. Y-12 Document dated February 2004. "Identification and Analysis of SP-100 Reactor Shield Information, Fabrication Considerations and Resource Assessment of Space Reactor Shielding."

1.1.d. NASA Technical Memorandum, X-483, "Compilation of the Properties of Lithium Hydride", Roger L. Smith and James W. Miser, Lewis Research Center, Cleveland, OH, January 1963.

1.1.e. Mueller, William M., James P. Blackedge, and George G. Libowitz. 1968. *Metal Hydrides.* New York: Academic Press.

1.1.f. Naval Research Laboratory Document NRL/MR/6720--96-7868. R.E. Terry. 1996. *Lithium Hydride Debris Shields for Plasma Radiation Studies.*

1.1.g. ORNL Document, ORNL/TM-12766, dated September 1994. "The Effect of Gamma Irradiation on the Thermophyscial Properties of LiH + 2% Li."

1.1.h. Atomics International Document NAA-SR-9400. Frank H. Welch. 1964. *Lithium Hydride Technology: I. Properties of Lithium Hydride and Corrosion Studies.*

1.1.i. R.K. Disney, "Status Report on the SP-100 Program Investigations of Irradiation-Induced Swelling of Lithium Hydride Shield Materials," Westinghouse Electric Corporation, February 25, 1993.

1.1.j. Mel'nikova, T.N. and K.A. Yakimovich. 1980. "Thermal Properties of Lithium Hydride and Its Isotopic Modifications in a Crystalline State", *High Temperature*. 18,2:250-256.

1.1.k. Zalkin, A. 1953. USAEC Report URCL-4239.

1.1.l. Atomics International Document NAA-SR-MEMO-7991. Lundberg, L.B. 1962. *Mechanical Properties of LiH Part I – Compression Tests.*

1.1.m. LANL Document, LA-2463. Frank Pretzel et. al. August 24, 1961. *Radiation Effects on Lithium Hydride.*

1.1.n. Atomics International Document NAA-SR-9400 Volume III. Frank H. Welch. 1973. *Lithium Hydride Technology: III. Properties of Lithium Hydride For SNAP Shielding Applications.*

1.1.o. KAPL Document MDO-723-0048, "The evaluation of lithium hydride for use in a space nuclear reactor shield, including a historical perspective, For Information (U)", to be issued

1.2 Beryllium (Be)

Many different industrial grades of Be are available (Brush Wellman, Elmore, OH). Data for the structural grades of Be (S-65, S-65H, S-200F and S-200FH) are most commonly reported in the literature. The main differences between the various grades are impurity levels (particularly the BeO content) and processing/fabrication method. S-65 and S-200F grade Be are vacuum hot pressed (VHP) materials while S-65H and S-200FH grade Be are hot isostatically pressed (HIP) materials. The S-65 and S-65H material has a maximum BeO content of 1% while the S-200 and S-200FH material has a maximum BeO content of 1.5%. Further information on the effect of processing and impurities in Be can be found in Reference 1.2.b and 1.2.c. Generally, Be is not recommended as a structural material for radiation environments due to loss of ductility at relatively low fluences (References 1.2.d and 1.2.e). Ductility and elongation are not presented here in, but could be studied if later needed.

1.2.1 Composition

Table 1.2.1 gives the composition of S-65 structural grade beryllium from Reference 1.2.f (Brush Wellman).

Table 1.2.1: S-65 Beryllium Composition (Brush Wellman)

Element (max unless otherwise stated)	wt%
Be (min %)	99
BeO	1.0
Al	0.06
C	0.10
Fe	0.08
Mg	0.06
Si	0.06
Other metallic impurities	0.04

1.2.2 Melting Temperature and Maximum Use Temperature

The melting temperature of beryllium is (Reference 1.2.g):

$T_{melt} = 1558 \pm 10\ K$

For structural application in a radiation environment, the maximum use temperature is **823K**. Above 873K embrittlement and reduction in strength are limiting factors (section 1.2.8 and **1.2.10)**.

1.2.3 Density

From Scaffidi-Argentina (Reference 1.2.b) for all grades of Be, the room temperature **(293K)** theoretical density is 1.85 g/cm^3. The following curve is recommended for the temperature range 293K ≤T ≤1500K.

$$\rho = 1.823 - 6.933x10^{-5} \cdot (T - 273) - 1.514x10^{-8} \cdot (T - 273)^2$$

where
ρ = density, g/cm^3
T = temperature, K

Dombroski (Reference 1.2.c) includes a data table of the variation in density of S-65 grade beryllium (Brush Wellman) with temperature (Table 1.2.2). Figure 1.1.1 shows some slight variation (+/-0.02) is observed at higher temperatures because the equation was fit to data from industrially available Be grades and the tabular data is only for S-65 grade Be, shown in Figure 1.2.1.

For the density of Be, the equation given by Scaffidi-Argentina (Reference 1.2.b) is recommended.

Table 1.2.2: Density data for Be

	Scaffidi-Argentina (2000)	S-65 Dombrowski (1995)
T (K)	Density (g/cc)	Density (g/cc)
324	1.819	1.82
412	1.813	1.814
456	1.810	1.811
515	1.805	1.806
564	1.802	1.801
609	1.798	1.797
673	1.793	1.791
737	1.788	1.785
816	1.781	1.777
892	1.774	1.769
973	1.767	1.76
1127	1.753	1.742
1269	1.739	1.725

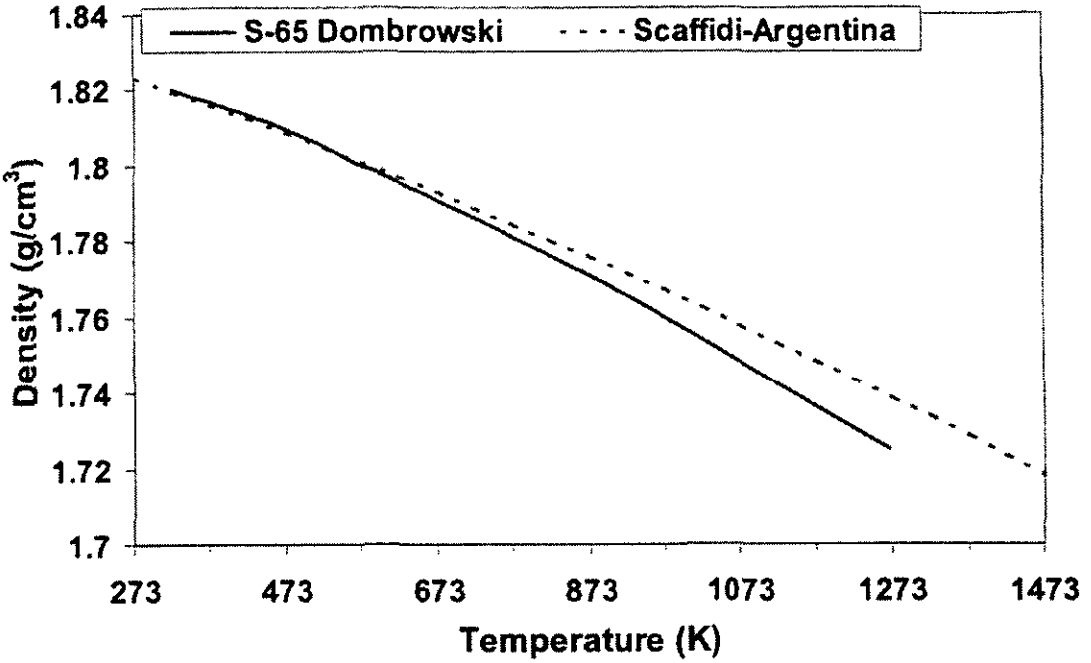

Figure 1.2.1: Density of Be

1.2.4 Thermal Conductivity

1.2.4.1 Unirradiated

From Scaffidi-Argentina (Reference 1.2.b) the unirradiated, thermal conductivity of Be is given by the following curve for the temperature range 293K ≤T ≤1500K.

$$k = 189.8 - 0.2694 \cdot (T - 273) + 2.543x10^{-4} \cdot (T - 273)^2 - 1.010x10^{-7} \cdot (T - 273)^3$$

where
k = thermal conductivity, W/m-K
T = temperature, K

Billone (Reference1.2.h) also proposed an equation for the thermal conductivity of Be based on data from various grades of Be up to 973K. This equation accounts for the fact that thermal conductivity is dependent upon the porosity of the material. This equation for the effective thermal conductivity is for hot pressed Be in the 0-50% porosity range.

$$k = \left(\frac{1 - p}{1 + 3.7p^2} \right) \cdot \left(291 - 0.48015 \cdot T + 4.2602x10^{-4} \cdot T^2 - 1.4914x10^{-7} \cdot T^3 \right)$$

where
k = thermal conductivity, W/m-K
p = fraction porosity
T = temperature, K

Dombroski (Reference 1.2.c) includes a data table of the variation in thermal conductivity of S-65 grade Be with temperature. Again, some variation is observed at higher temperatures (T>1073K) because the equation was fit to data from industrially available Be grades and the tabular data is only for S-65 grade Be.

The tabulated data (Table 1.2.3) for S-65 grade Be from Reference 1.2.c and the predicted values from the equations given in Reference 1.2.b and Reference 1.2.g assuming zero porosity are plotted in Figure 1.2.2. At temperatures between 400 – 973K, little variation is observed between the three sources.

For the thermal conductivity of Be, the equation given by Billone (Reference 1.2.h) is recommended. This curve is recommended because it accounts for the porosity of the material (0-50% range). This curve is given for T ≤973K.

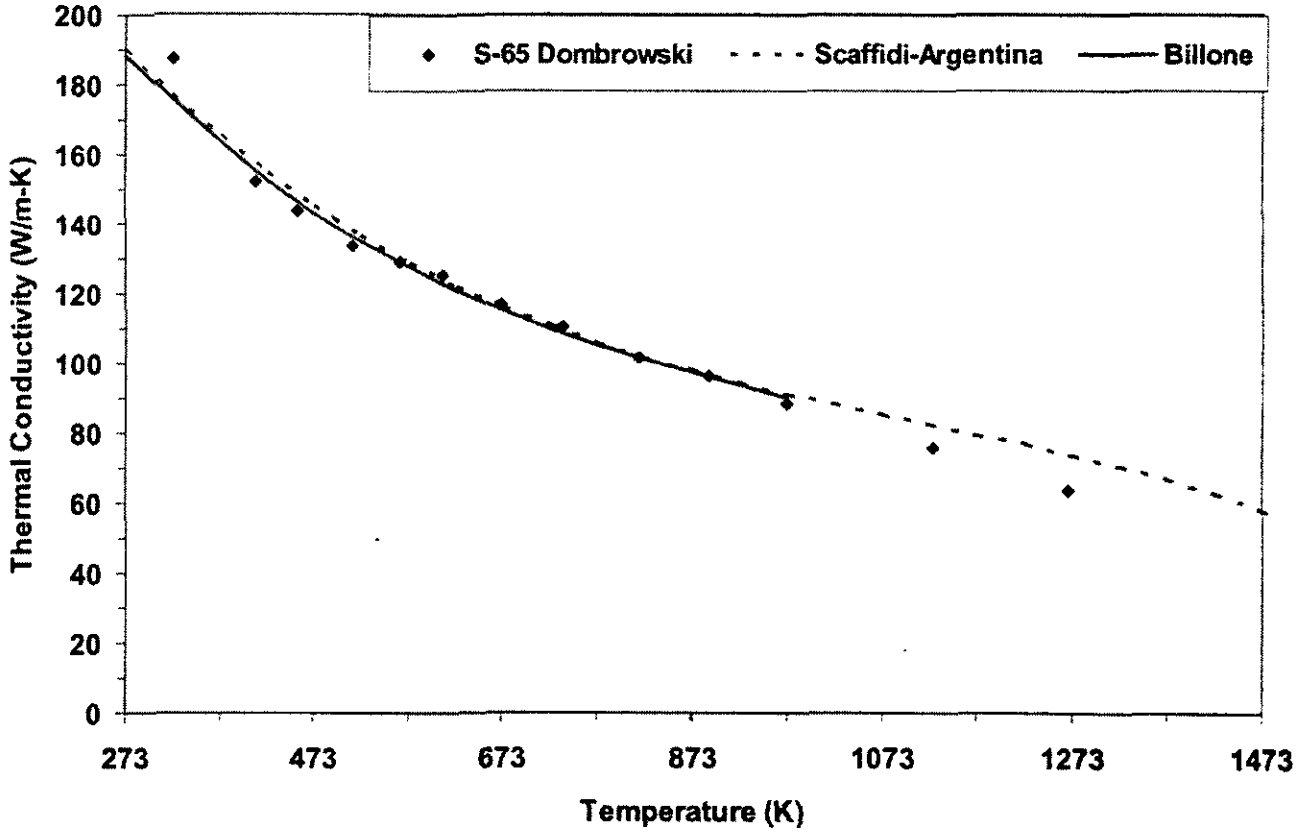

Figure 1.2.2: Thermal Conductivity of Be

Table 1.2.3: Thermal Conductivity Data for Be

S-65	Dombrowski (1995)
T (K)	Thermal Conductivity (W/m-K)
324	187.3
412	152.3
456	143.8
515	133.8
564	128.8
609	125.2
673	116.6
737	110.4
816	101.8
892	96.1
973	88.4
1127	75.8
1269	63.8

	Scaffidi-Argentina (2000)	Billone (1995)
T(K)	W/m-K	W/m-K
273	189.8	188.6
373	165.3	163.4
473	145.3	143.4
573	129.1	127.7
673	116.3	115.4
773	106.0	105.5
873	97.88	97.28
973	91.17	89.76
1073	85.29	
1173	79.66	
1273	73.65	
1373	66.67	
1473	58.10	
1573	47.35	

1.2.4.2 Irradiated

The irradiated thermal properties, including thermal conductivity, have been studied for beryllium. Snead and Barabash (References 1.2.i and 1.2.j) summarize the neutron irradiation data for S-65 and S-200F Brush Wellman beryllium grades. Snead (Reference 1.2.i) reported that significant reductions in thermal conductivity of Be are not expected until He bubbles and swelling become more prominent (He bubbles form at grain boundaries from 598 – 873K and form at dislocations within the grain at temperatures around 723 – 823K). This is because for irradiations above 573 K the He is no longer in solid solution and therefore He diffusion and bubble formation begin to occur. Snead (Reference 1.2.i) showed that the effect of radiation on the thermal conductivity of S-65 Be at ~$1x10^{21}$ n/cm^2 (E>0.1 MeV) and approximately 573K was within the ~4% experimental error of the unirradiated value. For S-200F Be irradiated to fluences of $4.5x10^{20}$ n/cm^2 (E>1MeV) at 473K, the thermal conductivity decreased approximately 5% (Reference 1.2.j). At this time there is no recommended equation for irradiated thermal conductivity of Be.

1.2.5 Thermal Expansion

It should be noted that due to the anisotropic nature of the hexagonal lattice, some amount of anisotropy is expected in thermal expansion. However, as described by Scaffidi-Argentina (Reference 1.2.b), there is little difference (less than a few percent) observed for polycrystalline, isotropic sintered Be parts (S-65 Brush Wellman grade Be). Extruded grades of Be may exhibit 15-20% differences in the longitudinal and transverse thermal expansion, while HIP Be (S-65H and S-200FH) are more isotropic.

1.2.5.1 Unirradiated Linear Expansion

Billone (Reference 1.2.h) reports the following equation, plotted in Figure 1.2.3, developed for the percent change in length ($\Delta L/L_0$) of Be based on data up to 1558K. The unirradiated percent change in length ($\Delta L/L_0$) is given by:

$$\frac{\Delta L}{L_0} = 8.43x10^{-4} \cdot (1 + 1.36x10^{-3} \cdot T - 3.53x10^{-7} \cdot T^2) \cdot (T - 298)$$

where
$\Delta L/L_0$ = change in length from 298K, percent
T = temperature, K

T (K)	% Linear Expansion
298	0
373	0.092
473	0.231
573	0.386
673	0.555
773	0.737
873	0.930
973	1.13

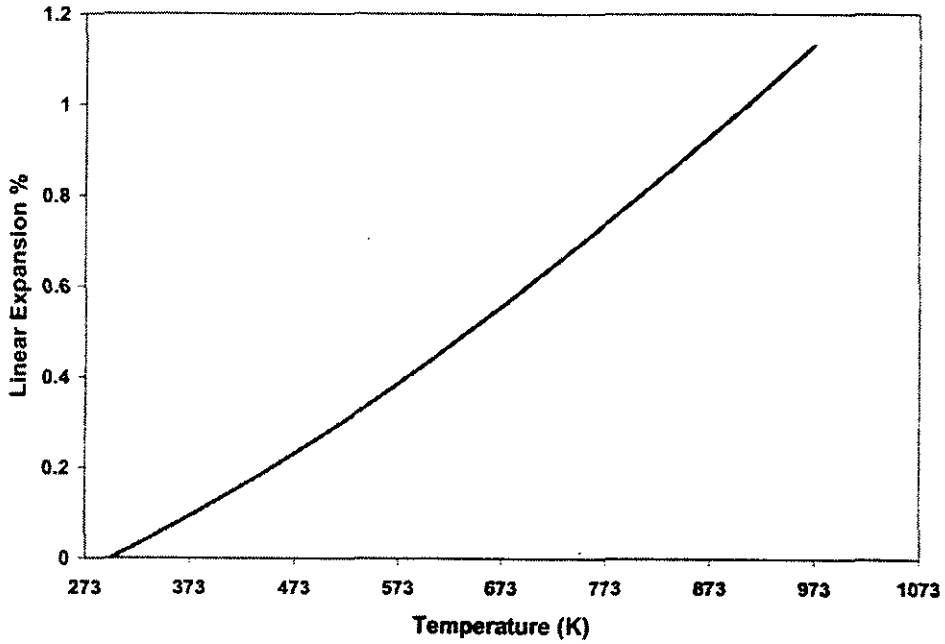

Figure 1.2.3: Linear Expansion of Be with Data Table Included

1.2.5.2 Unirradiated Instantaneous Coefficient of Thermal Expansion

From Scaffidi-Argentina (Reference 1.2.b), for the temperature range 293K ≤T ≤1473K the unirradiated instantaneous coefficient of thermal expansion (α_i) is given by the following equation.

$$\alpha_i = 10.8 + 0.022 \cdot (T - 273) - 1.35x10^{-5} \cdot (T - 273)^2 + 3.45x10^{-9} \cdot (T - 273)^3$$

where
α_i = instantaneous coefficient of thermal expansion, 10^{-6} K^{-1}
T = temperature, K and the reference temperature is 293K

1.2.5.3 Unirradiated Mean Coefficient of Thermal Expansion

From Scaffidi-Argentina (Reference 1.2.b), for the temperature range 293K < T < 1473K the unirradiated mean coefficient of thermal expansion (α_m) is given by:

$$\alpha_m = 11.04 + 0.0109 \cdot (T - 273) - 4.474x10^{-6} \cdot (T - 273)^2 + 8.631x10^{-10} \cdot (T - 273)^3$$

where
α_m = mean coefficient of thermal expansion, 10^{-6} K^{-1}
T = temperature, K and the reference temperature is 293K

Figure 1.2.4 includes the instantaneous coefficient of thermal expansion (α_i) and the mean coefficient of thermal expansion (α_m) as determined by Scaffidi-Argentina (Reference 1.2.b) for all grades of Be, and the mean thermal expansion coefficient as determined by Dombrowski (Reference 1.2.c) for S-65 Be containing 0.9% BeO. The values are tabulated in Table 1.2.4.

For the mean coefficient of thermal expansion of Be, the equation given by Scaffidi-Argentina (Reference 1.2.b) is recommended.

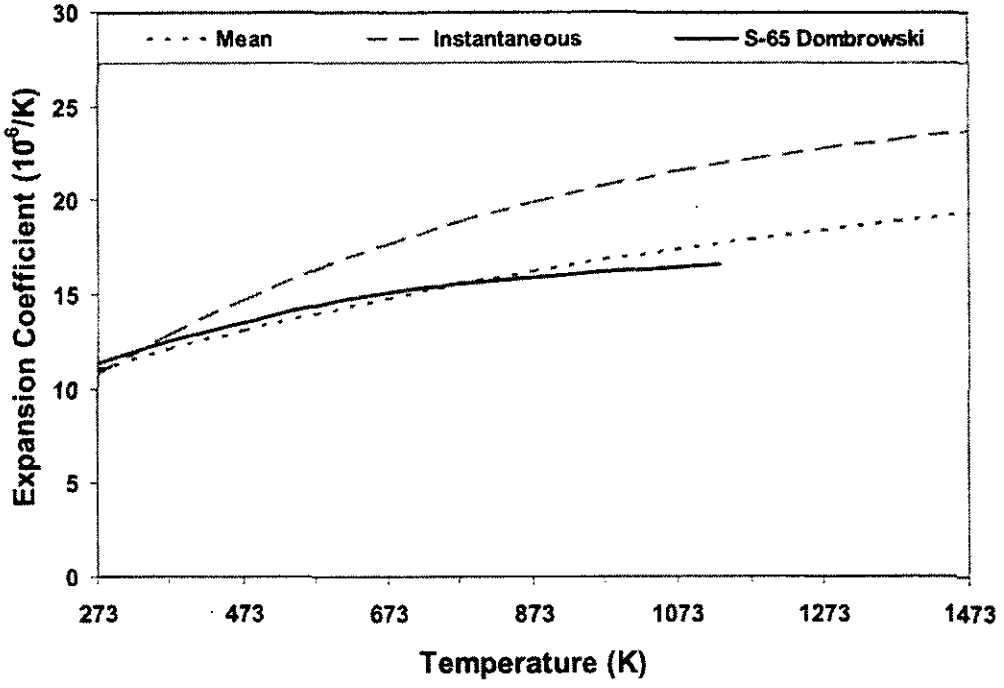

Figure 1.2.4: Mean and Instantaneous Thermal Expansion Coefficient of Be

Table 1.2.4: Mean and Instantaneous Thermal Expansion Data for Be

S-65	Dombrowski (1995)
T (K)	*CTE (10^{-6})/K*
270	11.32
381	12.58
524	14.00
607	14.66
688	15.14
758	15.44
952	16.10
1130	16.61

	Scaffidi-Argentina (2000)	
	instantaneous	mean
T(K)	CTE (10^{-6})/K	CTE (10^{-6})/K
273	10.80	11.04
373	12.87	12.10
473	14.69	13.07
573	16.28	13.96
673	17.66	14.78
773	18.86	15.53
873	19.89	16.22
973	20.77	16.85
1073	21.53	17.42
1173	22.18	17.95
1273	22.75	18.43
1373	23.26	18.88
1473	23.72	19.29
1573	24.16	19.68

1.2.5.4 Irradiated

From Reference 1.2.b it is expected that the coefficient of thermal expansion in isotropic Be grades is not affected by neutron irradiation.

1.2.6 Specific Heat

1.2.6.1 Unirradiated

From Scaffidi-Argentina (Reference 1.2.b), the unirradiated specific heat of Be is given by the following equation. This equation is based on experimental data from Be grades with ≤1% BeO content (S-65 Brush Wellman Be). The equation is valid for 293 ≤T ≤1558K.

$$C_p = 1741.8 + 3.3358 \cdot (T - 273) - 3.1125x10^{-3} \cdot (T - 273)^2 + 1.2748x10^{-6} \cdot (T - 273)^3$$

where
C_p = specific heat, J/kg-K
T = temperature, K

Billone (Reference 1.2.h) proposed an equation for the specific heat based on data from various grades of Be up to 973K.

$$C_p = 2432 + 0.6428 \cdot (T - 273) - 0.7111 \cdot (T - 273)^{-2}$$

where
C_p = specific heat, J/kg-K
T = temperature, K

Dombrowski (Reference 1.2.c) includes a data table of the variation in specific heat of S-65 grade Be with temperature. Figure 1.2.5 is of the tabular data, given in Table 1.2.5, for S-65 Be from Reference 1.2.c and the predicted values from the equations given in Reference 1.2.a and Reference 1.2.h for the unirradiated specific heat of Be. Some variation is observed between Reference 1.2.a and 1.2.h at lower temperatures (T<573K).

For the specific heat of Be, the equation given by Scaffidi-Argentina (Reference 1.2.b) is recommended.

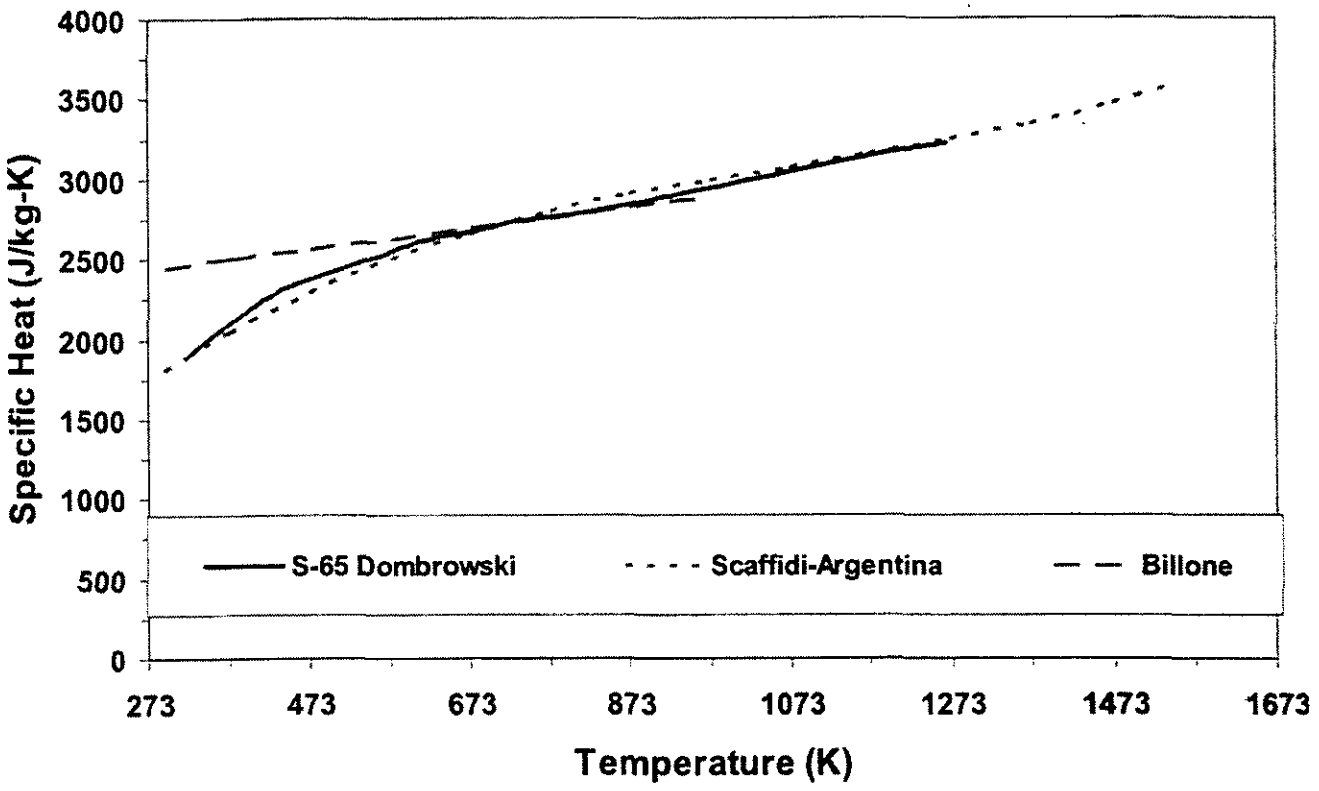

Figure 1.2.5: Specific Heat of Be

Table 1.2.5: Specific Heat Data for Be

S-65	Dombrowski (1995)
T (K)	Cp (J/kg-K)
324	1905
412	2240
456	2344
515	2441
564	2529
609	2613
673	2667
737	2734
816	2780
892	2860
973	2939
1127	3086
1269	3220

	Scaffidi-Argentina (2000)	Billone (1995)
T(K)	Cp (J/kg-K)	Cp (J/kg-K)
293	1807	2445
373	2046	2496
473	2295	2561
573	2497	2625
673	2660	2689
773	2791	2753
873	2898	2818
973	2989	2882
1073	3071	
1173	3152	
1273	3240	
1373	3342	
1473	3466	
1550	3581	

1.2.6.2 Irradiated

Scaffidi-Argentina (Reference 1.2.b) reports minimal effects on the specific heat of irradiated Be. It was also reported that the specific heat remains fairly independent of the Be grade. At this time it is assumed that the specific heat of Be will remain independent of irradiation.

1.2.7 Modulus of Elasticity

1.2.7.1 Unirradiated

Variation in the elastic modulus of S-65 Be with temperature is given by Dombrowski (Reference 1.2.c) over the temperature range 273K ≤T ≤1273K, shown in Figure 1.2.6. Based on the limited data points reported, no equation is given at this time.

T (K)	Young's Modulus (GPa)
273	310
473	300
673	290
873	230
1073	97
1273	48

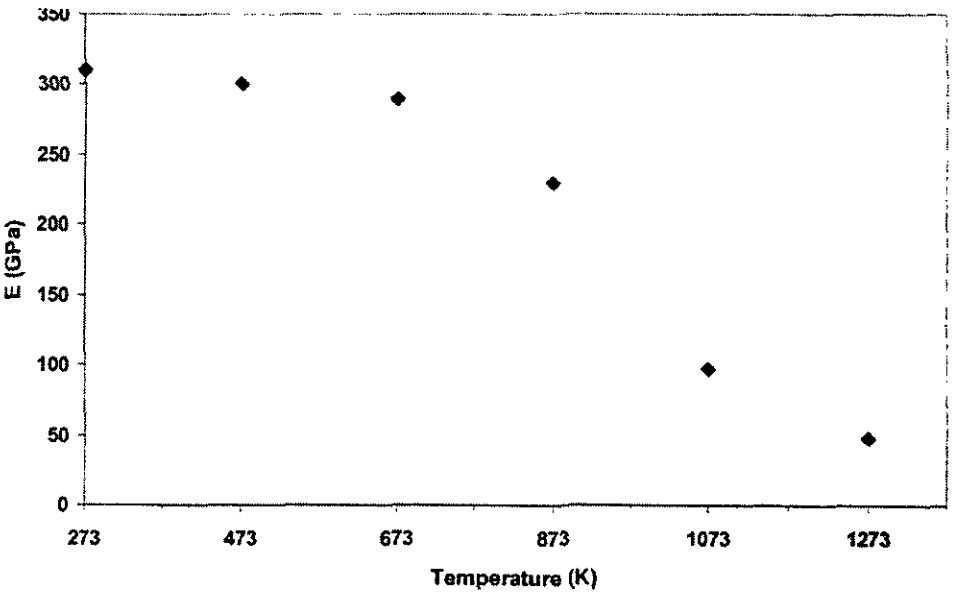

Figure 1.2.6: Elastic Modulus of Be with Data Table Included.

1.2.7.2 Irradiated

Hickman (Reference 1.2.e) reports that radiation effects in Be are expected to be negligible because of the lack of significant displacement type damage above 373K (no fluence limit was reported by Hickman). Some variation in the elastic modulus of Be may occur due to helium bubble formation and swelling. Generally, variations in the elastic modulus are related to temperature as shown above.

1.2.8 Tensile Yield Strength

1.2.8.1 Unirradiated

Multiple references have reported on the unirradiated tensile yield strength of Be (References 1.2.d, 1.2.k, 1.2.l and 1.2.m). The below equations are based on data from unirradiated VHP (S-65 and S-200F Brush Wellman) and HIP (S-65H and S-200FH Brush Wellman) Be grades. In general, HIP grade Be exhibits a higher tensile yield strength than VHP grade Be. These equations are linear regressions of the data in the temperature range 293K ≤T ≤1228K (See Figures 1.1.7 and 1.1.8 below in section 1.2.8.2).

$$VHP\ \ YS = -0.2574 \cdot T + 350.1$$

$$HIP\ \ YS = -0.3289 \cdot T + 449.3$$

where

VHP YS = tensile yield strength of VHP Be, MPa
HIP YS = tensile yield strength of HIP Be, MPa
T = temperature, K

1.2.8.2 Irradiated

Irradiation effects on the tensile yield strength of multiple grades of Be (S-65, S-65H, S-200F and S-200FH) have been studied by many references (References 1.2.d, 1.2.k, 1.2.l and 1.2.m) Irradiated Be exhibits a higher yield strength than in the unirradiated state. Below is a linear regression fit to the irradiated VHP Be and HIP Be data over a temperature range of 293K ≤T ≤823K and fluence range of 0.75 – 2.45x10^{21} n/cm^2 (E>1 MeV). The plot of irradiated and unirradiated tensile yield strength data for multiple grades of Be is also shown below (Figure 1.1.7 and 1.1.8). Neutron irradiation studies have observed that above 823K the strength of irradiated Be dramatically decreases due to He bubble formation. In beryllium He bubbles begin to form at grain boundaries at T>673K and at dislocations within the grains at T>823K. Additionally, Be has a high fast neutron cross-section for (n,α) reactions and therefore at higher temperatures He embrittlement becomes a concern (corresponding to 0.5 T_{melt}). All high temperature irradiated data (T ≥823K) was excluded from the regression analysis. Additionally, Moons (Reference 1.2.d) performed thermal ageing studies to isolate thermal effects from radiation effects. The thermal results are not included in this linear regression analysis. Data reported from Reference 1.2.d, 1.2.k, 1.2.l and 1.2.m were from samples tested at the irradiation temperature. The equations exhibit a good fit for 293 – 823K.

$$VHP\ YS_{irr} = -0.6270 \cdot T + 692.5$$

$$HIP\ YS_{irr} = -0.6985 \cdot T + 791.7$$

where
VHP YS_{irr} = irradiated tensile yield strength of VHP Be, MPa
HIP YS_{irr} = irradiated tensile yield strength of HIP Be, MPa
T = temperature, K

The unirradiated and irradiated tensile yield strength of Be is plotted in Figure 1.2.7 for VHP and HIP grades are plotted in Figure 1.2.8. The 95% confidence intervals for the least square fits to the data are shown on the graphs. Further study is required to define the effects on yield strength for fluences below 0.75x10^{21} n/cm^2 (E>1MeV).

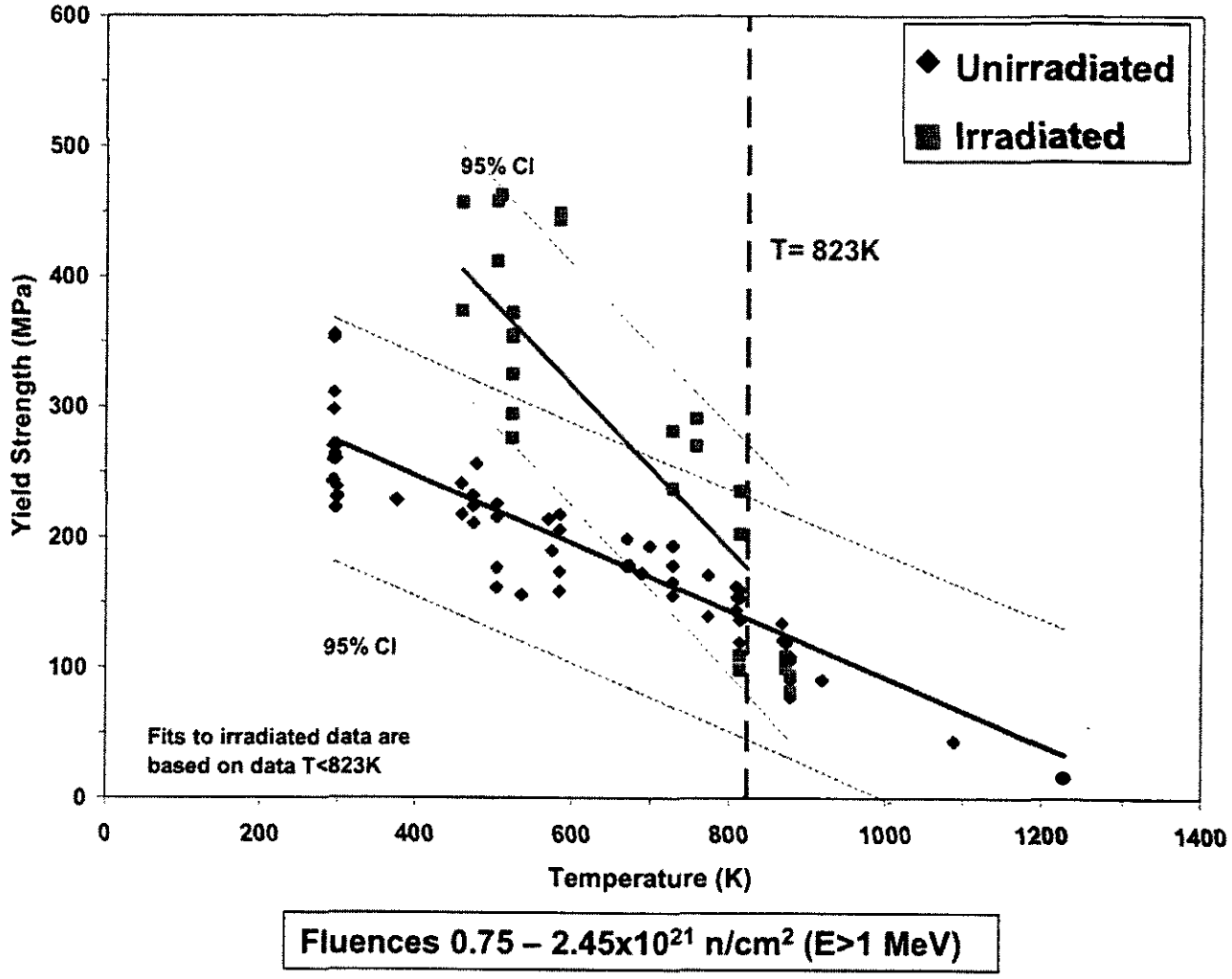

Figure 1.2.7: Irradiated and Unirradiated Tensile Yield Strength of VHP Be

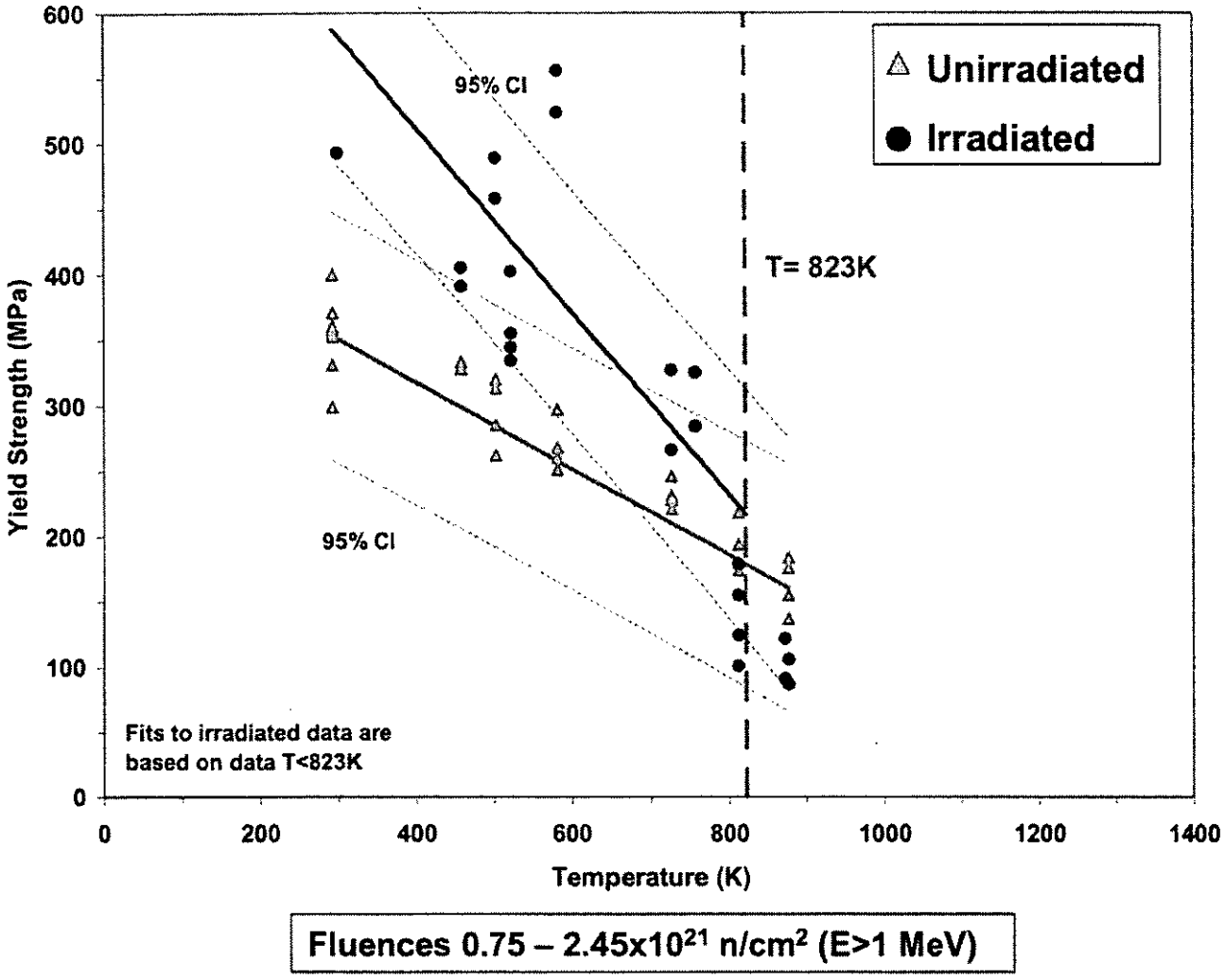

Figure 1.2.8: Irradiated and Unirradiated Tensile Yield Strength of HIP Be

1.2.9 Emissivity

Reference 1.2.g reports the emissivity of Be for $T < T_m$:

$$\varepsilon = 0.61$$

The emissivity of Be is not expected to vary with irradiation, however the emissivity may vary with material processing (i.e. surface finish).

1.2.10 Ultimate Tensile Strength

1.2.10.1 Unirradiated

Multiple references have reported on the unirradiated ultimate tensile strength of Be (References 1.2.d, 1.2.k, 1.2.l and 1.2.m). The below equations are based on data from unirradiated VHP (S-65 and S-200F Brush Wellman) and HIP (S-65H and S-200FH Brush Wellman) Be grades. In general,

HIP grade Be exhibits a higher ultimate tensile strength than VHP grade Be. These equations are based on data in the temperature range 293K ≤T ≤923K (See Figures 1.1.9 and 1.1.10 below in section 1.2.10.2).

$$VHP\ UTS = -0.4139 \cdot T + 515.3$$

$$HIP\ UTS = -0.4897 \cdot T + 609.9$$

where
VHP UTS = ultimate tensile strength of VHP Be, MPa
HIP UTS = ultimate tensile strength of HIP Be, MPa
T = temperature, K

1.2.10.2 Irradiated

Irradiation effects on the ultimate tensile strength of multiple grades of Be (S-65, S-65H, S-200F and S-200FH) have been studied by many references (References 1.2.d, 1.2.k, 1.2.l and 1.2.m). Irradiated Be exhibits a slightly higher ultimate tensile strength than in the unirradiated state. Below is a fit to the VHP Be and HIP Be data over a temperature range of 293K ≤T ≤823K and fluence range of 0.75 – 2.45x10^{21} n/cm^2 (E>1 MeV). The plot of irradiated and unirradiated ultimate tensile strength data for multiple grades of Be are shown in Figure 1.2.9 and Figure 1.2.10. Neutron irradiation studies have observed that above 823K the strength of irradiated Be dramatically decreases due to He bubble formation. In beryllium He bubbles begin to form at grain boundaries at T>673K and at dislocations within the grains at T>823K. Additionally, Be has a high fast neutron cross-section for (n,α) reactions and therefore at higher temperatures He embrittlement becomes a concern (corresponding to 0.5 T_{melt}). All high temperature irradiated data (T ≥823K) was excluded from the regression analysis. Additionally, Moons (Reference 1.2.d) performed thermal ageing studies to isolate thermal effects from radiation effects. The thermal results are not included in this linear regression analysis. Data reported from Reference 1.2.d, 1.2.k, 1.2.l and 1.2.m were from samples tested at the irradiation temperature. The equations exhibit a good fit for 293 – 823K.

$$VHP\ UTS_{irr} = -0.7980 \cdot T + 849.0$$

$$HIP\ UTS_{irr} = -0.8738 \cdot T + 943.6$$

where
VHP UTS_{irr} = irradiated ultimate tensile strength of VHP Be, MPa
HIP UTS_{irr} = irradiated ultimate tensile strength of HIP Be, MPa
T = temperature, K

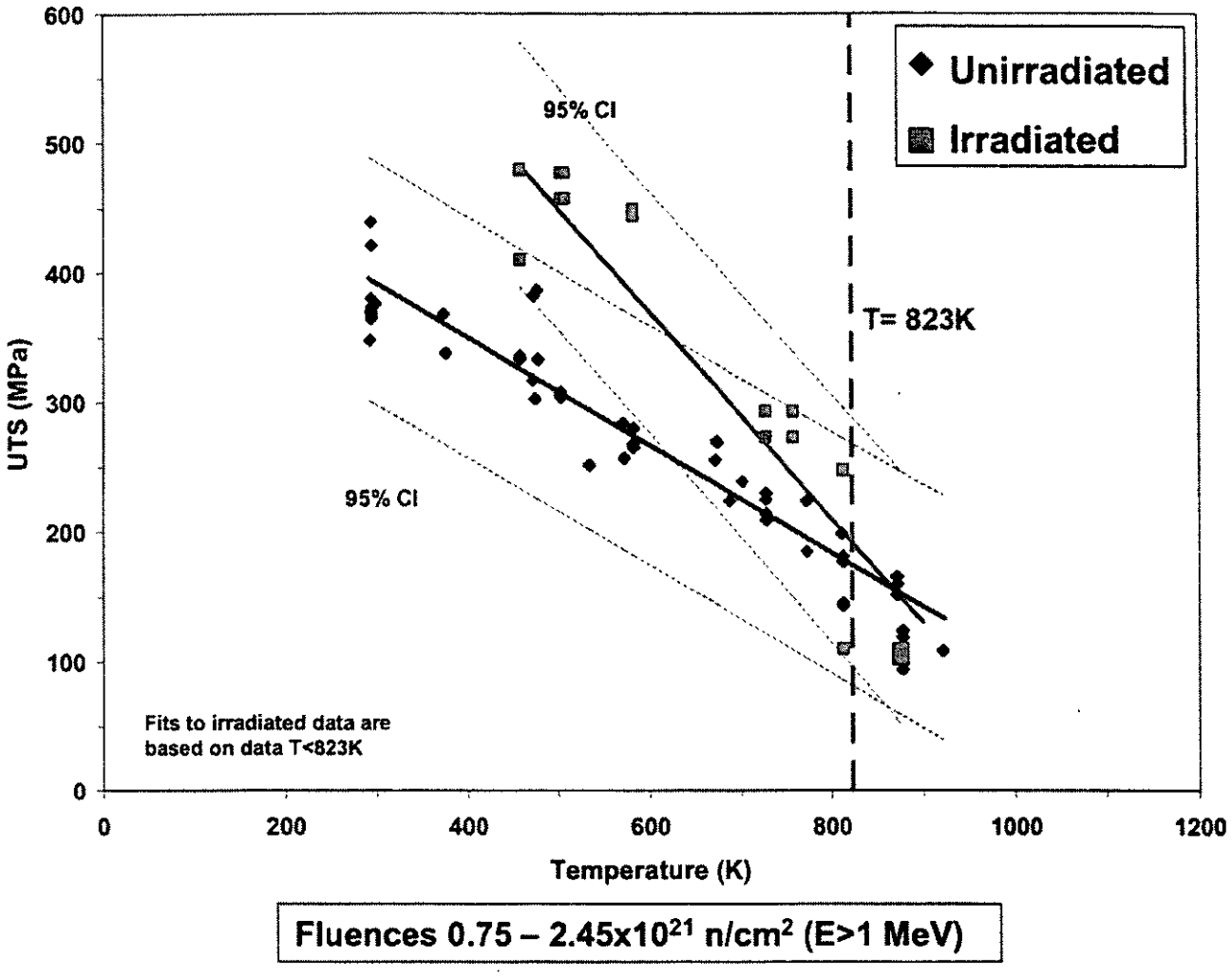

Figure 1.2.9: Irradiated and Unirradiated Ultimate Tensile Strength of VHP Be

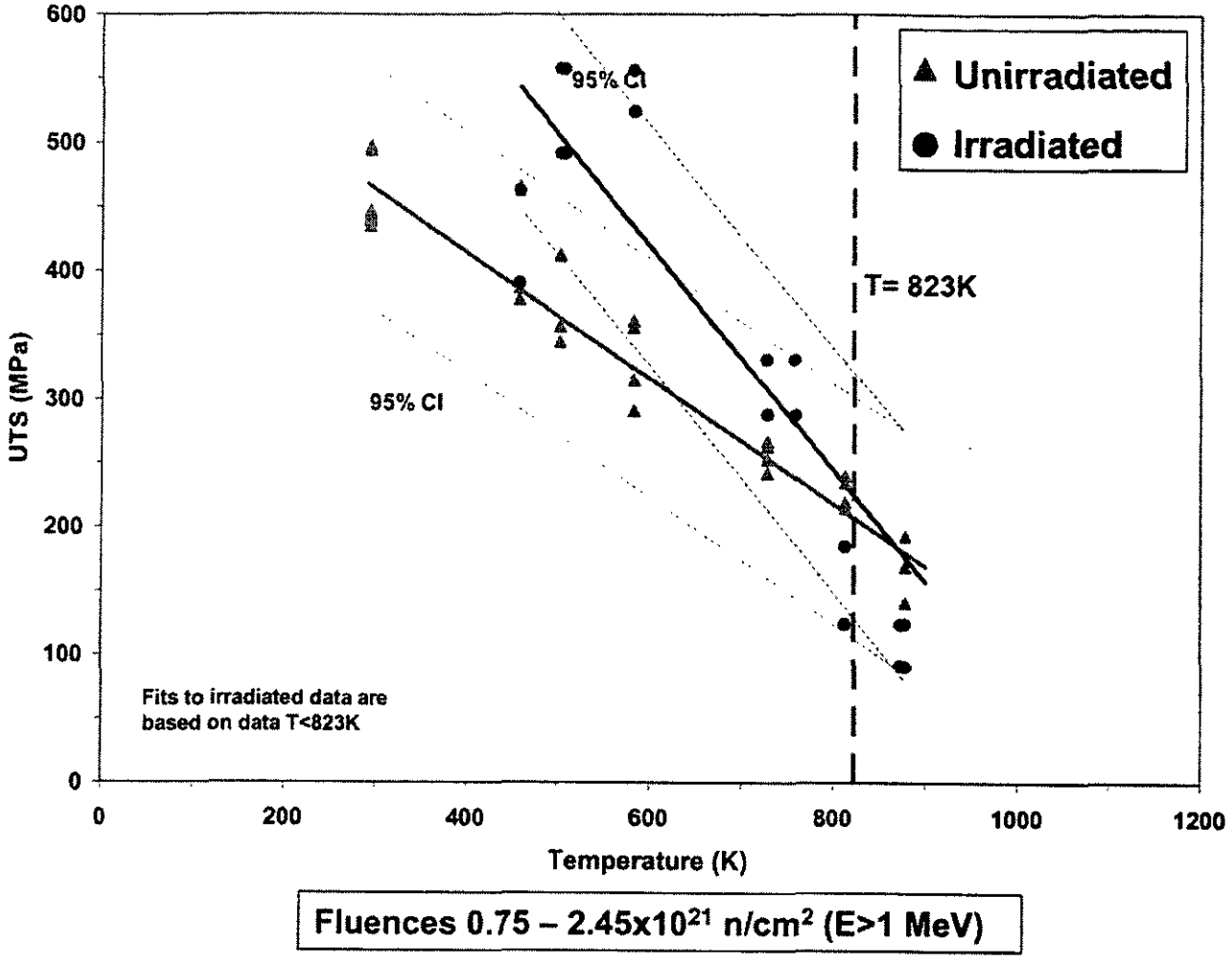

Figure 1.2.10: Irradiated and Unirradiated Ultimate Tensile Strength of HIP Be

1.2.11 Poisson's Ratio

Dombrowski (Reference 1.2.c) gives a table (Table 1.2.6) of room temperature data for Poisson's ratio of Brush Wellman Be grade S-200F. Note, scatter in the data is possibly attributed to the low value of the measurements. Because Be grades S-200F and S-65 are similarly processed, these results should be similar for S-65 grade Be.

Table 1.2.6: Poisson Ratio Data for S-200F Be

Orientation	Stress Axis	Direction of Orthogonal Strain	Poisson's Ratio
LC	Longitudinal	Circumferential	0.102 0.064 0.072
LR	Longitudinal	Radial	0.102 0.080 0.105

Orientation	Stress Axis	Direction of Orthogonal Strain	Poisson's Ratio
TL	Transverse	Longitudinal	0.069 0.071 0.108
TR	Transverse	Radial	0.102 0.058 0.066

Scaffidi-Argentina (Reference 1.2.b) reported that Poisson's ratio ranges between 0.01 – 0.13 (0.07 +/- 0.06) while Billone (Reference 1.2.h) reported Poisson's ratio at room temperature to be 0.08 +/- 0.02. Reference 1.2.a also reported that Poisson's ratio is generally independent of temperature, grain size, porosity and radiation damage. Additional data on S-65 grade Be may be required to validate these assumptions.

1.2.12 Irradiation Swelling

As described by Scaffidi-Argentina and Gelles (References 1.2.b and 1.2.n), damage due to irradiation in Be occurs primarily from fast neutron transmutation reactions resulting in the formation of helium (He) and tritium (^{3}H) via the following reactions:

$$^9Be + n \rightarrow {}^8Be + 2n \text{ (threshold energy 2.7 MeV)}$$

$$^8Be \rightarrow 2\,{}^4He$$

$$^9Be + n \rightarrow {}^6He + {}^4He \text{ (threshold energy 1.4MeV)}$$

$$^6He \rightarrow {}^6Li$$

$$^6Li + n \rightarrow {}^4He + {}^3H \text{ (primarily thermal neutrons)}$$

Swelling is considered an important irradiation effect. The He formed by the transmutation reactions is responsible for swelling at high fluences and high temperatures. Gelles (Reference 1.2.n) determined that minimum swelling at high temperatures occurred in Be grades with the smallest grain size and highest BeO content. Helium migration and the formation of large helium bubbles are limited by the large quantity of small BeO particles. The swelling of Be was also examined by Dalle Donne (Reference 1.2.o) in an attempt to characterize the behavior of the material in solid breeder blanket applications. It was established by Scaffidi-Argentina (Reference 1.2.b) that swelling generated from a given gas concentration was dependent on the He bubble size and therefore dependent upon the bubble density. Dalle Donne (Reference 1.2.o), using this and other constitutive relationships for Be (surface tension, grain boundary energy, self-diffusion, He diffusion, vapor pressure etc.) created the computer code ANFIBE (Analysis of Fusion Irradiated Beryllium). The ANFIBE code accounts for the important mechanistic processes that affect the gas generation and swelling behavior in Be.

Reference 1.2.o illustrates how the ANFIBE code has shown agreement with a variety of experimental data. Experimental data ranges from 2.1-50 x 10^{21} n/cm^2 (E>1MeV) from 300-973K. Experimental data was obtained from S-65 and S-200F beryllium irradiated in the EBR-II (fast reactor), BR2 (fast reactor) and the ATR (PWR reactor). Swelling predictions from the ANFIBE model were reported by Dalle Donne to fluences of 25x10^{21} n/cm^2 (E>1MeV) and temperatures of 973K. Dalle Donne (Reference 1.2.o) presented a comparison of the ANFIBE calculated swelling versus experimental

swelling shown for a range of data (Figure 1.2.11). Additionally, the ANFIBE predictions for swelling at 0.5-10 x 10^{21} n/cm^2 (E>1MeV) over the temperature range of 273-973K are shown in Figure 1.2.12.

Efforts continue to develop the ANFIBE code, providing greater capability and confidence in the model (References 1.2.b and 1.2.p). While much of the data used in validating the code is for higher fluences at lower temperatures or lower fluences at higher temperatures, the model is expected to yield reasonable predictions at higher temperatures and higher fluences.

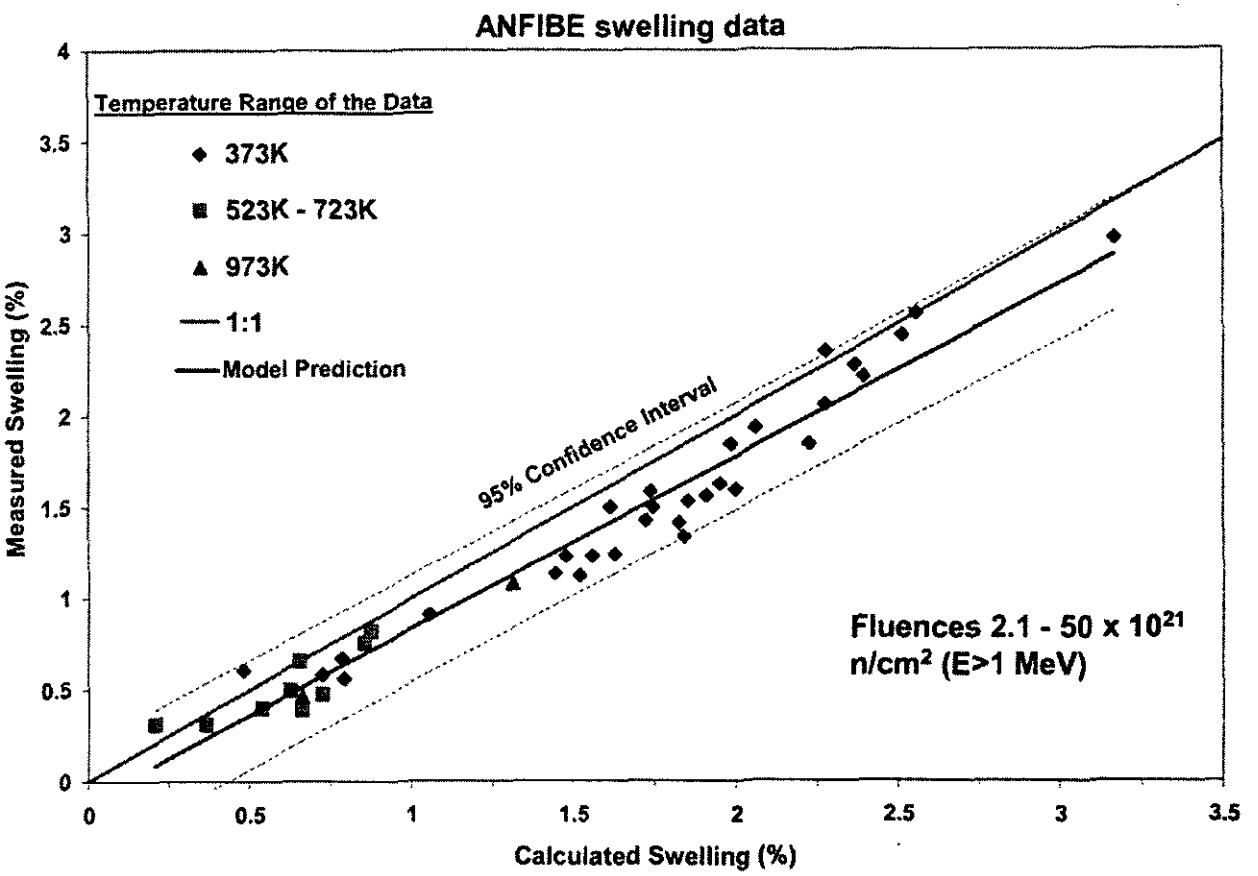

Figure 1.2.11: Measured Be Swelling Data Versus the ANFIBE Calculated Swelling

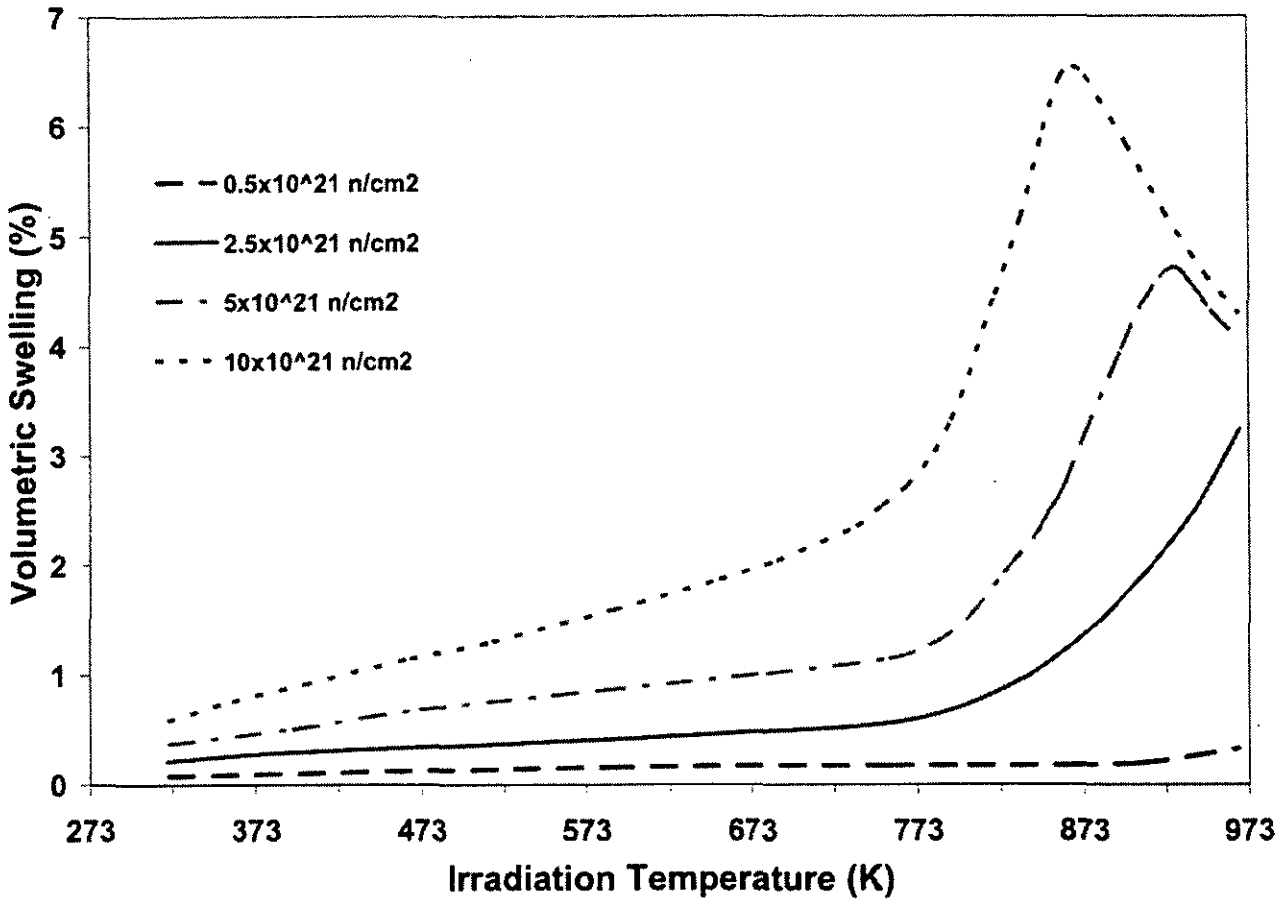

Figure 1.2.12: Predicted Be Swelling Based on ANFIBE Code

1.2.13 References

1.2.a J. Neter, M. H. Kutner, C. J. Nachtsheim and W. Wasserman, *Applied Linear Statistical Models* 4th ed., McGraw-Hill (1996).

1.2.b F. Scaffidi-Argentina, G. R. Longhurst, V. Shestakov and H. Kawamura, "Beryllium R&D for fusion applications", *Fusion Eng. and Design*, **51-52** (2000) 23-41.

1.2.c D. E. Dombrowski, E. Deksnis and M. A. Pick, "Thermomechanical Properties of Beryllium", Brush Wellman Report TR-1182, February 20, 1995.

1.2.d SCK CEN Progress report FT/Mol/96-03 ITER Task 23 "Beryllium Characterization: Tensile tests on neutron irradiated and reference beryllium", F. Moons, February 1996.

1.2.e B. S. Hickman, "Radiation Effects in Beryllium and Beryllium Oxide", *Studies in Radiation Effects, Series A Physical and Chemical Vol. 1*, 1966.

1.2.f Brush Wellman specification, S-65 Structural Grade Beryllium Block, Rev C, July 1, 1987.

1.2.g J. M. Beeston, "Beryllium metal as a neutron moderator and reflector material", *Nuclear Eng. and Design*, **14** (1970) 445-474.

1.2.h M. C. Billone, "Recommended design correlations for S-65 beryllium", Proceedings 2nd IEA International Workshop on Beryllium Technology for Fusion, September 6-8, 1995 pp. 348 – 363.

1.2.i L. L. Snead, "Low-temperature low-dose irradiation effects on beryllium", *J. Nucl. Mat.*, **326** (2004) 114-124.

1.2.j V. Barabash, G. Federici, M. Rödig, L. L. Snead and C. H. Wu, "Neutron irradiation effects on plasma facing materials", *J. Nucl. Mat.*, **283-287** (2000) 138-146.

1.2.k M. F. Smith, R. D. Watson, J. B. Whitley and J. M. McDonald, "Thermomechanical testing of beryllium for limiters in ISX-B and JET", *Fusion Technology*, **8** (1985) 1174-1183.

1.2.l S. H. Goods and D. E. Dombrowski. 1997. "Mechanical properties of S-65C grade beryllium at elevated temperatures", Proceedings of the 3rd IEA International Workshop on Beryllium Technology for Fusion, Mito City, Japan, 22-24 October.

1.2.m R. Chaouadi, F. Moons and J. L. Puzzolante. 1997. "Tensile and fracture toughness test results of neutron irradiated beryllium", Proceedings of the 3rd IEA International Workshop on Beryllium Technology for Fusion, Mito City, Japan, 22-24 October.

1.2.n D. S. Gelles, G. A. Sernyaev, M. Dalle Donne and H. Kawamura, "Radiation effects in beryllium used for plasma protection", *J. Nucl. Mat.*, **212-215** (1994) 29-38.

1.2.o M. Dalle Donne, F. Scaffidi-Argentina, C. Ferrero and C. Ronchi, "Modeling of swelling and tritium release in irradiated beryllium", *J. Nucl. Mat.*, **212-215** (1994) 954-960.

1.2.p E. Rabaglino, C. Ferrero, J. Reimann, C. Ronchi and T. Schulenberg, "Study of the microstructure of neutron irradiated beryllium for the validation of the ANFIBE code", *Fusion Eng. and Design*, **61-62** (2002) 769-773.

This Page Intentionally Left Blank

Distribution to
MDO-723-0042

CONCURRENCE/DESIGN CHECK FORM FOR DOCUMENT NO. MDO-723-0042 **Date:** 11/2/2005

DOCUMENT TITLE: Shield and Reflector Material Properties for Project Prometheus (U)

REFERENCES ENCLOSURES:

1. ADSARS: PERMANENT RECORD: Yes X No ___ Repository MFLIB Corporate Author: KAPL NR PROGRAM 08S

Key Words:	Shield	Reflector	LiH	Be	BeO	Prometheus			
Need to Know Categories	REP	REC	SGN						
Available Sites:	PRNR								
Design File Location(s)									

2. DESIGN CHECK

Type of Check	Signature(s)	Comments: (Including Reference to Check Document If Appropriate)
A. No check considered necessary		
B. Check vs. previous results/issues		
C. Checked calculations made	BG	J.Nash for LiH, B. Gurau for Be and BeO
D. Checked computer input and/or output		
E. Computer Programs approved/qualified		
F. Performed independent audit	BG	J. Nash for LiH, B. Gurau for Be and BeO
G. Spot checked significant points		
H. Reviewed methods used	BG	J. Nash for LiH, B. Gurau for Be and BeO
I. Reviewed results for reasonableness	DTP	
J. Comparison with test data		
K. Reviewed vs. drawings		
L. Verified procedures		
M. Technical content reviewed	BG	J Nash for LiH, B. Gurau for Be and BeO
N. Management verification of adequate review by others		
O. Performed Lessons Learned Search		
P. Used Measurement Uncertainty Methods		
Q. Other Checks (Describe)		

3. CONCURRENCE REQUIREMENTS: Indicate signatures required by X:

___ ARP MANAGER	___ NCSG	___ FLUID DYNAM
___ NUCLEAR ENGINEERING	___ ADVANCED CONCEPTS	___ STRUC. ENGRG
___ REACTOR TH/MECH DESIGN	___ NOISE & ELEC. TECH.	___ DRAFTING
___ REACTOR EQUIPMENT	___ SHIELDING	___ QA
___ POWER PLANT MECHANICAL	___ REACTOR SAFETY	___ OTHER
___ POWER PLANT ELECTRICAL	___ TO	Bhupta for W Ohrenberger 11/1/05
___ FINANCE	___ RSO	___ BPM per telecon
___ NEW SHIP PROGRAMS	___ FSO	___ ADMIN REVIEW
___ PROGRAM COORDINATION	MDQ/Sm 11/2/05	

Cognizant Manager B. Campbell BC
(Must Be Subsection or Higher for External Letters)

4. AUTHORIZED CLASSIFIER: **Reviewed By:** B. Campbell BC **CLASSIFICATION:** UNCL

5. RELATED SUBJECTS:

UTRS Implication (Y/N)	N	Commitment Made (Y/N)	N	Commitment Complete (Y/N)	N
Safety Council Review (Y/N)	N	Design Basis Info. (Y/N)	N	UTRS Doc. #	
		Design Review (Y/N)	N		

6. Distribution:

NR

DI Curtis
JD Yoxtheimer
JP Mosquera
ST Bell
CH Oosterman

PNR

JF Koury
JA Andes

SNR

D Potts
D Clapper
GM Millis

BETTIS

CD Eshelman, 36E/SE
D Hagerty **
RC Jewart **
CA White **
J Hack **
M Zika **
HA Karnes **
W Ohlinger **
R Baranwal **
M Wilke **
TL Pepple **
JL Bowman **

KAPL

JM Ashcroft **
PF Baldasaro **
CF Dempsey **
KC Loomis **
DF McCoy, 111
H. Schwartzman **
SA Simonson **
MJ Wollman **
BC Campbell **
BS Gurau **
JM Nash **
R Lewis **
MT Collins **
E Pheil **
W Burdge **
G Stasik **
W Gideon **
DL Hjelmar **
JT Ward **
JK Witter **
CM Maercklein **
S Samuel **
J Kokinos **

SM File
ADSARS

** Electronic Copy Only